SCIENCE IN PARLIAMENT

THE increasing importance of scientific research and technology and the impact that it has on the peoples of every nation is well reflected in government edicts of every country in the world. Particularly, therefore, where there is a system of government such as exists in the countries of the British Commonwealth, it is essential for the members comprising Parliament to be kept apprised of new developments.

The Parliamentary and Scientific Committee was therefore formed in 1939 to ". . . provide Members of Parliament with authoritative scientific and technical information . . . and to ensure that proper regard is had for the scientific point of view." There could not be any greater tribute to its efficiency and usefulness than the fact that similar committees have since been established in many countries throughout the world.

The Institution was one of the first of the professional bodies to obtain membership of the Parliamentary and Scientific Committee. The membership now includes representatives of 102 institutions and research associations and 180 members of both Houses of Parliament.

The Parliamentary and Scientific Committee is, of course, non-party. In addition to providing a permanent link between scientific bodies and Parliament, it is a centre for the consideration and discussion of scientific information bearing on proceedings in Parliament. Thus, its work covers the whole field of science, and addresses and discussions have included such topics as the Development of Inventions Bill, scientific research in the universities and colleges of technology, technological manpower, nuclear power development, transonic flight, education and manpower, etc.

In addition, the Committee circulates extracts from the official reports of both Houses of Parliament, arranges visits to research stations and important industrial organizations and, through its various sub-committees, keeps watch on legislation likely to affect scientific development.

On February 28th last, the Annual Luncheon of the Committee was honoured by the presence of H.R.H. Prince Philip, Duke of Edinburgh. In his speech, His Royal Highness mentioned the developments which had taken place in the scientific world since he last attended the Committee's Luncheon in 1953. After referring to Britain's scientific achievements, His Royal Highness concluded: ". . . there is one more thing that science can do for us, perhaps the most valuable and important thing. We have seen in the International Geophysical Year the way in which scientists of all nations, notwithstanding the military, commercial, diplomatic and all the other arguments, are working in harmony. This sort of thing does not happen so often that it can be dismissed as of no account. Could this possibly be an opening to a better understanding between the nations of the world? Perhaps the Parliamentary and Scientific Committee may help to answer that question."

Science and its applications is now a regular topic in the Parliaments of the world. No greater service could have been rendered to those who govern, or to those who are actively engaged in science and technology, than that opportunity should have been provided for members of both sects to meet dispassionately under such an aegis as the Parliamentary and Scientific Committee.

INSTITUTION NOTICES

OBITUARY

The Council has learned with regret of the death of the following Associate Members and has expressed sympathy with their relatives.

Ronald Ainslie Lanchester died recently at his home in Sydney, Australia, aged 53 years. Elected to Associate Membership in 1946 while serving as a Port Radar Officer with the Royal Indian Navy, Mr. Lanchester had long experience in many branches of radio. After completing his technical education he held appointments with Standard Telephones and Cables, the Marconi-Osram Valve Co., and the Telephone Manufacturing Co.; after the war, following two years with the Supply Department of the Government of India, he joined the Australian Department of Civil Aviation. At the time of his death he was a senior airways engineer.

*　　*　　*

Hendrikur Theodorus Joseph Wiegerinck died on 11th January last as a result of injuries received in a road accident. He was 46 years of age. Mr. Wiegerinck was born in Holland and worked with the Philips organization from 1936-1945, being concerned with development of domestic and communications receivers and measuring instruments. For the next two years he was in charge of the Communications Section of the Netherlands War Office in London, and in 1947 joined Pye Ltd., Cambridge. Here he was again concerned with domestic radio development, and in 1952 he was appointed to take charge of electrical design with an associated company, TV Manufacturing Ltd., Lowestoft, the position he held at the time of his death. Mr. Wiegerinck was elected to Associate Membership of the Institution in 1952.

Institution Dinner

The official guests at the Institution's Dinner, to be held on Thursday, 1st May, at the Savoy Hotel, London, will include Sir Ben Barnett (chairman of the Commonwealth Telecommunications Board) and Sir Cyril Hinshelwood, President of the Royal Society, who will be one of the speakers.

Details, together with an application form for tickets, were included in the February issue of the *Journal*. In view of the number of applicants, members who wish to bring guests are reminded that the form should be returned not later than 25th March.

Group Provident Scheme

The Council has under consideration starting a Provident Scheme for members. It will be operated through the British United Provident Association and the principal object will be to assist members against expense of private treatment for major illnesses and operations.

Treatment in nursing homes and private specialist consulting fees do not, of course, come under the National Health Service. The Provident Scheme would enable members, and their dependants, to make the best arrangements without having to worry about the cost. Thus the Scheme is not intended to displace the National Health Service, but to provide supplementary benefits.

Members who already contribute to the B.U.P.A. may apply for transfer to the Group Scheme which will be operated by the Institution, and thereby obtain the benefit of a 20 per cent. reduction in fees.

Members interested in joining this Group Scheme are asked to write to the General Secretary of the Institution for details.

Closing Dates for Graduateship Examination

The last date for receiving entries from candidates wishing to sit the May 1958 Graduateship Examination at centres in the United Kingdom is 1st April. The examination will take place on 21st-22nd May.

Overseas candidates are reminded that entries for the November 1958 examination should be received by the Institution by 1st May, 1958.

Radio and Electronic Component Show

This year's Radio and Electronic Component Show will be held at Grosvenor House, London, W.1, from 14th-17th April. The exhibition will be open from 10 a.m. to 6 p.m. daily. Members may obtain tickets from the Institution.

Corrections

The following corrections should be made in the paper "Approximate Relations between Transient and Frequency Response", published in the January 1958 issue:

Page 58: The fraction in eqn. (3) should be $200/\pi$.

Page 64: On the right-hand side of eqn. (37), the symbol j should be inserted before $1/2\pi$.

INDUSTRIAL APPLICATIONS OF A.C. POLAROGRAPHY*

by

R. L. Faircloth, B.Sc.† and D. J. Ferrett, M.A., D.Phil.†

*A paper presented at the Convention on "Electronics in Automation" in Cambridge
on 28th June 1957.
In the Chair : Dr. Denis Taylor (Member)*

SUMMARY

The a.c. polarographs that have recently been developed, such as the Mervyu-Harwell square-wave polarograph, have very greatly extended the range and usefulness of techniques for analysis of metals and non-metals.

Concentrations of 1 in 10,000,000 can be measured and these instruments overcome many of the disadvantages of conventional polarographs. The principles of the square-wave polarograph are discussed and recent work on the pulse polarograph and the r.f. polarograph is described. The range and versatility of these instruments offer many opportunities for plant-control and instrumentation.

1. Introduction

Polarography is an electrochemical technique of considerable value in both qualitative and quantitative analysis. Fig. 1 shows the apparatus used. The solution to be analysed is contained in a cell whose anode is a large pool of mercury. Mercury is also used as the cathode of the cell, but here it is in the form of very small droplets which emerge from the tip of a capillary tube. As well as the small unknown amount of ions that take part in the electrode reaction and which are to be analysed, there is present in the solution an excess concentration of an electrochemically inert electrolyte (generally referred to as the base-electrolyte) which conducts the current passing through the cell.

In the conventional polarographic technique a gradually increasing potential difference is applied to the two electrodes and the current flowing is recorded continuously, either on photographic paper or with a pen-recorder. For most electrochemically reducible species, e.g. metals such as iron, lead, copper, zinc, gases such as oxygen, and sulphur dioxide, and organic materials such as trinitrotoluene, vitamin C, streptomycin, etc., the current-voltage curves have the general form shown in Fig. 2.
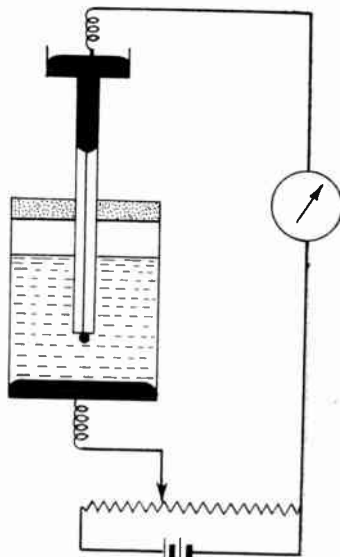

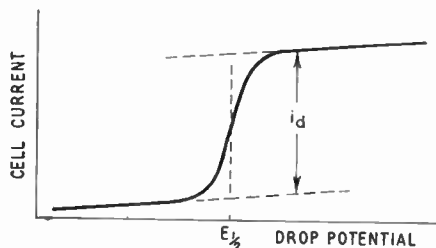Fig. 1. Schematic drawing of apparatus used in conventional polarography.

Fig. 2. Typical current–voltage curve obtained in conventional polarography.

Over the initial part of the wave, only a small current flows but when a potential is reached at which one ionic species begins to take part in an electrode process at the cathode, the current will increase rapidly. Finally a potential is attained at which as fast as ions arrive at the electrode surface they undergo reaction and the current becomes once more nearly constant. From diffusion theory it can be shown that this limiting current at 25°C is given by

$$i_d = 706n \, CD^{\frac{1}{2}}m^{2/3}t^{1/6} \qquad \ldots\ldots\ldots(1)$$

where i_d = the current in microamperes flowing t seconds from the beginning of the formation of a drop;

n = the number of electrons involved in the electrode reaction;

D = the diffusion coefficient of the reacting species in units of cm² sec⁻¹;

C = the concentration of this species in moles/litre;

and m = the rate of flow of mercury to the drop in mg. sec⁻¹.

This equation was first derived by Ilkovic.

The current-time relationship during the life of each drop is therefore a 1/6th order one and the smooth curves shown in Fig. 2 are not therefore obtainable in practice although close approximations may be achieved by using recorders of long time-constant. The diffusion current given by the wave height is directly proportional to the concentration of the reacting species in the solution and this forms the basis of quantitative polarographic analysis. It must be noted however that to ensure the accuracy of the analysis the temperature of the system, the concentration and nature of the base electrolyte and the capillary constants (m and t) must be controlled.

The potential at which the current is one-half of its limiting value, $E_{\frac{1}{2}}$—the half-wave potential—is characteristic of a given ion species in the solution studied and is a useful guide for qualitative analysis.

The limitation of conventional polarographic techniques is determined by the fact that a small current (the residual current) always flows through the cell, even in the complete absence of electro-reducible species. This current is due to the charging of the double-layer of ions that form a capacitor on the growing surface of the drop, and this capacitive current may be as much as 0·2 microampere. Since the diffusion current for a 10⁻⁴ M (10 p.p.m.) solution of (say) cadmium is about 1 microampere, adequate compensation for the residual current even at this concentration must be made. Since the current varies in an approximately linear fashion with potential it is possible to compensate to some extent, but even with this facility it is difficult to extend conventional d.c. polarography to concentrations below 10⁻⁵ M.

A further limitation to the analysis of solutions of mixtures of ions is that the current flowing due to the reduction of a large concentration of one ion, may well mask the diffusion current of another ion that is reduced at a more negative potential. This limitation may be partly overcome by recording the derivative of the current–voltage curve. The response from individual ions is then in the form of peaks and less interference in mixtures is encountered. The height of the derivative wave is directly related to the slope of the normal polarogram, however, so that any irregularities in the former are reproduced and the method gains little in sensitivity over normal polarography.

A form of derivative polarogram may be obtained by superimposing a small a.c. sinusoidal voltage upon the slowly changing d.c. potential and recording the alternating component of the current flowing. This method gives well-defined peaks but it suffers a considerable loss in sensitivity because of the large background current caused by the low a.c. impedance of the electrical double-layer of ions at the electrode/solution interface. This capacitive current flows continuously through the cell and small polarographic waves may be completed masked.

2. Square-Wave Polarography

The use of an alternating-voltage of square-wave form to eliminate the large background current associated with sinusoidal voltages was suggested by Barker and Jenkins[1], the method having initially been developed by Dr. G. C. Barker for studying electrode reaction kinetics.

Figure 3 shows the electrical equivalent for alternating components of a polarographic cell.
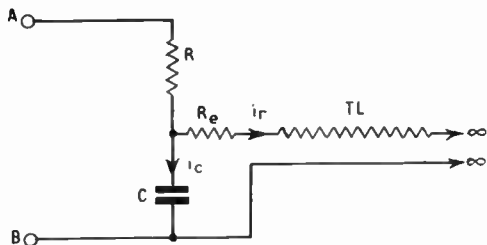
Fig. 3. Equivalent electrical circuit.

Resistance R represents the sum of the output impedance of any voltage source applied to the terminals of the cell AB, the resistance of the thread of mercury in the capillary of the electrode, and the resistance of the solution lying between the anode and the cathode. Capacitance C represents the double-layer capacitance of the electrode-solution interface. In parallel with this is R_e, representing the thermodynamic irreversibility of the electrode reaction, which can be ignored for reversible reductions and TL a transmission line of infinite length without inductance but with distributed shunt capacitance and series resistance along its length which represents the diffusion of reducible material from the bulk of the solution to the interface.

If therefore a square-wave voltage is applied to AB, currents i_r and i_c will flow, i_c giving rise to the interfering background current. i_r and i_c may be separated however by applying a square-wave voltage to AB, whose half-period τ is very much longer than the time-constant RC. Current voltage curves as in Fig. 4 are obtained.

It can be seen that at a given time t, i_c has decayed to virtually zero while i_r still has a finite value. An almost perfect separation of i_c and i_r may be obtained therefore if the a.c. component of the cell is measured just before each change in sign of the applied voltage. In practice, because of signal/noise ratio considerations, the average current flowing over a period of time at the end of each square-wave cycle is actually measured. In Square Wave Polarograph Type 1336A which is commercially available as the Mervyn-Harwell Square Wave Polarograph, a 225 c/s square-wave is used; τ is then 2·2 milliseconds. The average current is measured over the last 0·2 milliseconds and

hence t is a little over 2 milliseconds. The time-constant RC for most experimental conditions will be of the order of 20 microseconds.

From an extension of diffusion theory, it can be shown[2] that for the particular instrument at 25°C, the current amplitude ΔI (in Fig. 4) is given by

$$\Delta I = 5 \cdot 61 \times 10^7 \, n^2 \, D^{\frac{1}{2}} \Delta E \, CA \left(\frac{P}{1+P} \right)^2 \text{ amperes}$$

$$\ldots\ldots(2)$$

where ΔE = square-wave amplitude

$$P = \exp \frac{(E - E_{\frac{1}{2}})nF}{RT}$$

A = electrode area

E = electrode potential
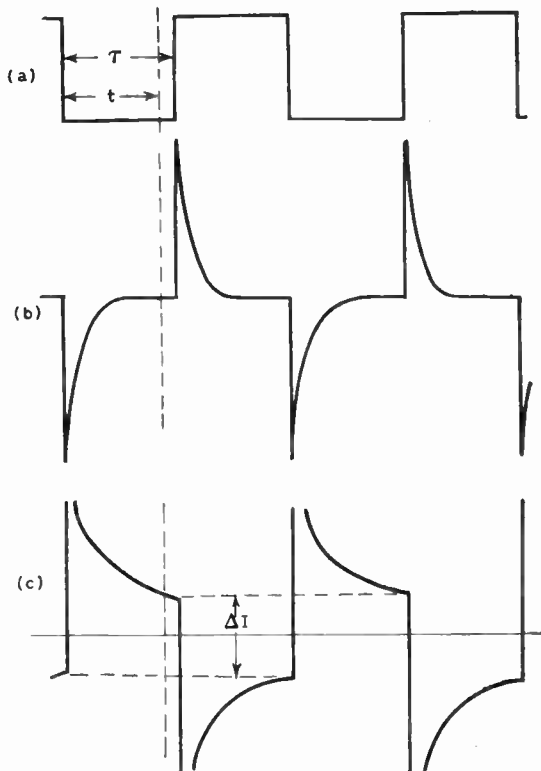
and $E_{\frac{1}{2}}$ = half-wave potential.

Fig. 4. Voltage and current waveforms.
(a) Square wave voltage. (b) Capacitance current i_c.
(c) Electrode reaction current i_r.

The current amplitude is therefore directly proportional to the electrode area, so that it
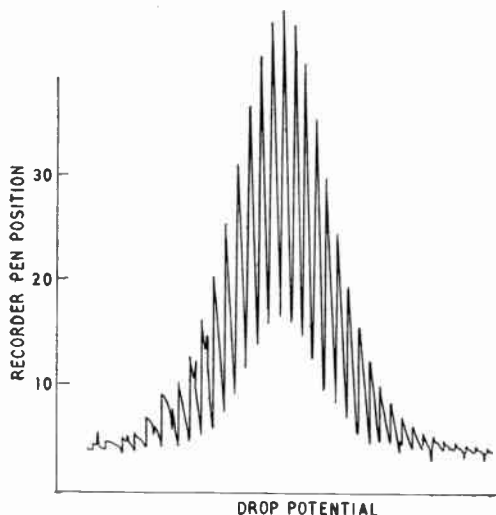
Fig. 5. Continuous output polarogram.

will change continuously during the life of each drop (see Fig. 5). It is however more useful to measure the current at a definite time in the life of each drop. This would then correspond to an electrode of constant area. If this is done, a polarogram of the form shown in Fig. 6, and known as a strobe polarogram is obtained. The time between the fall of a drop and the instant of current measurement is about 1·8 seconds. It is therefore important to use an electrode whose drop-time is not less than 3 seconds.

The facilities available in the square-wave polarograph offer a means of absolute calibration, which may well be advantageous in control analyses, where no large change in the characteristics of the solutions to be analysed
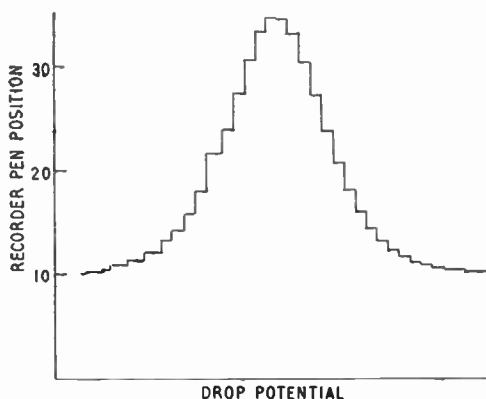

Fig. 6. Strobe output polarogram.

are expected. As the square-wave polarograph measures effectively the a.c. impedance of the cell, for a potential equal to the half-wave potential equation eq. (2) may be rewritten

$$G_{\frac{1}{2}} = 1·402 \times 10^7 n^2 D^{\frac{1}{2}} C \text{ mhos/cm}^2 \quad \ldots\ldots\ldots(3)$$

where G is the apparent conductance of the electrode/solution interface.

The vertical height of the strobe polarogram may therefore be calibrated in absolute units of reciprocal ohms per cm². This is rapidly and accurately done by comparing the response of the cell with that obtained when the cell is replaced by a standard resistance of suitable value. The double-layer capacitance of the electrode at this time can also be measured with the square-wave polarograph, and if capacitance data for this electrolyte at this temperature are known, the surface area of the drop can be obtained.

The simplified block diagram, Fig. 7, shows the equipment, and the controls available. The square-wave voltage is variable in both amplitude and frequency, the frequency being adjusted by reference to the small c.r.t. to 225 c/s. The square-wave voltage is fed to a modulator and mixed with a d.c. voltage supplied by a linear-voltage sweep generator. The speed and direction of the voltage sweep can be controlled and the potential for the start of the sweep can be fixed. The composite polarizing voltage which is the output of the modulator is then applied to the cell, or to a resistance for calibration.

The current waveform produced is filtered, amplified and fed into a time-sensitive detector which monitors the amplitude of the wave-form over the last 0·2 milliseconds of each half-wave cycle. The output voltage of the detector is passed to the output voltage selector where it is connected for 20 milliseconds to a storage capacitor at a pretermined strobe time in the life of the drop. The voltage across the capacitor varies in a step-wise manner from drop to drop and controls a high speed pen-recorder. The strobing time delay is achieved by passing a 1 Mc/s current through the cell. The sudden increase in cell impedance when the drop falls operates a delay circuit. The square-wave voltage is normally only applied to the cell around the strobing time but it can
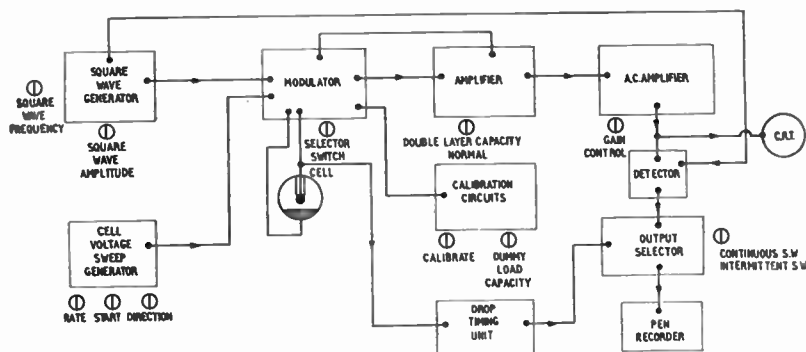
146

Fig. 7. Block diagram of equipment and controls.

potential slowly changes continuously but the pulse size remains constant.

Yet another advance in polarography which is in the early stages of development at Harwell involves radio-frequency voltages. It is believed that this method will be applicable to a number of types of electrode other than the dropping mercury electrode, such as solid platinum micro-electrodes. This would be of particular value in such cases as the

be applied continuously, when polarograms as in Fig. 5 are obtained.

3. Pulse Polarography

Another type of polarograph which has been developed at Harwell by Dr. G. C. Barker is known as the pulse polarograph.[3] The sensitivity of this instrument is appreciably greater than that of the square-wave polarograph, particularly for electrode reactions which are irreversible (see Fig. 8). It may also have particular advantages in control work since both normal and derivative polarograms may be obtained.

To obtain a normal polarogram the dropping mercury electrode is held for most of its life at a constant potential but at a predetermined time in the life of each drop a polarizing pulse changes the drop potential for $1/25$ second to a value which gradually becomes more negative while the polarogram is being recorded. The difference between the average cell current during the second half of the polarizing pulse and the corresponding current which would have been flowing if the drop potential had remained unchanged are computed and recorded. The polarogram so obtained closely resembles the type of record obtained with a conventional polarograph, but with the pulse polarograph there is automatic compensation for currents associated with reactions proceeding at the electrode prior to the occurrence of the voltage pulse.

The same circuits are used to record a derivative polarogram but in this case the drop

Fig. 8. Pulse and square wave polarograms for Cd^{++} and Ni^{++} $1M$ NH_4OH, $1M$ NH_4Cl containing 125 p.p.m. Cu, 1.25 p.p.m. Ni and 2.5 p.p.m. Cd.

continuous analysis for corrosion products in reactor loops where a simple dropping mercury electrode would present practical difficulties.

4. Industrial Applications of Polarography

In the thirty years since its discovery, polarography has found wide use in industry both in control of product purity, and in the

147

surveying of effluent control, raw-material analysis and control-testing. The range of the technique is very wide, for all substances that can take part in an electrode reaction, whether oxidation, reduction or absorption, at a dropping mercury electrode can be analytically determined. This includes such metals as iron, zinc, copper and uranium, and substances such as vitamins and steroids.

The analytical technique normally used is that known as standard addition. In this method, a known volume of the solution is transferred to the cell and the polarogram recorded. A smaller volume of a standard solution is then added, which contains a known concentration of the substance present, and the polarogram recorded again. A comparison of the two polarograms gives the concentration of the test solution. Once this data has been prepared for a given solution a calibration graph can be obtained and, provided that the solution conditions do not differ greatly from those formerly studied, unknown concentration can be accurately and rapidly determined.

The square-wave polarograph has to date been chiefly used for the analysis of metals, where its sensitivity is greatest. The increase of a hundredfold in sensitivity over conventional polarograms lowers both the sample size needed for analysis and the limits of detection. This latter feature is of fundamental importance in the control of the purity of foodstuffs. For example, the standard techniques for the determination of lead in foodstuffs require the use of considerable quantities of a large number of reagents and the problem of controlling the amount of lead in these reagents makes the determination of 1 p.p.m. or less of lead very difficult. Using the square-wave polarograph, however, lead in cocoa[4], a particularly difficult foodstuff to analyse, can be rapidly determined at the 0·7 p.p.m. level, and the quantities needed are such as to limit the lead content of the reagents used to 0·05 p.p.m.

Thus the increased sensitivity is also of value in determining impurity levels in the reagents themselves. The manufacture of reagents with a known and low impurity content is an important feature of present day chemical industry. The square-wave polarograph has been succesfully used for the rapid analysis of lead and copper in such reagents as sodium carbonate, citric acid and potassium chloride at levels down to 0·1 p.p.m.[5] The pulse polarograph can be used for the detection of such ions at levels below 0·005 p.p.m.[3] (see Fig. 9).
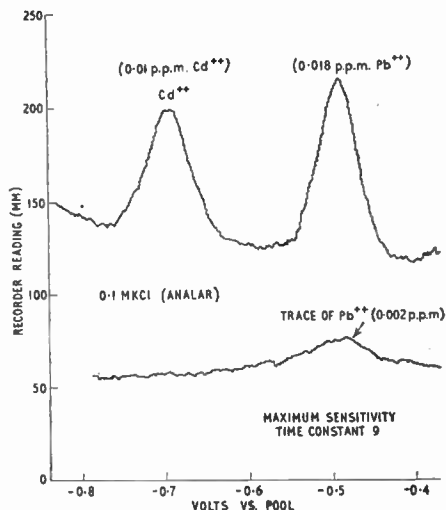
Fig. 9.   Derivative pulse polarograms at maximum sensitivity.

The derivative response of the square-wave and pulse polarographs compared with the step-wise response of conventional polarography makes the instruments of great use in the control analysis of alloys. Thus a single voltage sweep, which can be carried out in 5–15 minutes will determine copper, lead, cadmium, and zinc in an aluminium alloy (see Fig. 10). The analysis of zinc and nickel in copper alloys, brasses and bronzes can also be rapidly carried out while copper, lead, tin and chromium can be determined in steels at very low levels—Fig. 11 shows the copper and tin peaks in a steel equivalent to 0·002% copper and 0·00052% tin[6].
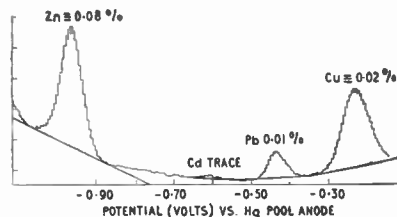
Fig. 10.   Square-wave polarogram for aluminium-base alloy (20mg/100 ml) in 1M KCl.

The analysis of water supplies and the control of effluent are both routine analytical problems where the high sensitivity available with the square-wave polarograph has been applied. One of the purposes of the experimental reactor loop constructed at A.E.R.E. Harwell is to obtain data on the corrosion

Fig. 11. Steel B.C.S. No. 149. 1mg/ml 5M HCl.

problems associated with stainless steel/water systems. At the temperatures and pressures used and under the high incidence of radiation that is possible, corrosion takes place and it is obviously necessary to have analytical techniques to follow and determine the extent of the corrosion. With the square-wave polarograph it has been possible to detect such important ions in corrosion effluents as 0·2 p.p.m. iron, and chromium, 0·06 p.p.m. of

nickel and 0·4 p.p.m. of manganese in only 2 ml. of sample[7]. Such ions can be detected at even lower levels with the pulse polarograph.

Investigations into the industrial potentialities of the square-wave and pulse polarographs were carried out on batch samples and studies on the application of the techniques to plant control and the analysis of flowing samples are now being made. Problems of interest being investigated in industry are the determination of sulphur dioxide in fruit juices, and the analysis of gas-work effluents for cyanide and thiocyanate.

The controlled circulation of liquid past the electrode presents little difficulty: of greater importance is the need to keep the potential of the dropping mercury electrode versus the solution constant, if a derivative polarogram is being recorded. The stability is determined both by instrumental factors, e.g. the stability of the linear voltage sweep, and by the composition of the solution flowing past the electrode. For a typical 2-electron reduction control of current amplitude within ±5 per cent. demands that the potential is held constant within ±12 mV. This degree of control can be instrumentally maintained but large fluctuations in the composition of the flowing sample could produce anomalous results. This difficulty can be overcome almost completely by using the normal polarogram facility of the pulse polarograph.

5. References
1. G. C. Barker and I. L. Jenkins, *Analyst*, **77**, p. 685, 1952.
2. G. C. Barker, R. L. Faircloth and A. W. Gardner, A.E.R.E. Report C/R 1786.
3. G. C. Barker and A. W. Gardner. Unpublished work.
4. D. J. Ferrett, G. W. C. Milner and A. A. Smales, *Analyst*, **79**, p. 731, 1954.
5. D. J. Ferrett and G. W. C. Milner, *Analyst*, **80**, p. 132, 1955.
6. D. J. Ferrett and G. W. C. Milner, *Analyst*, **81**, p. 193, 1956.
7. D. J. Ferrett and G. W. C. Milner, *Proc. Int. Conf. Atomic Energy, Geneva*, 1955, Vol. 9, p. 436.

APPLICANTS FOR ELECTION AND TRANSFER

As a result of its February meeting the Membership Committee recommended the following elections and transfers to the Council.

In accordance with a resolution of Council and in the absence of any objections, the election or transfer of the candidates to the class indicated will be confirmed fourteen days after the date of circulation of this list. Any objections or communications concerning these elections should be addressed to the General Secretary for submission to the Council.

Direct Election to Member
CARD, Group Captain Leslie Thomas, C.B.E., R.A.F. *Ewell.*
CHEESEMAN, Victor Alfred, B.Sc. *Wembley.*
PHILPS, Charles Lionel. *Glasgow.*
SHIRLEY, Lt. Col. John Robertson, O.B.E. *Napier, New Zealand.*

Transfer from Associate Member to Member
NEILL, Stanley Francis Mundy. *Potters Bar.*

Direct Election to Associate Member
BROWN, Arthur, B.Sc.* *Durham.*
EVATT, William Henry Royle. *Reading.*
FITZGERALD, James Arthur. *Marlborough.*
GREENACRE, James Alan, B.Sc. *Wigan.*
HUDSON, Alan Douglas, B.Sc. *Beckenham.*
MURTY, Satanarayana Dangety, M.A., M.Sc., D.Sc. *London, N.12.*
O'RILEY, Vincent, B.Eng. *Cork.*

Transfer from Associate to Associate Member
BILBROUGH, Jack. *Newcastle-upon-Tyne.*
CASTLE, John Lucas. *South Godstone.*

Transfer from Graduate to Associate Member
BEAGLES, Ralph Edward. *Manchester.*
CHAPMAN, Kenneth Samuel, B.Sc.Eng. *Chelmsford.*
DAMON, Lionel. *Malvern Link.*
PEARSON, Gordon Pitt. *Warlingham.*

Transfer from Student to Associate Member
LOGIE, Frank McLean. *London, N.W.2.*
LUFF, William. *Boreham Wood.*
TUCKER, John Drew. *Old Coulsdon.*

Direct Election to Associate
LOOI, Imm Meng. *Singapore.*
MOSELEY, Sidney Robert. *Rayleigh.*
SOE MYINT, Flt. Lt., Burma Air Force. *Rangoon.*
WALTHO, Ronald Eardley. *Ilford.*

Transfer from Student to Associate
DELANOY, Donald Brian. *Stapleford.*

Direct Election to Graduate
BEX, John Charles Arnold, B.Sc. *Worthing.*
BONVINI, Leonard Alfred. *Old Windsor.*
CLARE, Norman Victor. *Hayes, Middlesex.*
CLARK, James Oliver, B.Eng. *Leeds.*
DAMERAL, Thomas Charles. *Torpoint.*
DOBSON, Raymond Percival. *Stockport.*
GILHAM, Maurice Peter. *Tonbridge.*
HARRINGTON, Peter Frederick. *London, E.11.*
ISHAM, Douglas Cecil. *Luton.*
LAKSHMANAN, Krishna. *New Delhi.*
NEWMAN, Henry John. *Great Bookham.*
POWRIE, John Reginald, B.Sc.(Eng.). *London, S.W.14.*
SYMONDS, Robert Frank, B.Sc. *Weymouth.*
TOWELL, Douglas John. *Bromley.*

Transfer from Student to Graduate
DEVAN, Deva Das. *Brighton.*
HALTON, Dennis Lewin. *Wantage.*
HOLTZHAUSEN, Petrus Johannes. *Pretoria.*
HORN, Peter Jack. *Hitchin.*
LAWSON, Oswald Edward. *Lagos.*
JATHAR, Nilakanath Balakrishna. *Bangalore.*
SRINIVASAN, Ramachandran, B.Sc. *Bangalore.*
TSAMOUSSIS, Efstratios. *Athens.*

STUDENTSHIP REGISTRATIONS

ARMSTRONG, Thomas James Turner. *Chester-le-Street.*
BOULOHERI, Korallia. *Athens.*
BRIKAS, Evangelos Kyriazis. *Athens.*
CAWTHORN, Lewis. *Bath.*
CHRISTIE, Stanley. *Blackrock, Co. Dublin.*
DERMIT, Major William, R.Sigs. *London, W.1.*
DIXON, John Clive, B.Sc. *Rugby.*
DOBLE, Reginald George. *Gillingham.*
GOLDMANN, Rudolf. *Sao Paulo.*
GOODING, Patrick Michael. *Barnsley.*
GRIFFIN, Michael John. *Chorley Wood.*
HARPER, Terence William. *Reading.*
HART, Princewill. *Bristol.*
HUNG CHEUNG LOY. *Hong Kong.*
INDRASAN, Pandey. *Deoria.*

LATTIMORE, Ronald Victor. *London, N.W.7.*
LEUNG CHEUK SING. *Hong Kong.*
MAINWARING, Wynford John. *Swansea.*
MANLY-ROLLINGS, Thomas Cecil. *Southampton.*
MERRICK, Peter Hugh Crosbie. *Enfield.*
MILLAR, James Tait. *Stevenage.*
NAGARAJA, Birur Shamanna. *Bombay.*
OULTON, Richard John. *Maghull.*
PRATTEN, Peter E. J. *London, N.3.*
PUTLEY, Derek Edward. *Cheltenham.*
ROOME, Gordon, B.Sc. *Malvern Link.*
WHITHAM, Brian. *Shoreham-by-Sea.*
WONG SAU CHAN, Anthony. *Hong Kong.*

* Reinstatement.

THE ELECTRONIC SYNTHESIS OF FLEXIBLE BEAM BEHAVIOUR*

by

M. Squires, B.Sc.✝ and W. G. Hughes, B.Sc., D.I.C., A.R.C.S.✝

SUMMARY

The paper relates to the use of electronic analogue computers to evaluate and display the vibrations of flexible beams and related structures. The method is characterized by the speed and continuity with which the desired information is presented and by the fact that it provides a continous mental picture or model of the physical system being studied. The techniques described are applicable to "thin" beams in general and are capable of yielding static as well as dynamic information. They have, however, been evolved primarily to deal with problems in dynamics whose complexity makes them unsuitable for treatment by "classical" methods. A simple hypothesis concerning structural energy dissipation is discussed. It is shown to possess valuable practical advantages except where the detailed mechanism of structural energy loss is itself the subject of investigation. The essential correctness of the basic premises, and the practicability of realizing a useful synthetic "beam" have been demonstrated experimentally. Much further development remains to be completed however. The paper concludes with a review of certain directions in which progress is hoped for in the immediate future.

TABLE OF CONTENTS

¡LIST OF PRINCIPAL SYMBOLS

$B(x, t)$ Bending moment—a function of x and t

E Young's modulus

I Second moment of cross-sectional area

$EI(x, t)$ Mechanical rigidity, a function of x and t

L Total length of beam

M Total mass of beam

$Q(x, t)$ Shear force, a function of x and t

j Order of flexural vibration

$(k_j L)$ Constant associated with the jth mode of flexural vibration with given boundary conditions.

m_r Mass associated with the rth cell of a discrete-cell model, counting from the origin of co-ordinates (see Fig. 2)

p Laplace operator

t Time

x Distance parallel to x-axis (Fig. 1) measured from y-axis

$y(x, t)$ Distance parallel to y-axis (Fig. 1) measured from x-axis, a function of x and t

x Distance parallel to x-axis (Fig. 1) of the rth bounding section, measured from y-axis

x'_r Distance parallel to x-axis (Fig. 1) of the mass-centre of the rth cell

$\gamma(x, t)$ Mass per unit length measured parallel to x-axis, a function of x and t

$\psi(x, t)$ Inclination of beam-axis to x-axis, a function of x and t

ψ_r $\dfrac{(y_{r+1} - y_r)}{(x_{r+1} - x_r)}$

λ Coefficient of structural energy dissipation rate

1. Introduction

A variety of analytical and numerical methods exist for evaluating the behaviour of flexible beams and related structures. Generally speaking, however, they cannot be applied to any but relatively simple beam configurations without protracted and tedious labour. The dynamic data yielded by these methods is usually in the form of critical frequencies, mode shapes of vibration etc. which, although essential as a rule, are often subsidiary in practical importance to the overall behaviour of the beam under service conditions. This is the case, for example, when the "beam" is the fuselage of an aircraft for which an autopilot control is to be designed.

There are, too, important instances in which beam-like structures are complex not only in the sense that the mass per unit length and/or rigidity varies along the x-axis (Fig. 1); these properties may, in addition, change rapidly and profoundly with time. Both spatial and temporal variations may also take place in the surrounding medium and in the nature of the beam's interaction with that medium (due, for example, to variations in the beam's relative velocity as a whole). By way of illustration, consider, say, an aircraft, the greater part of whose take-off weight is made up of fuel. This fuel may, on occasion, be totally consumed or jettisoned in a matter of minutes during which

the aircraft may have climbed from the relatively dense atmosphere at sea level, gaining rapidly in speed the while, into the semi-vacuum prevailing at great heights. What may be termed "classical" methods of design calculation are difficult to apply in such circumstances, if indeed they are applicable at all, especially if the temporal variations are so rapid as to occasion serious doubts concerning the validity of "constant coefficient" solutions to the describing equations.

The electronic analogue computer is capable of providing an alternative approach of the kind for which such problems appear to call. An analogue machine of moderate capacity can be so arranged as to provide an electronic model or analogue of a flexible beam which will perform without significant delay, calculations of the type implicit in the previous paragraph.

The main desiderata of an electronic beam model are:

(a) There must be provision whereby the widest possible range of non-uniform beam configurations can be accommodated. This range should include, as far as possible, even the most complex and irregular long thin structures likely to be encountered in physical or engineering practice.

(b) It must provide in the form of electrical potentials or currents, continuous, virtually instantaneous and, within limits depending

on the problem, accurate information as to whichever aspects of the beam's behaviour are of interest.

(c) The electrical output data must be directly applicable not only to measuring and recording apparatus, but also to other components, simulated or real, which, together with the beam, form a model of any wider system being investigated or developed.

(d) It should be possible to observe the sequence of events at all "sensitive" points along the x-axis of the beam, simultaneously if need be. Such points might include those at which excitation is applied, or at which control surfaces, measuring instruments etc., are located.

(e) The model must function in response to the kind of input data which would normally be available such as mass and rigidity distributions within the beam, the nature of the environment and the nature of any externally applied forces.

(f) The model must truly be a model in the sense that it readily conveys to the experimenter a mental picture of the original, and is, therefore, a source of intuitive insight. A satisfactory model might, for this reason, be thought of primarily as a physical rather than a mathematical tool.

"Behaviour" as it is to be understood in (b) above, includes such quantitative information as critical frequencies, structural gains etc. where relevant. This kind of information is necessary in the present context as a means of enabling experiments whose object is the study or optimization of overall behaviour, to be economically planned and executed, and results to be intelligently interpreted.

The present paper is largely an account of progress made up to the date of submission, towards achieving the aims outlined above. The argument is invariably illustrated, where necessary, by reference to the "free-free" beam. This bias is due to the authors' preoccupation with airborne structures. The argument is nevertheless applicable to supported beams, which differ, apart from certain problems characteristic of the free-free case (which are discussed in the paper) only in respect of their boundary conditions. These can be taken

account of by using the methods described herein.

The account presented is necessarily very incomplete since much remains to be done before the model itself is sufficiently advanced for application to any but relatively simple problems. The authors would excuse themselves for presenting the paper at this stage. In doing so they are motivated by the hope that it will stimulate interest which, in its turn, may result in helpful criticism and advice being offered them.

2. Some Preliminary Assumptions

We take as our starting point the idealized "thin" beam for which the classical equations are well known. The rigidity and mass distributions along the x-axis (Fig. 1) will be assumed arbitrary in the first instance so that the principal restrictions implied are:

(a) Only flexural vibrations take place and these together with any motion executed by the beam regarded as a rigid body, are confined to the x-y plane (Fig. 1).

(b) The beam obeys Hooke's law.
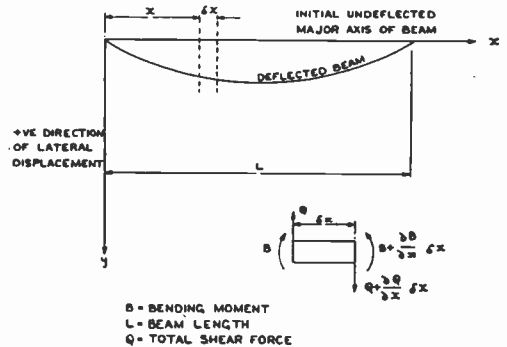
Fig. 1. Illustrating sign conventions adopted for forces, etc.
(Adapted from Timoshenko[3], Fig. 203.)

(c) The translatory motion of any part of the beam takes place wholly in the directions at right-angles to the x-axis of the undeflected beam (Fig. 1). By implication, all deflection angles are small.

(d) The beam does not buckle; the shape and area of any cross-section perpendicular to the x-axis are constant.

(e) The beam is "thin" in the sense that the

dimensions of any cross-section are small compared with length along the x-axis. This implies that the moment of inertia of any thin "slice" of the beam bounded by adjacent cross-sections, about any axis perpendicular to the x-axis, is negligible.

(f) All external forces acting on the beam are applied in directions at right-angles to the x-axis.

(g) The slope of the deflection curve depends only on the rotation of cross-sections, and does not include the effect of shear (Sect. 10.3.1).

We shall also make approximations in respect of elastic energy losses or dissipative effects due to distortion within the material of which the beam is constructed. These are more fully discussed in Section 3, in which the standard equation is extended to take account of them.

3. The Beam Equation with Extension to include Structural Energy Losses

By using the familiar static deflection properties of the flexible beam, and applying d'Alembert's principle[4 et al.] so as to embrace the dynamic situation, we obtain the standard form

$$\frac{\partial^2}{\partial x^2}\left[EI(x,t).\frac{\partial^2 y(x,t)}{\partial x^2}\right] + \gamma(x,t)\frac{\partial^2 y(x,t)}{\partial t^2} + P(x,t) = 0 \qquad \ldots\ldots\ldots(1)$$

where

E is Young's Modulus for the material of the beam $[ML^{-1}T^{-2}]$.

I is the second moment of cross-sectional area $[L^4]$.

$EI(x,t)$ is the "rigidity" factor, a function of x and t.

$\gamma(x,t)$ is the mass per unit length along the x-axis, a function of x and t $[ML^{-1}]$.

x is distance measured along the x-axis from the left-hand end of the beam in Fig. 1 which is taken as the origin co-ordinates.

$y(x,t)$ is translation of a point on the beam at x in a direction in the x-y plane, perpendicular to the x-axis.

t is time.

$P(x,t)$ is the lateral force per unit length—a function of x and t.

Equation (1) takes no account of elastic losses occurring within the substance of the beam consequent on bending. The complex nature of this phenomenon in, for example, impure metals such as carbon steel, would pose an analogue computing problem in its own right if considered in any detail. We have not felt called upon for our purposes to take any such close account of it. On the other hand, it is impossible to ignore its broader effects.

We have therefore sought a reasonably simple formula whereby the observed dynamic effects of structural energy dissipation could be given expression in an analogue computer model and, if possible, be conveniently handled analytically.

This has led us to assume that something in the nature of a viscous force acts along the length of all elemental longitudinal filaments of the beam which have an instantaneous time rate of change of length, and that this force is proportional to that rate of change. Equivalently (Appendix 2), it is proportional to the time rate of change of curvature at the point in question, or, considering a short length of beam, to the time rate of change of the angle between its bounding cross-sections which, in the undistorted state, would be parallel to each other.

This hypothesis commends itself in the first place in that it does not fly in the face of experimentally established facts (given sufficiently small amplitude and temperature ranges; but see Sect. 3.8). It is also attractive in that it leads to expressions which are convenient from the analytical standpoint, and is easy to translate into analogue computer settings. Thus, when a term expressing this hypothesis is added into the standard beam equation (Appendix 1), the resulting partial differential equation is

$$\gamma(x,t)\frac{\partial^2 y}{\partial t^2} + \frac{\partial^2}{\partial x^2}\left\{EI(x,t)\left[\frac{\partial^2 y}{\partial x^2} + \frac{\lambda\partial^3 y}{\partial t\partial x^2}\right]\right\} + P(x,t) = 0 \qquad \ldots\ldots\ldots(2)$$

in which λ is a disposable constant. If EI and γ are assumed constant and we set $P(x,t)=0$, and if in addition a solution of the form $y=\tau(t).\chi(x)$ is assumed then it is shown in Appendix 1 that equation (2) is separable into the two ordinary differential equations

$$\ddot{\tau} + \lambda(k_j L)^4\frac{EI}{ML^3}\dot{\tau} + (k_j L)^4\frac{EI}{ML^3}\tau = 0 \ldots\ldots(3)$$

where $M = \gamma L$

and

$$\frac{\partial^4 \chi}{\partial n^4} - \frac{(k_j L)^4}{L^4} \chi = 0 \qquad \ldots\ldots\ldots (4)$$

This form lends itself readily to physical interpretation and where necessary, to analytical solution.

Here $k_j L$ is independent both of x and t. It depends only on j which defines the mode of vibration considered ($j = 0, 1, 2, \ldots$ where $j = 0$ corresponds to rigid-body or collinear motion) and on the boundary conditions for the beam (Appendix 4).

Given these boundary conditions, solutions to eq. (4) exist for an infinite number of definite "eigenvalues" of $k_j L$. Substitution of these values into eq. (3) defines corresponding undamped natural or critical frequencies for the beam if a value is assigned to EI/ML^3.

If, in addition, a numerical value is assigned to λ, a rate of oscillatory decay is defined for all modes of vibration. It will appear in Section 6 that it is a straightforward matter to translate this decay rate into analogue computer settings. Thus we may either (a) ascribe values to λ and then observe the effect, or else we may, as a result of experiments carried out on an actual beam, (b) interpret the observed decay rate in a particular mode in terms of the coefficient of $\dot{\tau}$ in equation (3) which of course includes λ as a factor, and then set up the analogue computer accordingly.

By implication, having selected one value for λ, the decay rate is fixed for all modes throughout the spectrum. The effect is, as is shown in Appendix 1, to give a decay exponent which increases as the square of the frequency, and a damping factor (which defines oscillatory attenuation per cycle), which increases linearly with frequency. The extent to which this property accords with reality, even within very restricted ranges of conditions, seems at present to be conjectural. It is also difficult to foresee the importance of disagreement at this point between theory and experiment. One can at least assert, however, that a law of this kind will not, when built into our electronic model, tend to produce a spurious instability at the higher overtones.

A sufficiently clear distinction is not always made between energy dissipation due to internal causes, and that which is due to vibration in a viscous medium. In the former case, the losses are related to structural deformation rates; that is, to velocities of elemental components of the beam towards or away from their unstrained positions, and not relative to any fixed set of axes in space. In the latter case one is concerned with velocities relative to the external medium; this would mean, in still air or water for example, velocities relative to fixed space co-ordinates. The distinction is illustrated by a beam moving in a direction normal to its fore-and-aft axis, in which no mechanical distortion is present. In this case there is viscous damping due to movement through the medium, but no structural losses occur. These two sources of energy loss are taken account of by different sets of interconnections in the electronic model.

4. Derivation of Equations for Analogue Computer Treatment—No Structural Energy Losses

4.1. *General*

A suitable basic approach consists in adapting to our purposes the familiar method of numerical analysis used for evaluating partial differential equations of the type which concern us. The method consists in replacing the continuous range of one or more of the independent variables by a series of discrete, fixed levels or tabular points. In our case, the two independent variables being x and t, we realize the kind of model we require by treating x in this way. The partial differential equation is then replaced by a system of linear, second order, simultaneous ordinary differential equations in which the only independent variable is time t. Such equations can, as is well known, be handled by a standard electronic analogue computer.

Looked at physically, the method consists of dividing the beam notionally into, say, n discrete elements or cells distributed along the x-axis. Each cell is assumed to be self-rigid and homogeneous. We assume at this stage of the argument that these cells do not rotate individually. Their motion is then small, purely translational and in directions parallel to the y-axis. Each cell is acted upon solely by the shear forces at its bounding cross-sections, which likewise operate in directions parallel to the y-axis, together with any specified external lateral forces.

It is usual in solving partial differential equations by this numerical method, to space the tabular points at equal intervals in the range of interest. In our context this implies a restriction whereby our discrete cells must be of equal length along the x-axis, and have their centres of mass equally spaced. We are, of course, free to give individual masses different and time-varying values; we can also introduce stepwise variations in the rigidity along the x-axis. We can, therefore, reasonably expect to be able to deal with the type of problem outlined, for example, in Section 1.
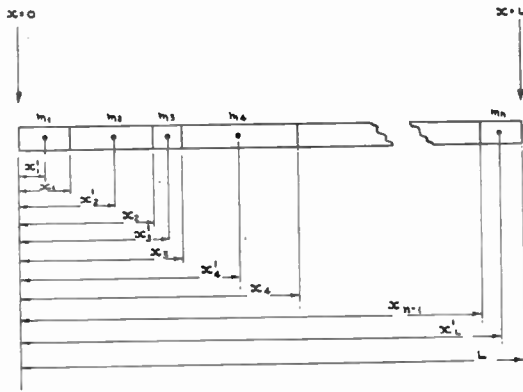
Fig. 2. Diagrammatic presentation of beam divided into cells or elements by normal sections.

However, if we accept this restriction, we may be compelled at times to take significantly more tabular points than would otherwise be necessary. As will appear from subsequent sections, this would undesirably increase the amount of computing equipment required and possibly, on that account, increase susceptibility to error. We are in the process of considering extensions to our technique with the object of removing the restriction in question. We shall assume for the purposes of this present section, notwithstanding the more general form of subdivision depicted in Fig. 2, that the restrictions outlined above are in force.

If we divide the beam into n cells as already defined, we have $(n-1)$ equally-spaced bounding cross-sections. In Fig. 2, the rth cell from the origin or left-hand end of the beam, has mass m_r centred at x'_r from the origin, and is bounded by cross-sections at x_r and x_{-1}

from the origin. If the displacement of m_r is y_r and if the shear force at $x=x_r$ is Q_r, we have, using the sign convention of Fig. 1,

$$m_r \ddot{y}_r = Q_r - Q_{r-1} \qquad \ldots\ldots(5)$$

From static considerations,

$$Q_r = - \frac{\partial}{\partial x} EI \left(\frac{\partial^2 y}{\partial x^2} \right) \bigg|_{x=x_r} \qquad \ldots\ldots(6)$$

From (5) and (6)

$$m_r \ddot{y}_r = \frac{\partial}{\partial x} \left[EI \frac{\partial^2 y}{\partial x^2} \right]_{x=x_r} - \frac{\partial}{\partial x} \left[EI \frac{\partial^2 y}{\partial x^2} \right]_{x=x_{r-1}} \qquad \ldots\ldots(7)$$

Thus far in our work we have made the assumption that between any two mass-centres situated at, say x'_{r-1} and x'_r (Fig. 2), the inclination of the beam to the x-axis is constant at a given instant in time, and is therefore represented by

$$\psi_r = \frac{y_r - y_{r-1}}{x'_r - x'_{r-1}} \qquad \ldots\ldots(8)$$

The shear-force Q_r at $x=x_r$ is then given by

$$-Q_r \rightarrow \left\{ EI_{(x_r<x<x_{r+1})} \frac{\dfrac{y_{r+2}-y_{r+1}}{x'_{r+2}-x'_{r+1}} - \dfrac{y_{r+1}-y_r}{x'_{r+1}-x'_r}}{(x_r-x_{r-1})\ (x'_{r+1}-x'_r)} \right.$$
$$\left. - EI_{(x_{r-1}<x<x_r)} \frac{\dfrac{y_{r+1}-y_r}{x'_{r+1}-x'_r} - \dfrac{y_r-y_{r-1}}{x'_r-x'_{r-1}}}{(x_{r-1}-x_{r-2})\ (x'_{r+1}-x'_r)} \right\} \qquad \ldots\ldots(9)$$

in which the symbol $\rightarrow$ denotes transition from the partial differential coefficient to the finite difference form. On replacing the right-hand side of equation (7) by that of eq. (9) with reversed sign, and subtracting from it the corresponding expression for Q_{r-1} we have an expression for the time-rate of change of transverse momentum of the rth cell in terms of its own displacement together with those of its two immediate neighbours to either side, and of certain predetermined lengths measured along the x-axis, which do not change in the course of the computation. To the extent, therefore, that our approximations are valid, we have here a complete theoretical basis for the construction of an electronic beam model of the required character.

4.2. The Uniform Beam

Our first check on the validity of the reasoning outlined in section 4.1 above consisted in applying it to the idealized beam defined

in Section 2, with the further restrictions that γ and EI are constant with respect both to x and t. Corresponding restrictions were imposed on the discrete-cell model of section 4.1 in that, for example, the cells were assumed all to be of equal mass. The describing equation for such a beam as well as those relating to its discrete-cell analogue have easily ascertained analytical solutions and are thus well suited to our immediate purpose.

Consequently we have:

$$m_1 = m_2 = \ldots \ldots = m \qquad \ldots\ldots\ldots(10)$$

and

$$x_1 = (x_2 - x_1) = \ldots = (x_r - x_{r-1}) = \ldots = (L - x_n) =$$
$$(x'_2 - x'_1) = \ldots = (x'_r - x'_{r-1}) = \ldots = (x'_n - x'_{n-1}) = x$$
$$\ldots\ldots\ldots(11)$$

In addition

$$x'_1 = (L - x'_n) = \tfrac{1}{2}x \qquad \ldots\ldots\ldots(12)$$

which expresses the assumption that the end cells of the discrete-cell model have their mass-centres at $\tfrac{1}{2}x$ from the nearer ends of the "beam."

If, then, we have n cells,

$$nm = M \qquad \ldots\ldots\ldots(13)$$

$$nx = L \qquad \ldots\ldots (14)$$

Making these substitutions in the finite-difference form of equation (7), we obtain

$$m\ddot{y}_r = -\frac{EI}{x^3}\left[y_{r+2} - 4y_{r+1} + 6y_r - 4y_{r-1} + y_{r-2} \right]$$
$$\ldots\ldots\ldots(15)$$

Equation (15) typifies the group of equations to be solved simultaneously by the analogue computer. If we postulate n cells, there are $(n-4)$ such equations since this form is not directly applicable to the two cells at each end of the beam. The motions of these, i.e. those

for which $r = 1, 2, (n-1)$ and n, are susceptible to the boundary conditions for, as eq. (15) shows, it is necessary in the general case to have information concerning two cells to either side of any one in question.

Modifications of eq. (15) appropriate to the cases $r = 1, 2 (n-1), n$, in a "free-free" beam are developed in Appendix 3.

For $r = 1$:

$$m\ddot{y}_1 = -\frac{EI}{x^3}\left[y_3 - 2y_2 + y_1 \right] \qquad \ldots\ldots\ldots(16)$$

For $r = 2$:

$$m\ddot{y}_2 = -\frac{EI}{x^3}\left[y_4 - 4y_3 + 5y_2 - 2y_1 \right]\ldots\ldots(17)$$

For $r = n - 1$:

$$m\ddot{y}_{n-1} = -\frac{EI}{x^3}\left[-2y_n + 5y_{n-1} - 4y_{n-2} + y_{n-3} \right]$$
$$\ldots\ldots\ldots(18)$$

For $r = n$:

$$m\ddot{y}_n = \frac{EI}{x^3}\left[y_n - 2y_{n-1} + y_{n-2} \right]\ldots\ldots(19)$$

A useful check may be applied to these equations. Thus if $y_{r-2}, y_{r-1}, y_r, y_{+1}, y_{+2}$ are in arithmetical progression, the rate of change of momentum $m_r\ddot{y}_r$ is zero. That is, as one would expect, collinear cells are in equilibrium in the absence of external forces.

4.3. Computer Set-up—Five-Cell Model to Represent Uniform Beam without Structural Energy Losses

Figure 3 shows in block form, a computer set up to perform the calculations specified above. It represents a sub-division of the beam into five equal lengths or cells. This is the least number capable of yielding a representative check since no smaller number could, for the reasons stated above, include a cell whose motion was described by the prototype equation (15).

Each rectangular block contains computing units which together perform a double integration with appropriate sign control. Since from eq. (15) through (19) the input quantities to each block represent the total transverse accelerating force (for a freely-moving beam) the output quantities
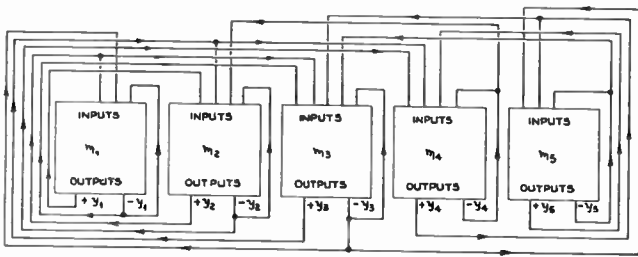

Fig. 3. Block schematic of computer set-up for a five-cell model.

represent the corresponding lateral displacements. This model displays the collinear motion of the beam together with the fundamental mode of flexural vibration and the first two overtones.

An important practical consideration when setting up the computer is the precision with which the input quantities to the blocks can be scaled. Equation (15) shows, for example, that excessive y_{r+2}, y_r, or y_{r-2} input amplitudes to the rth block correspond to excessive restoring force. Excessive y_{r+1} or y_{r-1} inputs, on the other hand, give rise to spurious divergence. With adequate care, we have not found this a serious difficulty.

In Section 5, we analyse this model and compare its behaviour with that of a uniform beam whose mass and dimensions it has been designed to reflect.

5. Comparative Analysis of the Five-Cell Model without Structural Energy Losses— (Free-Free Beam).

5.1. General

A discrete-element system is a sufficiently true synthesis of a loss-free beam if:

(a) The former has a sufficient number of critical frequencies for the purpose in hand, and these are substantially equal to the related frequencies for the original beam.

(b) The y-displacements of the mass centres at a given instant, plotted against x when the analogue is in sustained vibration at one critical frequency, lie sufficiently close to the plot of the corresponding normal function. (Criteria for accuracy here will be sensitive to particular requirements.)

(c) Transfer functions relating excitation at any relevant point on the x-axis, to responses

at the same or at other points on this axis, must agree to an acceptable extent, with those which characterize the original beam.

In testing the analogue from the standpoints (a), (b) and (c) above, certain restrictions in addition to the finite spectrum must be accepted. Firstly, it must be assumed that excitation is applied at one of the mass centres (although this is not, we consider, an absolute restriction and can probably be circumvented). Also y-displacements are directly registered only at those points; angular, or translational displacements at intermediate points must be inferred from these in the light of the postulated method of interpolation (in our case, linear). These restrictions can be an important factor in the choice of the masses associated with individual cells.

5.2. The Frequency Spectrum

If in eq. (15) to (19) we write

$$x = \frac{L}{n}; \quad \frac{EI}{mx^3} = \alpha^2 \qquad \ldots\ldots(20)$$

and finally, using Laplacian notation we put

$$\frac{p^2 m x^3}{EI} = \frac{p^2}{\alpha^2} = s \qquad \ldots\ldots\ldots(21)$$

then the system of equations for an unspecified number of discrete cells becomes:

$$
\begin{aligned}
& y_1(s+1) - 2y_2 + y_3 = 0 \\
& -2y_1 + y_2(s+5) - 4y_3 + y_4 = 0 \\
& y_1 - 4y_2 + y_3(s+6) - 4y_4 + y_5 = 0 \\
& \overline{y_{r-2} - 4y_{r-1} + y_r(s+6) - 4y_{r+1} + y_{r+2} = 0} \cdot \ldots(22) \\
& y_{n-1} - 4y_{n-3} + y_{n-2}(s+6) - 4y_{n-1} + y_n = 0 \\
& y_{n-3} - 4y_{n-2} + y_{n-1}(s+5) - 2v_n = 0 \\
& y_{n-2} - 2y_{n-1} + y_n(s+1) = 0
\end{aligned}
$$

leading to the following conditions for a nontrivial solution:

$$
\Delta = \begin{vmatrix}
s+1 & -2 & 1 & & & & & & \\
-2 & s+5 & -4 & 1 & & & & & \\
1 & -4 & s+6 & -4 & 1 & & & & \\
0 & 1 & -4 & s+6 & -4 & 1 & & & \\
& & & & 1 & -4 & s+6 & -4 & 1 & 0 \\
& & & & & 1 & -4 & s+6 & -4 & 1 \\
& & & & & & 1 & -4 & s+5 & -2 \\
& & & & & & & 1 & -2 & s+1
\end{vmatrix} = 0 \qquad \ldots\ldots\ldots(23)
$$

In particular if we divide the beam into five equal elements, the determinant becomes

$$\begin{vmatrix} s+1 & -2 & 1 & 0 & 0 \\ -2 & s+5 & -4 & 1 & 0 \\ 1 & -4 & s+6 & -4 & 1 \\ 0 & 1 & -4 & s+5 & -2 \\ 0 & 0 & 1 & -2 & s+1 \end{vmatrix} = 0 \quad \ldots\ldots(24)$$

Equation (24) reduces to

$$s^5 + 18s^4 + 75s^3 + 50s^2 = 0 \quad \ldots\ldots(25)$$

Two roots of eq. (25) are clearly zero, and a third is $s = -5$. The remaining roots therefore follow when the residual quadratic equation is solved. Equation (25) then becomes

$$s^2 (s+0\cdot8215)(s+5)(s+12\cdot1785) = 0 \quad \ldots(26)$$

Using eq. (20) and (21) to re-express eq. (26) in terms of the Laplace operator p

$$p^4 \left(p^2 + \frac{513\cdot4375\,EI}{ML^3} \right) \left(p^2 + \frac{3125\,EI}{ML^3} \right)$$
$$\left(p^2 + \frac{7611\cdot5625\,EI}{ML^3} \right) = 0 \quad \ldots\ldots(27)$$

which is the factorized form of the characteristic equation for a five-element model of a uniform beam, there being three non-zero critical frequencies.

The critical frequencies follow directly from (27). The zero roots of eq. (27) relate to the "rigid body" response of the uniform beam model.

Denoting the fundamental critical angular frequency by ω_1, and the successive overtones by ω_2, ω_3 etc. we have from (27)

$$\omega_1 = 22\cdot659 \sqrt{\frac{EI}{ML^3}} \qquad \text{rad/sec} \quad \ldots\ldots(28)$$

$$\omega_2 = 55\cdot97 \sqrt{\frac{EI}{ML^3}} \qquad \text{rad/sec} \quad \ldots\ldots(29)$$

$$\omega_3 = 87\cdot24 \sqrt{\frac{EI}{ML^3}} \qquad \text{rad/sec} \quad \ldots\ldots(30)$$

The corresponding figures given by analytical treatment of the uniform thin beam are

$$\omega_1 = 22\cdot3729 \sqrt{\frac{EI}{ML^3}} \qquad \text{rad/sec} \quad \ldots\ldots(31)$$

$$\omega_2 = 61\cdot62 \sqrt{\frac{EI}{ML^3}} \qquad \text{rad/sec} \quad \ldots\ldots(32)$$

$$\omega_3 = 120\cdot9120 \sqrt{\frac{EI}{ML^3}} \qquad \text{rad/sec} \quad \ldots\ldots(33)$$

On comparing (28) with (31) and so on, the percentage errors in frequency given by a five-element system are respectively

$$+ 1\cdot28 \text{ per cent. for } \omega_1 \qquad \ldots\ldots(34)$$

$$- 9\cdot17 \text{ per cent. for } \omega_2 \qquad \ldots\ldots(35)$$

$$- 27\cdot85 \text{ per cent. for } \omega_3 \qquad \ldots\ldots(36)$$

The error in fundamental frequency ω_1 is certainly within acceptable limits for a wide range of practical purposes.

However, it is natural to ask what improvement can be expected from increases in the number of sub-divisions of the beam, especially in the overtone frequencies. The form of the determinant is such that it can be broken down into determinants of much lower order before expanding. The results of increasing the number of beam cells from five to seven, say, or higher, can, therefore, be ascertained without undue labour.

In the seven-cell case, for example, where we have five non-zero critical frequencies, a distinctly better agreement is found to exist between the uniform and the discrete cell concepts. Table 1 shows collected values of $(k_jL)^2$ for the uniform beam, and the corresponding coefficients of $\sqrt{\dfrac{EI}{ML^3}}$ for the 5, 7 and 10-cell models. These, together with the tabulated percentage errors, give some notion of the kind of improvement to be expected from an increase in the number of discrete cells.

5.3. Normalized Frequency Response

The application of lateral forces to the beam model may be expressed by adding suitable terms to the right-hand side of the appropriate members of the equation system set out in eq. (22).

Confining ourselves to the five-cell model we have considered the effects of an exciting force $F(t)$ applied to the cell nearest the origin of co-ordinates $(x/L = 0\cdot1)$. The following normalized frequency responses are then obtained for the mass-centres at $x/L = 0\cdot1$, $0\cdot3$, ... $0\cdot9$:

$$y_1 = \frac{\Delta_1}{\Delta}$$
$$= \left\{ \frac{F(t)}{125M} \left[\frac{EI}{ML^3} \right] \right\} \left\{ \frac{s^3 + 17s^2 + 63s + 30}{\Delta/s} \right\}$$
$$\ldots\ldots(37)$$

Table 1

I		Uniform Beam	5-Cell Model		7-Cell Model		10-Cell Model	
		$(k_jL)^2$		% Error		% Error		% Error
1	Fundamental	22·3729	22·659	+ 1·28	22·5625	+ 0·847	22·45	+ 0·46
2	1st overtone	61·6225	55·97	− 9·17	59·29	− 3·47	60·68	− 1·51
3	2nd overtone	120·9120	87·24	− 27·85	106·09	− 12·31	114·4	− 5·59
4	3rd overtone	199·9396	—	—	151·29	− 24·3	177·7	− 11
5	4th overtone	298·5984	—	—	184·145	·· 38·3	244	− 18·16
6	5th overtone	417	—	—	—	—	305·4	− 26·65
7	6th overtone	554·7	—	—	—	—	356	− 35·9
8	7th overtone	712·5	—	—	—	—	388·7	− 45·6

where Δ is defined by the left-hand side of equation (25) or (26).

$$y_2 = \frac{\Delta_2}{\Delta}$$
$$= \left\{ \frac{F(t)}{125M} \left[\frac{EI}{ML^3} \right] \right\} \left\{ \frac{2(s^2 + 10s + 10)}{\Delta/s} \right\}$$
.........(38)

$$y_3 = \frac{\Delta_3}{\Delta}$$
$$= \left\{ \frac{F(t)}{125M} \left[\frac{EI}{ML^3} \right] \right\} \left\{ \frac{-(s^2 + 3s - 10)}{\Delta/s} \right\}$$
.........(39)

$$y_4 = \frac{\Delta_4}{\Delta} = \left\{ \frac{F(t)}{125M} \left[\frac{EI}{ML^3} \right] \right\} \left\{ \frac{-6s}{\Delta/s} \right\}$$
.........(40)

$$y_5 = \frac{\Delta_5}{\Delta} = \left\{ \frac{F(t)}{125M} \left[\frac{EI}{ML^3} \right] \right\} \left\{ \frac{s - 10}{\Delta/s} \right\}$$
.........(41)

Using the relationship

$$s = p^2/625 \left[\frac{EI}{ML^3} \right] \qquad ....(42)$$

and the definition of Δ, the frequency responses at the values of x/L specified above for the five-cell model are determined.

5.4. *The Response Functions*

Corresponding to (*b*) and (*c*) in Section 5.1 we compare the five-cell model with the true beam by considering firstly the absolute

responses (i.e. the transverse motions of the mass-centres) to a lateral excitation applied at a selected point on the *x*-axis of the synthetic beam. We then compare these responses with those of the true beam under similar excitation. In the case of the five-cell model, the points on the *x*-axis at which observations can conveniently be made are: $x/L = 0·1, 0·3, 0·5, 0·7$ and 0·9. Thus far the only excitation point considered is $x/L = 0·1$. We necessarily concentrate on the same values of x/L when studying the true beam.

Using eq. (42) to eliminate s from eq. (37), we have by some rearrangement of eq. (37), and dividing up into partial fractions

$$\bar{y}_1 = \frac{F(t)}{M} \left\{ \frac{3}{p^2} + \frac{1·4}{\left(p^2 + 513·4 \frac{EI}{ML^3} \right)} + \right.$$
$$\left. + \frac{0·5}{\left(p^2 + 3125 \frac{EI}{ML^3} \right)} + \frac{0·115}{\left(p^2 + 7611·6 \frac{EI}{ML^3} \right)} \right\}$$
.........(43)

Similar expressions for y_2, y_3, y_4, y_5 are obtained by applying the procedure outlined above for equation (37) successively to equations (38) through (41).

Table 2 below shows the values taken by the bracketed numerators in eq. (43) together with the corresponding numbers for y_2, y_3, y_4, y_5.

Each row of numbers in Table 2 would, if our model were perfect, yield a series of points lying exactly on a graphical plot to the same scale, of the corresponding normal function X.

From direct analysis of the uniform beam, if X_j (Appendix 4) is the normal function for translatory motion in the jth mode ($j = 0$, 1, 2, ...) the displacement corresponding to $\overline{y}_1$ in equation (43) is given by

$$\overline{y}_{(x/L = 0\cdot 1)} = \frac{F(t)}{M} \sum_{j=0}^{\infty} \frac{X_{j(x/L=0.1)} \cdot X_{j(x/L=0.1)}}{p^2 + (k_j L)^4 \dfrac{EI}{ML^3}} \quad \ldots\ldots(44)$$

$$\text{or } \overline{y}_{(x/L = 0\cdot 1)} = \frac{F(t)}{M} \left\{ \frac{2\cdot 92}{p^2} + \frac{1\cdot 14}{\left(p^2 + 501\,\dfrac{EI}{ML^3}\right)} + \frac{0\cdot 206}{\left(p^2 + 3796\,\dfrac{EI}{ML^3}\right)} + \frac{0\cdot 0108}{\left(p^2 + 14619\,\dfrac{EI}{ML^3}\right) + \ldots} \right\}$$

$$\ldots\ldots(45)$$

Values of X_j are tabulated in Appendix D from from which $\overline{y}$ for other values of x/L can be directly calculated, using equation (53) below.

Table 3 shows the values taken by the bracketed numerators in equation (45) together

with the corresponding numbers of $x/L = 0\cdot 3$, $0\cdot 5$, $0\cdot 7$, $0\cdot 9$. They are given by the products:

$$X_{j(x/L = 0.1)} \cdot X_{j(x/L = 0.1, \, 0.3 \ldots 0.9)} \quad \ldots\ldots(46)$$

The numerical values of X_j are taken as before, from Appendix 4. The row corresponding to $j = 0$ follows directly from the application of rigid-body dynamics to the undistorted beam.

Strictly, in order to compare term for term, the responses expressed by equations such as (43) and (45) it is necessary to take account of their denominators. More especially, if we wish to compare the resonant responses at the critical frequencies in each case, it is useful to postulate linear damping which introduces into the denominator a term in the operator p (excluding the case $j = 0$) and at resonance in the jth mode, the denominator of the relevant term takes the form

$$2u_j \, \omega^2_j \qquad \ldots\ldots(47)$$

where u and ω have their customary meanings. Nevertheless, we can gain a useful preliminary impression by directly comparing Tables 2 and 3, insofar as we compare corresponding modes while disregarding frequency errors.

Tables 2 and 3 indicate fair agreement in the rigid-body and fundamental flexural modes. In

Table 2

Discrete Cell Synthesis (Excitation at $x/L = 0\cdot 1$)

Mode	x/L 0·1	0·3	0·5	0·7	0·9
Rigid Body	3	2	1	0	− 1
Fundamental	1·4	− 0·63	− 1·55	− 0·62	1·35
1st Overtone	0·5	− 1	0·003	0·98	− 0·45
2nd Overtone	0·115	− 0·36	0·103	− 0·36	0·1

Table 3

Uniform Beam (Excitation at $x/L = 0\cdot 1$)

Values of $X_{j(x/L = 0.1)} . X_{j(x/L = 0.1, \, 0.3, \, \ldots \, 0.9)}$

j	Mode	x/L 0·1	0·3	0·5	0·7	0·9	
0	Rigid Body	2·92	1·96	1·003	0·034	− 0·9178	(zero at $x/L =$
1	Fundamental	1·14	− 0·583	− 1·305	− 0·584	1·15	0·708)
2	1st Overtone	0·206	− 0·601	0·002	0·601	− 0·2075	
3	2nd Overtone	0·0108	0·0826	− 0·148	0·083	0·0144	

the case of the first overtone discrepancies of 50 per cent. or more are common; in the case of the second overtone it is not easy at first sight to discover any useful degree of correlation at all. Moreover the discrepancies are, generally speaking, in such a direction that they would be worsened by taking account of frequency errors (Table 1 and the previous paragraph).

The immediate cause of these large discrepancies is to be found in the choice of excitation point $(x/L = 0.1)$. Equations (43) (45) relate to responses at the point to which the excitation is applied. Reference to the numerator terms to the right of the summation sign in eq. (44) indicates that the numerators of successive terms inside the bracket on the right-hand side of eq. (45) are, therefore, in fact $(X_j)^2_{j(=1, 2 \ldots)(x/L=0.1)}$. It is therefore legitimate to compare the square roots of these with the square roots of the bracketed numerators in eq. (43) for successive values of j. The "equivalent" $X_{j(x/L=0.1)}$ in eq. (43) are:

$+1.732$; $+1.183$; $+0.707$ and $+0.339$

the signs of the roots being inferred from responses at other values of x/L. The comparable true values of X_j from Appendix 4 and, for the case $j = 0$, from elementary rigid-body dynamics are

$+1.7088$; $+1.0743$; $+0.454$ and -0.104.

The maxima of X_j, which occur at $x/L = 0$ are invariably equal to two. The discrepancies in "equivalent" X_j at $x/L = 0.1$ expressed as percentages of two are respectively

1.15%; 5.45%; 12.65% and 22.15%.

These are by no means as large, at any rate for the overtones, as the differences between Tables 2 and 3 for these modes might lead one to expect. The large tabulated discrepancies are thus clearly related to the large percentage differences between true and "equivalent" values for X_j for the overtones in the vicinity of $x/L = 0.1$; that is, to the fact that excitation occurs at a point which is close to a node for the two overtones. In the case of the first overtone the tabulated discrepancies would almost vanish if the value of x/L were changed by something less than 2 per cent. The corresponding required change in x/L to correct the second overtone is about $2\frac{1}{4}$ per cent.

This sensitiveness of response to small changes in the point of application of the transverse force (and the symmetry of eq. (44) shows that similar remarks apply to points at which responses are measured) is potentially of great significance in the sphere of practical design. Our most immediately important inference is, however, that a limited body of data which does not include a sufficiently representative variety of excitation points for example, or in which such points are not carefully chosen, can completely mislead one as to the possibilities and/or limitations of a given beam model.

One would be on safer ground if one could so choose an excitation point that X_j approximated to its positive maximum for all relevant values of j; that is, x/L sufficiently close to zero. In the form of beam model considered thus far, it is not convenient to apply excitation at points other than discrete mass-centres. Given a uniform distribution of mass-centres therefore, it seems likely that the effect of increasing the number of sub-divisions will only be to transpose the difficulty to higher order modes. This problem, together with considerations of frequency error as displayed in Table 1, have suggested to us that an empirical law should be observed, to the effect that if n modes are of interest, then the number of notional sub-divisions of the beam should be not less than $(2n + 3)$.

In view of the foregoing there can be no pretence that the information derived from a comparison between Tables 2 and 3 is in any sense representative. It is regarded rather as a preliminary test which indicates how further experiments may most usefully be designed. It is perhaps worth noting that the foregoing discussion of lateral translation in vibrating beam applies with equal force if suitably adapted in detail, to angular motion.

6. Introduction of Structural Dissipation into the Beam Model

Figure 4 shows in detail the circuits contained by the rectangles in Fig. 3, marked $m_1, \ldots m_5$. Additionally, however, the resistance R3 is introduced in Fig. 4. In Fig. 3, the rectangles depicting the cells which comprise the beam model, are shown as yielding outputs $\pm y_1, \ldots \pm y_5$ i.e. the lateral displacements with a choice

162

of sign. By writing down the describing equations of the circuit of Fig. 4 it is easily shown that, as a result of introducing R3 the available outputs from the rth cell take the form

$$\pm y_r \left[\frac{1}{T_2} + \frac{R_3}{R_2} p \right]$$ in which $T_2 = C_2 R_2$. That is

to say we have both the lateral displacements and their time-derivatives. These are independently variable by varying C_2 and R_3 respectively. The complex quantity is moreover available in both signs. It follows that we can give effect to the structural dissipation hypothesis (section 3) by choosing R_3.

From Fig. 4 we have in Laplacian notation:

$$p^2 y_r = -\left(\frac{1}{T_2} + \frac{R_3}{R_2} p \right) \left\{ \frac{y_{r-2}}{C_1 R_1} - \frac{y_{r-1}}{C_1 R_4} + \right.$$
$$\left. + \frac{y_r}{C_1 R_5} - \frac{y_{r+1}}{C_1 R_6} + \frac{y_{r+2}}{C_1 R_7} \right\} \quad \ldots\ldots(48)$$

From Appendix 1 we have, adopting similar notation:

$$p^2 y_r = -\frac{1}{\gamma(x, t)} \cdot \frac{\partial^2}{\partial x^2} \left\{ EI(x, t) \frac{\partial^2 y}{\partial x^2} [1 + \lambda p] \right\} \ldots(49)$$

or for the uniform beam

$$p^2 y_r = -\frac{EI}{\gamma} \frac{\partial^4 y}{\partial x^4} (1 + \lambda p) \quad \ldots\ldots(50)$$

Alternatively, by adapting eq. (15) which is applicable to the general cell of the discrete-cell model ($r \neq 1, 2, (n-1), n$),

$$p^2 y_r = -\frac{625\, EI}{ML^3} (1 + \lambda p) \left[y_{r-2} - 4_{r-1} + 6y_r - 4y_{r+1} + y_{r+2} \right] \quad \ldots\ldots(51)$$

Equating coefficients in (48) and (51):

$$\frac{1}{T_2 C_1 R_1} = \frac{1}{T_2 C_1 R_7} = \frac{625\, EI}{ML^3} \quad \Big| \qquad \frac{R_3}{R_2 C_1 R_1} = \frac{R_3}{R_2 C_1 R_7} = \lambda \quad \Big|$$

$$\frac{1}{T_2 C_1 R_4} = \frac{1}{T_2 C_1 R_6} = \frac{4.625\, EI}{ML^3} \quad \cdot \qquad \frac{R_3}{R_2 C_1 R_4} = \frac{R_3}{R_2 C_1 R_6} = 4\lambda \quad \ldots\ldots(52)$$

$$\frac{1}{T_2 C_1 R_5} = \frac{6.625\, EI}{ML^3} \Big| \qquad\qquad \frac{R_3}{R_2 C_1 R_5} = 6\lambda \Big|$$

We thus have the necessary relationships for fixing R_3 in order to reflect a specified value of λ.

Reference to Appendix 3 or to Section 4 above shows how the subject matter of Section 6 can be applied to the two cells at each end of the beam.
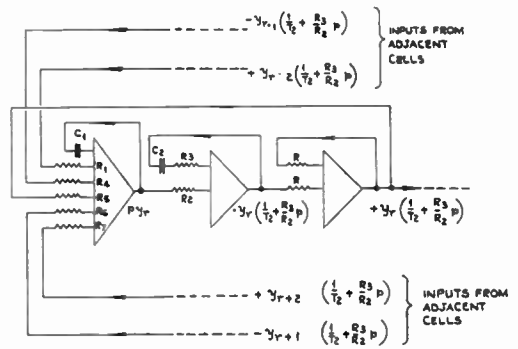

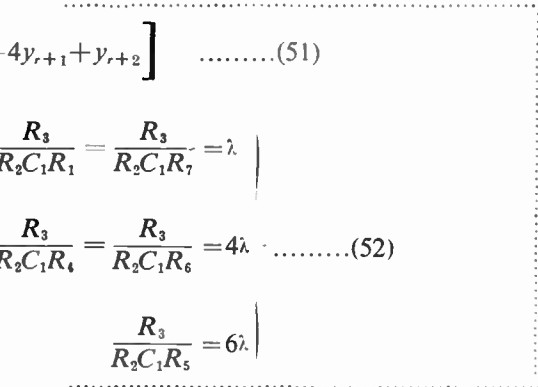Fig. 4. Detailed schematic circuit of the general cell in a discrete-cell model.

7. Practical Difficulties Associated with Free-Free Beams

The "free-free" beam category, that is to say the case for which the boundary conditions are:

$$\frac{\partial^2 y}{\partial x^2}_{(x=0)} = \frac{\partial^3 y}{\partial x^3}_{(x=0)} = 0$$

and

$$\frac{\partial^2 y}{\partial x^2}_{(x=L)} = \frac{\partial^3 y}{\partial x^3}_{(x=L)} = 0$$

includes such structures as ships' hulls, and aircraft fuselages and is therefore of considerable practical interest.

Beams of this type give rise to peculiar problems in electronic synthesis, especially if the object of that synthesis is to "highlight" vibrational effects. These problems reflect the fact that the "free-free" beam, unlike supported,

hinged or encastré beams, for example, is at no point fixed in space.

The motion in space of an uncontrolled free-free beam acted upon by external forces will, because it is unattached, generally include large rotational and translational displacements of the beam as a whole. In practically foreseeable circumstances these displacements would quickly: (a) invalidate any small-angle assumptions implicit in the analysis and (b) become so large as to make it difficult if not impossible for an external observer to distinguish vibrational effects at all. On the basis of this reasoning, we could be free of the difficulty only if we could perfectly protect the beam against all extraneous disturbances such as, say, gusts of wind, or else study it only in association with an effective control system which did not itself obscure vibrational effects.

In developing our model we have expressed the motion of the beam with respect to co-ordinates fixed in space. This is a natural consequence of taking the classical beam treatment as our starting point. Our analogue computer model as discussed thus far, therefore, makes no distinction between vibratory motions and rigid-body motions. To the extent, therefore, that we cannot shield such a model from unwanted excitation, the real-life problem just described is reflected in the electronic analogue, and must of necessity be dealt with.

If we could eliminate from the analogue computer all influences comparable with, say, the wind gusts etc., which would set a real free-free beam in translational and/or rotational motion as a whole, no practical difficulties would arise. In point of fact, random effects such as those of sudden supply voltage fluctuations, interference, amplifier drift etc., do produce comparable effects in the electronic model. As a result it has been found that when a free-free beam model is set up, even on a high-grade analogue computer, it tends to drift within a matter of seconds, to such an extent as to obscure the vibrational displacements which are the main objects of interest.

One superficially attractive way of dealing with this difficulty is to set up a separate, additional model which yields the collinear response only. On subtracting this from the response of the model proper, it might be argued, one is left with the desired information,

unobscured by the large unwanted drift component. It is, however, the very largeness of the unwanted component that makes this approach inappropriate; for what is then being attempted in effect, is to derive accurately a difference between two responses, which is, in general, small compared with the magnitudes of the responses themselves. This is notoriously a technique which is highly susceptible to error.

We have turned to an alternative and considerably more rewarding method of dealing with the difficulty. This consists essentially of re-expressing the basic beam equations in terms of angular displacements rather than linear displacements with respect to the x-axis. Lateral accelerations still appear in the formulation, but not displacements, so that only angular drift remains to be dealt with. This is a comparatively simple matter, the method being to apply a suitable heading-angle control system to the new model, which stabilizes the orientation of the fore-and-aft axis. The rigid-body translational and/or rotational motion of the beam in the x-y plane can then be set up separately in accordance with well established principles, the inputs and the output responses of the two models being combined as necessary, for connection to any external parts of the overall system or to, say, control surface actuators if the "beam" is a ship or an aircraft.

In Section 8, the derivation of this orientation model is outlined. It will also appear that the attachment of a simple control system can be turned to advantage when exploring the frequency spectrum of the model.

8. The "Angle" Model

It has been intimated in earlier sections that certain advantages are to be gained especially when dealing with "free-free" beams in isolation, by producing a model in which translational displacements do not appear explicitly. Unfortunately, it is not possible at this stage, owing to lack of time, to present a detailed description of such a model, although this is the type which we actually have in use. It must suffice here to say that by replacing $\partial y/\partial x$ in the describing equations by a symbol $\psi(x, t)$ to represent the orientation of the body at any point x on the x-axis, the equations take a form in which the lateral displacements only appear in the sense that $\ddot{y}$ remains explicitly.

Only the angular drift of the beam axis, therefore, remains to be corrected. This is achieved by taking the heading angle of the beam-axis, and its time-derivative, at some suitable point on that axis and generating additional forcing functions proportional thereto. The essential requirements are that the measured values of $\psi(x, t)$ and $\dot{\psi}(x, t)$ be fed back in such a way as to ensure stability, and not to obscure any behavioural features which are of interest.

Such a control system can be turned to advantage in measuring the critical frequencies of the beam. For example, suppose that no structural damping is assumed, and a forcing function in the form of a sinusoid is applied. Then those frequencies at which the beam oscillates, the error signal being zero (i.e. the difference between the applied forcing function and the fed back components $\psi_{(r)}$ and $\psi_{(z)}$, which is the nett excitation applied to the beam), are clearly the desired critical frequencies.

In work on the "angular" beam it has been found convenient to define and use a corresponding form of normal function. Generalizing eq. (44) we express the lateral deflection y of the uniform beam due to a force $F(t)$ applied at $x/L = c$ say, by,

$$\bar{y}(x, t) = \frac{F(t)}{M} \sum_{j=0}^{\infty} \frac{X_{j(x/L-c)} \cdot X_{j(x)}}{p^2 + (k_j L)^4 \left[\dfrac{EI}{ML^3} \right]} \quad .....(53)$$

where c is the fraction of the total beam length from the origin, to the point of excitation. We define a new dimensionless normal function $v_j(x)$ such that

$$\bar{\psi}(x, t) = \frac{F(t)}{M} \sum_{j=0}^{\infty} \frac{X_{j(x/L=c)} \cdot \left[\dfrac{k_j L}{L} \right] v_j(x)}{p^2 + (k_j L)^4 \left[\dfrac{EI}{ML^3} \right]} \quad .....(54)$$

v_j is in effect the normalized x-derivative of X_j to which it is therefore related as:

$$v_j = \frac{L}{k_j L} \cdot \frac{dX_j}{dx} \qquad ....(55)$$
(see Appendix 4)

To the extent that "free-free" beams are relevant in the fields of aerodynamics and hydrodynamics, they are likely in any case to be associated with control systems which inhibit random drifts. Therefore, even if it is difficult to study such a beam in isolation one can at least study it in association with its control system.

9. Experimental Checks

Enough experimental work has been carried out, using an electronic five-cell model of a uniform beam to show that our basic premises are (a) correct and (b) likely to remain so when eventually the method is extended to cases not susceptible of analysis.

In the case of the uniform beam it is, of course, possible to make generally valid checks. These consist of (a) comparing a given discrete-cell model with the original beam on paper, and (b) comparing an analysis of an n-discrete-cell model with the behaviour of the model as set up on the analogue computer. Check (a), with which Section 5 above is largely concerned, indicates the validity or otherwise of the process of dividing the independent space variable x into a limited number of discrete levels. Check (b) indicates the extent to which the discrete model is usefully realizable with existing computer equipment. The experimental results presented below, although in our view they establish the soundness of our general approach, are, at this stage, incomplete. To this extent the authors would ask the reader to bear with them.

Table 4 shows the angular frequencies relevant to a five-cell model. It shows a highly satisfactory measure of agreement in the case of the fundamental mode. In the cases of the first and second overtones, the theoretical and experimentally determined frequencies for the discrete-cell model are in excellent agreement.

We are, at the time of writing, investigating the behaviour of an electronic beam model which includes circuits to represent structural energy dissipation, the underlying theory being that set forth in Section 3 and Appendix 1.

The model in question is the "angle" model of Section 8 at a transitional phase in its development. It is still in a form corresponding to five-mass-centres at $x/L = 0.1$, 0.3, ... 0.9 respectively, but the explicit quantity measured is ψ_r (eq. 8) at the bounding sections of the five cells, i.e. at $x/L = 0.2$, 0.4, 0.6, 0.8.

We cannot, unfortunately, draw any conclusive inferences from our experiments for the

Table 4

Undamped Critical Frequencies (rad/sec)

	Fundamental	1st Overtone	2nd Overtone
Direct Analysis of the Uniform Beam	52·884	145·65	285·8
Analytical Values for 5-cell Model	52·8	132	206
Experimental Values for 5-cell Model	53·4	131	204

Table 5

Moduli of Angular Responses at Resonance, to Lateral Force $F(t)$ applied at $x/L = 0·1$

$\lambda = 0·001$

j	x/L 0·2 $\left|\dfrac{\psi}{F(t)}\right|$	0·4 $\left|\dfrac{\psi}{F(t)}\right|$	0·6 $\left|\dfrac{\psi}{F(t)}\right|$	0·8 (radians per lb.) $\left|\dfrac{\psi}{F(t)}\right|$
1	5×10^{-8}	$2·6 \times 10^{-8}$	$2·5 \times 10^{-8}$	$4·8 \times 10^{-8}$
2	$6·4 \times 10^{-9}$	$4·1 \times 10^{-9}$	$3·9 \times 10^{-9}$	$5·9 \times 10^{-9}$
3	$2·01 \times 10^{-9}$	$1·39 \times 10^{-9}$	$1·19 \times 10^{-9}$	$6·3 \times 10^{-10}$

moment because the calculated beam responses are not yet completely available for comparison. However, we give in Table 5 a sample set of results obtained from the analogue computer model, together with such comments as may usefully be made at this stage.

The experiment consisted of applying a sinusoidal excitation to represent a force $F(t)$ at the point $x/L = 0·1$ and, for a specified value of λ, in recording the modulus of $\psi/F(t)$ at $x/L = 0·2$, 0·4 etc. at the three critical frequencies corresponding to $j = 1$, 2, 3.

We draw the conclusion from these experiments that oscillatory decay does, in fact, occur. Additionally it was noticed that the rates of oscillatory decay increased with the mode order j, as the theory requires (Appendix 1).

Experience and theory relating to the loss-free beam lead one to expect, from considerations of symmetry

$$\left|\frac{\psi}{F(t)}\right|_{(x/L=0·2)} = \left|\frac{\psi}{F(t)}\right|_{(x/L=0·8)}$$

$$\left|\frac{\psi}{F(t)}\right|_{(x/L=0·4)} = \left|\frac{\psi}{F(t)}\right|_{(x/L=0·6)}$$

Table 5 shows a growing deviation from this state of affairs as j increases.

When however a damped beam is excited near to one end, one would expect from a consideration of the normal functions that attenuation of this kind would manifest itself towards the other end of the beams. We are not, of course, in a position, as yet, to satisfy ourselves that these experimental results are quantitatively in agreement with theoretical prediction.

We now have a ten-cell "angular" model in operation but it is impossible at this early stage to make any useful comment on its behaviour.

10. Some Outstanding Questions

10.1. General

Several lines of investigation need to be followed. These fall, broadly speaking into two categories. The first embraces refinements in techniques, designed to endow our model with all the realism and flexibility compatible with reasonable size. The second category reflects our need to shed as many of our simplifying assumption as possible in order to extend the range of reality to which this powerful technique can be applied.

10.2. *Refinement in Techniques*

Under this heading the most immediate needs are to determine the number of discrete cells into which a beam may most profitably be divided, and to enable ourselves to choose cells of arbitrary length along the x-axis. In regard to the former, two mutually opposed factors come into play which, between them, go far to restrict the range of choice. The importance of the latter is indicated in Section 4.

Let us suppose that we have a computer which is completely free from error. If, in addition, there are no restrictions on space or quantity of equipment then, clearly, the greater the number of elements or cells into which we divide a beam for our purpose, and the shorter their length measured along the x-axis, the more closely shall we approximate to the true solution of equations such as (1) and (2). If, as will generally be the case, space and technical resources are restricted, we fall back on an empirical law, suggested by our experimental results to the effect: "If n nodes (including collinear response) are of interest, use not less than $(2n+3)$ cells."

In any real analogue computer, each explicitly yielded quantity will include a component of error. Moreover, the process of solving difference equations as an alternative to dealing with differential coefficients consists substantially of determining differences between quantities (in our case the lateral displacements of neighbouring cells) which are likely to be very similar in magnitude. A determination of the curvature at such a point as $x=x_r$ for for example consists essentially of performing the two subtractions $(y_r - y_{r-1})$ and $(y_{r+1} - y_r)$, followed by the subtraction of one of these results from the other.

But the greater the number of cells, i.e. the more closely they are spaced, the more difficult it must become to distinguish y_{r-1} from y_r or y_r from y_{r-1}. Given a computer which is not wholly free from error, it is clear then that a point can be reached in the process of increasing the number of cells, at which the required differences $(y_{r+1} - y_r)$ etc. are substantially overlaid by computer errors. At this point the computer is rapidly becoming useless. Clearly some smaller number of cells would give more satisfactory answers, even though the number

of modes expressed is smaller.

For a given computer then, there must be an optimum number of cells. It is the order of this number, with representative equipment, that we need to determine. Experience suggests that ten is not excessive if the equipment is available. Five seems a very bare minimum.

Another technique problem which engages our attention is that of interpolation. Throughout this paper we have based ourselves on simple linear interpolation, and have assumed, further, that the inclination of the beam to the left of the first mass centre is the same as that between the first and second. An analogous assumption is made regarding the right-hand end of the beam.

It is well known that more sophisticated methods are available, e.g. polynomial curve fitting, for deriving smooth curves to pass through a finite number of points. In one recent paper[12], for example, specific proposals are made and analysed, which should receive our close attention. It would appear, however, that the methods proposed there imply the subjection of any given cell to the direct influence, not only of its two neighbours to either side, but of additional, remoter neighbours. Also, more equipment seems to be needed. We may well have to ask ourselves at some stage whether additional equipment is more profitably used in this way, or in increasing the number of cells under conditions of linear interpolation.

Other technique problems which occur to us are: are we taking account of boundary conditions in the best possible way, and should we take account of rotations of individual cells due to the applied couples? As to the first question, we have, thus far, seen no reason to hope for improvement; as to the second we are not, as yet, in a position to make any useful comment. It may be noticed, however, that the disagreement between eq. (43) and (45) in respect of rigid-body response to excitation, is due to the fact that the moment of inertia of the five-discrete-cell model in the x-y plane about the centre of gravity is less than that of the uniform beam. In this model, one of the masses is, of course, concentrated at the centre of gravity.

10.3. *Extending the Range of Usefulness*

10.3.1. Inherent properties of the beam

Examples occur in which it is not justifiable to regard the beam as "thin." If the beam cross-section has sufficiently large dimensions, it may be that any short length has moments of inertia about axes perpendicular to the x-axis, which exert a significant effect on the behaviour of the beam.

In Timoshenko,[3] for example, the standard beam equation is extended to take account of this possibility.

A further "second order" effect, which may sometimes be significant, is the beam deflection contributed by shear. In general it is assumed that the beam develops curvature and that this accounts substantially for the mode shapes. However, associated with the effect of shear forces, adjacent thin sections of a beam may be thought of as sliding relative to one another without any change in orientation of their planes being implied. Clearly this is an additional factor in determining the deflection of the beams.

10.3.2. External forces acting on the beam

We are here concerned with the effects of a viscous external medium on the beam's behaviour. If the position of the beam in space remains fixed, and the deflections are small, the effects of a static viscous medium may be regarded simply as a linear function of the transverse velocity $\dot{y}$ of any point on the beam. In the "angular" model of Section 7 the transverse acceleration $\ddot{y}$ for each cell appears explicitly. It is, therefore, merely necessary to integrate this quantity once with respect to time—a standard analogue process, and to feed the integrator output, with appropriate polarity, back to the input to the cell in question as an additional restoring force.

If the beam acquires velocity as a whole through the medium, say in a direction roughly parallel to the x-axis as in an aircraft, the situation is a little less simple. We now have to consider forces proportional to the incidence angle (i.e. the angle between the fore-and-aft axis and the direction of flight) and perhaps its time-derivative. The former will be in the nature of a restoring force. In addition there will be forces proportional to the rate of change of orientation of the fore-and-aft axis—a

damping force—and perhaps its time derivative. It will also be necessary to consider the moments produced by these forces. For the rigid-body mode, this involves a knowledge of the virtual point of application or centre of pressure of these forces and, more especially, the length and sign of the distance between this point and the centre of gravity of the beam as a whole. Alternatively, it will be necessary to know for each cell of which the model is built up, the appropriate constant by which these components of motion must be multiplied to give the local value of the force or moment in question. These will depend on such factors as the velocity of the beam through the medium, the density of the medium, and the local shape of the beam.

We need to consider how best to deal with the non-uniform beam. In principle there is no difficulty in arranging for the model to reflect changes or non-uniformities with respect either to x or t, in mass or rigidity.

However, if we consider a given beam-like structure whose mass-distribution, for example, is non-uniform, then, if we have solved the second problem mentioned in Section 10.2, there is, in general, a multitude of choices available as to how we shall distribute our discrete cell masses. In many cases, doubtless, one would wish to arrange the cells in such a way as to "highlight" any critical or important features of the corresponding mode shape. One could not always expect, however, to have enough prior knowledge to make a good arrangement from this point of view. As far as can be seen at this stage, there is no alternative to an initial choice based on intuition or experience. One might hope, as a result of one or two modifications of such an initial layout, to arrive at a disposition which met the essential requirements of the problem.

We may also need to investigate, insofar as we concern ourselves with powered craft, the effects of end-thrusts.

Finally, we are concerned with the restriction implicit in Section 5.1 to the effect that transverse forces must be applied to the discrete-cell model at mass centres. One potentially important disadvantage arising from this restriction is discussed in Section 5.4. It now seems to us that by treating laterally

applied external forces as discontinuities in shear force distribution along the beam, this difficulty will be circumvented. However, we have not thus far considered the point in any detail.

11. Conclusions

It is perfectly practicable to set up on a conventional electronic analogue computer of moderate size (say twenty amplifiers or thereabouts) a synthetic flexible "beam" in which account is taken of the broad, linearized effects of structural energy losses due to distortion, and which satisfies the requirements listed in Section 1.

The model is capable of rendering superfluous a number of laborious and time-consuming calculations commonly associated with the evaluation of critical frequencies etc. of all but the simplest beam configurations. It also conveys a mental picture of the beam's actual behaviour in a variety of circumstances.

The output of the model is characterized by $n - 1$ modes (including the zero-frequency or collinear response) when it is based on a notional division of the beam's x-axis into n equal lengths. The accuracy with which the true beam behaviour is reflected falls off as the mode order in question approaches the $(n - 1)$th. This fact has suggested an empirical rule, whereby if n modes are of interest, the beam should be sub-divided into not less than $(2n + 3)$ parts.

In dealing with "free-free" beams it is desirable wherever possible, so to arrange matters that only changes in orientation, as distinct from translational movement, appear explicitly. This goes far to mitigate the problems arising from the natural tendency of a "free-free" beam to drift in space under the influence of random perturbations or small computer maladjustments. Such an "angular" model has proved to be very tractable in use. It necessarily displays, in addition to angular information, the side-slip acceleration. This does not give rise to translational drift and is potentially an advantage in some control problems.

The linearized concept of structural energy losses introduced here, which is based on an assumed direct relationship between such losses and local time-rates of change or curvature, is capable of straightforward expression in computer terms. It has the further advantage of endowing the describing partial differential equations of uniform beams with a form which makes for ready analytical solution. It takes no direct account of the highly complex detailed factors known to contribute to the energy losses in question, and is therefore unsuitable for use where these factors are themselves under investigation.

Our energy-loss hypothesis is also less adaptable than could be desired. This shortcoming consists in the fact that, once the rate of oscillatory decay for one mode of vibration is fixed, the decay rates in all other vibratory modes are automatically fixed. Should this disadvantage prove at any stage to be a serious one, it is proposed to combine the use of the model with an alternative technique, not discussed in this paper. This alternative has none of the important labour-saving advantages of the beam syntheses which are the subject of this paper. On the other hand it enables decay rates to be set up completely independently for each vibratory mode.

A considerable programme of development remains to be completed before any but simple tasks can be assigned to our model. It seems clear, however, that there is no major obstacle likely to prevent it from emerging as an efficient and flexible research tool.

12. Acknowledgements

13. References and Bibliography

1. D. R. Hartree, "Calculating Instruments and Machines." (Cambridge University Press, 1956.)
2. R. H. Howe and V. S. Haneman, "The solution of partial differential equations by difference methods using the electronic differential analyzer," *Proc. Inst. Radio Engrs*, **41**, pp. 1497-1508, October 1953.
3. S. Timoshenko and D. H. Young, "Vibration Problems in Engineering," 3rd Edition. (D. van Nostrand, New York, 1955.)

4. E. J. Routh, "Rigid Dynamics," pp. 47-52, 2nd Edition. (Macmillan & Co., London, 1868.) (Concerning d'Alembert's Principle.)

5. Jack L. Beharrell and Hans R. Friedrich, "The transfer function of a rocket-type guided missile with consideration of its structural elasticity," *Journal of the Aeronautical Sciences*, **21**, pp. 454-458, July 1954.

6. I. T. Minhinnick, "The Theoretical Determination of Normal Modes and Frequencies of Vibration." (R. and M. No. 3039.

7. Clarence L. Johnson, "Analogue Computer Techniques," pp. 168-175. (McGraw-Hill, New York, 1956.)

8. Heinrich Holzer, "Biegungsschwingungen mit Berückschtigung der Stabmasse und der äusseren und inneren Dämpfung," *Zeitschrift für Angewandte Mathematik und Mechanik*, **8**, pp. 272-283, 1928.

9. K. Muto (Tokio), "Biegungsschwingungen mit Berückichtigung der Stabmasse und der äusseren und inneren Dämpfung," *ibid.*, **10**, pp. 346-353, 1930.

10. K. Sezawa (Tokio), "Die Wirkung des Enddrucks auf due Biegungschwingung eines Stabes mit inneren Dampfüng," *ibid.*, **12**, pp. 275-279, 1932.

11. Goodyear Aircraft Corporation, "Analysis of Transient Heating Problems with GEDA Equipment," U.S. Report, 12th June 1953.

12. Michael E. Fisher, "Higher order differences in the analogue solution of partial differential equations," *Journées Internationales du Calcul Analogique Bruxelles*, pp. 208-213, September 1955.

13. Dana Young and R. P. Felgar, "Tables of Normal Functions," University of Texas, Publ. No. 4912, 1949.

14. D. R. Hartree, "Numerical Analysis." (Oxford University Press, 1955.)

15. R. G. D. Bishop, "Treatment of damping forces in vibration theory," *Journal of the Royal Aeronautical Society*, **59**, p. 738, November 1955.

16. Václav Vodicka, "Biegungsschwingungen in zusammeugesetzten Stäben," *Z. angew. Math. Mech.*, **37**, No. 1/2, January/February 1957.

14. Appendix 1 : Modification of the Standard Thin Prismatic Beam Equation To Take Account of Internal Energy Dissipation

Elementary treatment of the static flexural behaviour of a thin beam is based on the assumption that Hooke's Law applies to all elemental, longitudinal filaments of the beam. On integrating over a cross-section it is found that the local bending moment B is proportional to the beam curvature. That is, for a short length of the beam δx in which the curvature is $\frac{\partial x^2}{\partial^2 y}$ we can write

$$-B = EI(x)\frac{\partial x^2}{\partial^2 y} \qquad \ldots\ldots(56)$$

If now we assume that the bending moment includes a further component proportional to the rate of change of beam curvature with time, then eq. (56) is replaced by

$$-B = EI(x)\left[\frac{\partial^2 y}{\partial x^2} + \lambda\frac{\partial^3 y}{\partial t\partial x^2}\right]\ldots\ldots(57)$$

where λ is a constant, and the describing partial differential equation for the thin prismatic beam becomes

$$\gamma(x,t)\frac{\partial^2 y}{\partial t^2} + \frac{\partial^2}{\partial x^2}\left\{EI(x,t)\left[\frac{\partial^2 y}{\partial x^2} + \lambda\frac{\partial^3 y}{\partial t\partial x^2}\right]\right\} + P(x,t) = 0 \qquad \ldots\ldots(58)$$

in which γ is the beam mass per unit length and $[P(x,t)]$ is an applied lateral force per unit length.

If in equation (58) we set γ and EI constant, and equate $P(x,t)$ to zero (i.e. confine ourselves to the free vibrations of a thin prismatic beam) we can write

$$\gamma\frac{\partial^2 y}{\partial t^2} + EI\left[\frac{\partial^4 y}{\partial x^4} + \gamma\frac{\partial^5 y}{\partial t\partial x^4}\right] = 0 \quad \ldots\ldots(59)$$

Now suppose the solution of (59) to be of the form

$$y(x,t) = \chi(x)\cdot\tau(t) \qquad \ldots\ldots(60)$$

in which $\chi(x)$, $\tau(t)$ are functions only of x and t respectively.

Substituting for y in (59) from (60) and rearranging:

$$\frac{\gamma\dot{\tau}}{EI(\tau+\lambda\dot\tau)} = \frac{\chi^{IV}}{\chi} = -k^4 \text{ say } \ldots\ldots(61)$$

in which k is a function neither of x nor of t.

Then

$$\ddot{\tau} + \lambda \frac{EI(kL)^4\dot{\tau}}{ML^3} + \frac{EI(kL)^4\tau}{ML^3} = 0 \quad \text{........(62)}$$

and

$$\chi^{IV} + \frac{(kL)^4\chi}{L^4} = 0 \quad \text{.........(63)}$$

Solutions of equation (63) exist for an infinite number of discrete eigenvalues (kL), the particular values being determined by the boundary conditions. On inserting these numerical values successively in eq. (62) the corresponding values of the coefficient of τ are measures of the time-rates of oscillatory decay at the corresponding critical frequencies for a given $\frac{EI}{ML^3}$ and λ. Denoting successive values of (kL) by $(k_jL)_{(j = 0, 1, 2, ...}$ the first few values for the "free-free" end conditions are shown in Table 6, Appendix 4.

It is very important to notice that having, for a given beam and boundary conditions, specified a value for λ, then in equations such as (62) the coefficient of $\dot{\tau}$ is determined for all values of j. That is to say, we can choose the damping coefficient for one mode only; the rest cannot then be independently controlled. This is potentially a disadvantage inherent in our assumptions in regard to structural energy losses. Much depends upon whether the variation of damping coefficient with j in eq. (62) is related in an acceptable manner, with reality.

It is, therefore, necessary to examine this particular consequence of our hypothesis a little more closely.

The undamped natural angular frequencies are given by equation (62) as

$$\omega_j = (k_jL)^2 \sqrt{\frac{EI}{ML^3}}_{(j = 0, 1, 2, ...)} \quad \text{.........(64)}$$

The coefficient of $\dot{\tau}$, may, therefore, be written as

$$\lambda(k_jL)^4 \frac{EI}{ML^3} \lambda\omega_j^2 \, (j = 0, 1, 2, ...) \quad \text{.........(65)}$$

This is the decay exponent of free oscillations in the jth mode, and it clearly increases as the square of the frequency.

Alternatively, equation (62) may be written in the form:

$$\ddot{\tau} + 2u_j\omega_j\dot{\tau} + \omega_j^2 = 0 \quad \text{........(66)}$$

Comparing the coefficient of $\dot{\tau}$ in (65) and (66) we see that

$$2u_j = \lambda\omega_j \quad \text{........(67)}$$

that is u_j, which is a measure of attenuation per cycle of oscillation, is proportional to ω_j. The clear implication is that vibrations are increasingly damped with increasing j, the rate of increase being outside our control. Such a situation has at least the practical advantage that in a lightly damped system, one may be reasonably confident that sustained oscillations will not develop at large values of j (other than by virtue of the characteristics of any feedback paths used). We do not know, however, how this relationship between oscillatory decay and vibration frequency compares with reality.

There is at least one other method of producing an electronic beam analogue (or for that matter an analogue of any other multi-mode vibratory system). This has none of the advantages inherent in the models which are the subject matter of this paper. It has, however, one potentially valuable property, namely that it permits of a completely independent setting of the oscillatory decay constant for each mode. Should this factor prove to be a serious drawback of our discrete cell system, it might be useful to use both techniques interchangeably at times. This, however, is a matter beyond our present scope.

15. Appendix 2: Fundamental Derivation of the Beam Equation, including the Effect of Structural Energy Dissipation

Consider the short length of uniform beam shown in Fig. 5. Its length along the neutral axis is

$$l_0 = R\theta \quad \text{.........(68)}$$

where R is the radius of curvature measured to the neutral axis (assumed constant with reference to x over the short length l_0); θ is the angle subtended by the arc l_0 at the centre of curvature.

Consider a corresponding section of length l of a filament parallel to the neutral axis and distant h therefrom. Then

171

$$l = (R + h)\theta$$

and

$$\frac{l - l_0}{l_0} = \frac{h}{R} = h\varphi \qquad \ldots\ldots\ldots(69)$$

where φ is the curvature.

Assuming that individual filaments obey Hooke's Law, we obtain the force dF required to strain the filament

$$dF = Eh\varphi dA \qquad \ldots\ldots\ldots(70)$$

where E is Young's modulus; dA is the cross-sectional area of the filament.

Equation (70) is the basis of static and of elementary dynamic treatments of a beam in flexure. To introduce structural energy losses we assume (Section 3) that a viscous force acts along the length of each filament which is proportional to the time-rate of change of length of that filament. For our purposes then we replace (70) by

$$dF = Eh(\varphi + \lambda\dot{\varphi})dA \qquad \ldots\ldots\ldots(71)$$

where λ is a constant.

The moment of this force about the neutral axis is hdF, so that by integration over the beam cross-section, we have the bending moment

$$B = EI(x)(\varphi + \lambda\dot{\varphi}) \qquad \ldots\ldots\ldots(72)$$

where I is the second moment of area of the cross-section about an axis through the neutral axis and perpendicular to the plane of flexure. Writing $EI(x)$ allows that the structural constants may vary along the beam axis (as also may λ, though we have not considered this).

16. Appendix 3 : Derivation of Boundary Conditions in Terms of Lateral Deflections of the Discrete Cells

It is shown in Section 4.2 that in a discrete-cell model of a thin uniform flexible beam, the lateral motion of the rth cell counted from one end of the beam is given by

$$m\ddot{y}_r = -\frac{EI}{x^3}\left[y_{r+2} - 4y_{r+1} + 6y_r - 4y_{r-1} + y_{r-2}\right]$$
$$\ldots\ldots\ldots(73)$$

where the beam model consists of n equally spaced cells, each of mass m, the length of the beam being $L = nx$. EI is the rigidity, assumed constant, and $3 \leqslant r \leqslant (n - 2)$.

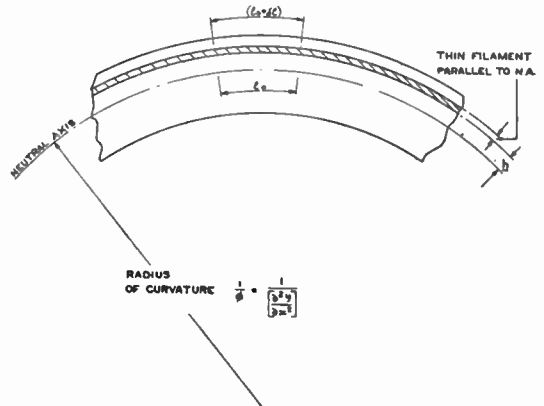The corresponding equations for the two

Fig. 5. Short section of deflected beam.

cells at each end of the beam depend upon the specified end conditions and upon the manner in which these are interpreted in finite-difference terms. We here illustrate the derivation of these equations by reference to the "free-free" beam.

We interpret the boundary conditions (Section 7.1) as meaning that the gradient $(y_2 - y_1)/x$ is applicable from the point x'_1 to the left-hand extremity of the beam and that analogous conditions prevail at the right-hand end. If $r = 1$ therefore, the second fraction on the right-hand side of eq. (9) is zero. Now the only shear force acting on the cell for which $r = 1$ is at its right-hand bounding section, and in consequence this is equal, for the uniform beam, to

$$Qx_1 = -EI\left[\frac{y_3 - 2y_2 + y_1}{x^3}\right] \qquad \ldots\ldots\ldots(74)$$

from eq. (9).

Hence the required equation for $r = 1$ is

$$m\ddot{y}_1 = -EI\left[\frac{y_3 - 2y_2 + y_1}{x^3}\right]\ldots\ldots\ldots(75)$$

For the case $r = 2$ we have to consider the shear forces acting both at x_1 and x_2 (Fig. 2). From eq. (9) if we express the boundary conditions in the manner specified above we have :

$$Q_{x=x1} = -EI\left[\frac{y_3 - 2y_2 + y_1}{x^3}\right]$$

and

$$Q_{x=x2} = -EI\left[\frac{y_4 - 2y_3 + y_2}{x^3}\right] - EI\left[\frac{y_3 - 2y_2 + y_1}{x^3}\right]$$
$$\ldots\ldots\ldots(76)$$

$$= - EI\left[\frac{y_4 - 3y_3 + 3y_2 - y_1}{x^3}\right] \qquad \ldots\ldots\ldots(77)$$

so that

$$m\ddot{y}_2 = - \frac{EI}{x^3}\left[y_4 - 4y_3 + 5y_2 - 2y_1\right] \ldots\ldots(78)$$

From considerations of symmetry, it follows that for $r = (n-1)$

$$m\ddot{y}_{n-1} = - \frac{EI}{x^3}\left[-2y_n + 5y_{n-1} - 4y_{n-2} + y_{n-3}\right]$$
$$\ldots\ldots\ldots(79)$$

and for $r = n$

$$m\ddot{y}_n = - \frac{EI}{x^3}\left[y_n - 2y_n - 1 + y_{r-2}\right] \ldots\ldots\ldots(80)$$

17. Appendix 4 : Normal Functions for Flexure —Prismatic "Free-Free" Beam

In the jth mode, the normal function X_j for translation is given by

$$X_j = C_1\left[\cos(k_jL)\frac{x}{L} + \cosh(k_jL)\frac{x}{L}\right]$$
$$+ C_3\left[\sin(k_jL)\frac{x}{L} + \sinh(k_jL)\frac{x}{L}\right]$$

The corresponding normal function v_j for rotation is given by

$$v_j = C_1\left[-\sin(k_jL)\frac{x}{L} + \sinh(k_jL)\frac{x}{L}\right] +$$
$$+ C_3\left[\cos(k_jL)\frac{x}{L} + \cosh(k_jL)\frac{x}{L}\right]$$

C_1, C_3, k_jL are given in Table 6 for various j. L is the length of the beam; and x is the distance along the axis of the beam from the left-hand end (Fig. 1). $j = 0$ corresponds to collinear motion; $j = 1$ corresponds to the fundamental flexural mode and so on.

Table 6

j	C_1	C_3	k_jL
0			
1	1	-0.9825	4.730
2	1	-1.00078	7.853
3	1	-0.999966	10.996
4	1	-1.0000	14.137
5	1	-1.0000	17.279

Higher values of k_jL are obtained by adding π to the next lower value.

Table 7

$\frac{x}{L}$	$j=1$ X_1	v_1	$j=2$ X_2	v_2	$j=3$ X_3	v_3	$j=4$ X_4	v_4	$j=5$ X_5	v_5
0	$+2.00000$	-1.9650	2.0000	-2.00156	2.000	-1.999932	2.0		2.0	
0.05	1.5355	-1.960847	1.216	-1.98348	0.907		0.604		0.312	
0.1	1.0743	-1.934829	0.454	-1.8717	-0.104		-0.588		-0.966	
0.15	0.6240	-1.856662	-0.235	-1.61619	-0.726		-1.255		-1.300	
0.2	0.1955	-1.748136	-0.794	-1.282128	-1.286	-0.331876	-1.210		-0.610	
0.25	-0.1977		-1.169		-1.242		-0.512		0.555	
0.3	-0.5432		-1.324		-0.794		0.451		1.351	
0.35	-0.8271		-1.249		-0.089		1.213		1.206	
0.4	-1.0400		-0.966		0.656		1.400		0.221	
0.45	-1.1700		-0.526		1.215		$+0.919$		-0.919	
0.5	-1.2149		0.004		1.422		0.000		-1.414	
0.55	-1.1713		0.525		1.212		-0.918		-0.918	
0.6	-1.0390		0.966		0.653		-1.397		0.221	
0.65	-0.8274		1.249		-0.092		-1.206		1.206	
0.7	-0.5436		1.323		-0.799		-0.437		1.345	
0.75	-0.1977		1.169		-1.249		0.541		0.541	
0.8	0.1956		0.792		-1.298		1.260		-0.642	
0.85	0.6239		0.232		-0.903		$+1.375$		-1.375	
0.9	1.0737		-0.457		-0.139		$+0.831$		-1.144	
0.95	1.5353		-1.2178		0.847		-0.111		-0.111	
1.0	1.9990		-1.994		1.984		-1.0		1.0	

# of current interest . . .

Emigration to Australia

Under an agreement recently signed by the Prime Ministers of the United Kingdom and of Australia, social security arrangements for emigrants and temporary residents have been substantially strengthened.

Previously persons going from the United Kingdom to Australia have had to depend on their National Insurance record in the United Kingdom to qualify for Australian social security benefits. Under the new agreement their residence in the United Kingdom will count as residence in Australia and so enable them to qualify for Australian benefits.

The new agreement will also extend and simplify the reciprocal arrangements between the two countries. For example, family allowance will now be paid during the journey to a family migrating from one country to the other. Another interesting feature of the new agreement is that it can be extended to apply to those British Colonies which have schemes of national insurance.

Electronic Engineering Association

At the recent annual general meeting of the Radio Communication and Electronic Engineering Association it was announced that the name of the association will in future be the Electronic Engineering Association. In his address, the chairman of the association emphasized the desirability of the industry having much greater freedom to talk of technical achievement under classified contracts.

Appointment of the First Director of the Rutherford High Energy Laboratory

The Rutherford High Energy Laboratory, named in commemoration of the work of the late Lord Rutherford in the development of nuclear physics, is now being built adjacent to the Atomic Energy Research Establishment, Harwell, for the National Institute for Research in Nuclear Science. It will house the Institute's first large accelerator, a research machine of which the main part is a magnet ring 120 ft. in diameter and weighing over 6,000 tons.

Dr. T. G. Pickavance, who is at present Deputy Head of the General Physics Division of the Research Establishment, has been appointed Director of the new Laboratory by the Governing Board of the Institute.

Extension of B.B.C. Television Coverage

The permanent television transmitting station at Douglas, Isle of Man, was opened on December 12th, replacing the temporary lower power station on the same site which was brought into operation in December 1953. The new station will operate on the same frequencies as the temporary station (Channel 5, vision 66·75 Mc/s, sound 63·25 Mc/s) with vertical polarization and will use a directional aerial giving a maximum effective radiated power of 2·8 kW—a ten-fold increase.

At present the vision signals for the Douglas transmitter are obtained by direct reception of the Holme Moss transmissions, and quality has been adversely effected during periods of poor reception conditions. A new link is now under construction and vision signals will be picked up at a receiving station on Snaefell, where a strong signal is obtained from Holme Moss, and then fed to the Douglas transmitter via a u.h.f. radio link.

An increase in power of the B.B.C's Norwich television station has recently been possible. The station has been working on reduced power in order to avoid interference with the Belgian low-power station at Liège, which shares the same frequency channel. The British Post Office and the Belgian authorities have agreed to an initial increase in the power of the Norwich station and to a further increase to full power next Spring, by which time it is expected that the Liège transmitter will be on high power. The Norwich station has a directional aerial, and the final e.r.p. will vary between 1-10 kW in different directions.

Technical Writing Premiums

The Radio Industry Council has recently announced its awards of premiums worth 25 guineas to authors of articles published in the Technical Press during 1957. Among the recipients is Mr. E. J. Gargini (Associate Member) whose article on "An Alternative Colour TV System" was published in *Wireless World* last August. Mr. Gargini is with E.M.I. Research Department and is the author of several papers and articles, principally on wired broadcasting.

DEVELOPMENTS IN COMPONENT DESIGN

A further selection of papers read at the International Symposium on Electronic Components, Malvern, September 1957.

Recent Developments in Fixed Resistors
R. W. Burkett*

Mr. Burkett opened his lecture by reviewing the range of resistive materials. He then gave the main factors of importance in choosing a resistor as follows: —

1, Price; 2, Reliability; 3, Stability in use; 4, Long storage life; 5, Mechanical strength; 6, Temperature coefficient; 7, Noise; 8, Linearity; 9, Low reactance.

He then summarized the faults of existing resistor types as follows: —

(a) Wirewound resistors—reactance, bulk and and price.

(b) Carbon film resistors—unreliability and instability in humidity.

(c) Metal film resistors—price, bulk and range.

(d) Metal oxide resistors—range and linearity.

(e) Composition resistors — instability and noise.

(f) Semi-conductor resistors — range and linearity.

Mr. Burkett then reviewed some recent developments in the resistor field. Dealing with wirewound resistors, he pointed out that nickel-chromium alloys of increased resistivity had become available but it was impracticable com-

* The Welwyn Electrical Co. Ltd., Bedlington, Northumberland.

mercially to produce wire of less than 0·0005 in. diameter. Protection by new resins such as epoxy or polyurethanes, improved the moisture resistance of lower temperature types. For vitreous enamelled resistors, craze-free enamels enabled them to withstand prolonged applications of condensation and direct currents. Pyrolytic carbon films have been slowly improved, enabled by the use of alkali-free ceramic rods as a basis for deposition. Further developments of the pyrolytic method were referred to and it was mentioned that independent tests had shown that in some cases it could operate at 250°C on full load. Reference was made also to a composition resistor using a carbon dispersion and it was suggested that the noise in this might be greatly reduced. Metal film resistors are liable to attack by moisture but are essentially stable and may have very low temperature coefficients if suitable alloys are chosen. Finally, the oxide film resistor deposited on glass was briefly described.

It was stated that improvements are possible in the pyrolytic carbon resistor which may make it cheap enough to act as a possible replacement for existing Grade II resistors. It is possible that the surface resistivity of metal film resistors might be further increased but there would be difficulties in making the film much thinner. The most promising line probably lay in the oxide film resistor on grounds of cost, stability, high temperature and performance.

The Design of High Performance Multi-gang Variable Capacitors
L. W. D. Sharp†

Mr. Sharp outlined briefly the developments which have taken place during the last ten years in design and manufacture of variable capacitors, in particular variable capacitors of the types used on communication equipments for the armed Services. The factors which have determined the main trend in development are the higher operational frequencies and the provision for the

† The Plessey Company Ltd., Ilford.

selection of a very large number of channels. The use of very high frequencies has involved to a much greater degree the integration of the gang capacitor into the design of equipment. The requirement for a high degree of selectivity has resulted in the demand for calibration and accuracy of repetition, and the tuning capacitor must therefore have a highly accurate law and must be matched between sections to very close limits.

Mr. Sharp then traced the development for variable capacitors, from the conventional four-gang unit, to a unit having three sections for transmitter circuits and three sections for receiver circuits, which are controlled by two spindles geared together.

A seven-gang capacitor produced by the latest techniques was next discussed. The accuracy required in the capacitor is determined by the design of a transmitter-receiver, and after analysing the relevant factors it was felt that would be more profitable to approach the problem as one in mechanical precision. The result was that a capacitor was produced which required no electrical tests or ganging adjustments. A method of jigging was devised in the assembly stages which gave the best possible concentricity and accuracy of range location.

The production of a capacitor in this manner for which normal electrical testing, with this capacitance measurement, has been eliminated, means that mechanical inspection of extreme accuracy is necessary. This was carried out satisfactorily and the final check was made by taking one capacitor from each batch and wiring it into a functional test set.

Mr. Sharp finally outlined the most recent developments which are connected with the introduction of continuously tuned multi-channel equipment on a v.h.f. band up to 400 Mc/s per second. Due to the need for a wide frequency range, nearly two to one, and to the great importance of stray inductance in variable capacitors and of stray capacitance in variable inductances at such frequencies, it has been found necessary to vary both inductance and capacitance simultaneously.

Life-Failure Statistics of Short Rated Oil-Paper Capacitor Elements

R. J. Peterson*

The problem which has arisen at A.W.R.E. has been to ensure the fastest possible discharge of maximum stored energy in a short time. Further, it was required that volume should be kept to a minimum and that the units should be as robust as possible. Normal capacitors worked at their normal ratings were completely inadequate and, expressing the effectiveness of a storage system in joules per litre, for normal capacitors, there are some 11 joules per litre or, allowing for packing, leads, etc., 16 joules per litre. By removing these sources of loss and reducing volume to a minimum, a storage of some 36 joules per litre could be realized.

This must be improved upon and it became clear that increasing the voltage rating would produce a great improvement, the storage being proportional to the square of the voltage. It was expected from the start that improved energy storage would be obtained only at the expense of shortened life and the purpose of the investigation was, therefore, to investigate the life shortening which must be tolerated in order to secure maximum voltage ratings at normal temperatures. For this study a number of $0.01 \mu F$ oil-impregnated paper capacitors were used having total thickness of insulant 60 microns. These were measured for

* Atomic Weapons Research Establishment, Aldermaston, England.
U.D.C. No. 621.319.4

internal resistance and discharge inception, and finally voltage breakdown was measured on a number which it was hoped was representative. For these units an ultimate breakdown strength of 15·2 kV was found. To allow for faults inherent in the assembly process, a number were broken open and the constituents were tested again for breakdown stress, giving a figure of 20 kV, the discrepancy being attributed to the presence of localized faults, etc., which could be eliminated in a later experiment. The remaining capacitors were tested for life under various voltage stresses on an automatic recording machine. The results may be briefly summarized as follows: Whilst it is known that the life falls off very rapidly with increasing voltage (a fifth power law being normally adopted), it was clear that the considerable number of low voltage breakdowns under relatively small stresses after a long time could not be expressed in this form and a modified law has been put forward using the empirical formula

$$x \propto V^5 \left(1 - \left(\frac{v}{u}\right)\right)^{\frac{1}{4}}$$

where v is the short term breakdown voltage.

The coefficient u can then be chosen to give a best fit, and this theoretical formula may be compared with practical results, but it is premature to say that it is a useful theoretical approximation, though it helps in discovering the facts by simplifying study.

176

The actual life tests on a limited number of samples show two things. First, whilst no exact correlation can be established between the life capacitors and the likelihood of failure as shown by discharge inception tests, it appears that the number of discharges which have taken place is an important contribution to the final breakdown, leading to the further conclusion that over-voltage will very rapidly shorten the life of a unit, as is well known and confirmed by the experiments. Secondly, other mechanisms play an important part in determining the long life of components under low stress. Experiments are continuing to investigate the true factors which limit the life of capacitors.

Metal Oxide Film Potentiometers

Dr. G. V. Planer*

Dr. Planer dealt first with metal film of platinum/gold alloy for which flat plate substrates normally of glass were used and fired on films of alloy solutions from paint solutions were used. He said that the range of film thicknesses found most suitable corresponded to about 20 to 50 ohms per square before the meandering pattern was applied.

The temperature coefficients are of the order of $+0.03\%$ per °C. Noise values measured on elements of between 70,000 and 550,000 ohms were within the range 0.013 to 0.033 microvolts per volt, and were effectively constant over the range 20 to 50 ohms per square; the value becomes worse for thicker films and better for very thin films.

In order to obtain high total resistance values it is necessary to produce meandered tracks. A photo-abrasion method has been developed to do this and has resulted in tracks of resistance up to 500,000 ohms in a 2 in. diameter. Line widths down to about 0.001 to 0.0015 can be obtained in this way, but in practice patterns of about 0.0045 with about 112 lines per inch and meandering ratios of between 10,000 and 15,000 were used.

In order to obtain reasonably long life of the track, the wear characteristics of the gold/platinum film have had to be improved by laying down a reinforced track for the wiper. Reinforcement is obtained by depositing a silver coating and laying down a rhodium coating on top. With these reinforced tracks, excellent wear characteristics were obtained. For example, with 300,000 ohm elements under a.c. and d.c. load at 70°C, resistance change was below 0.6% after 300,000 cycles. A thousand hour test under d.c. conditions and humidity gave rather higher variations due to an electrolytic attack. Unless special substrates

* G. V. Planer Ltd., Sunbury-on-Thames.
U.D.C. No. 621.316.82

and stringent climatic sealing methods are used, a d.c. rating limitation may have to be imposed.

Dr. Planer then turned to oxide films, which he considered to have greater possibilities in many respects than the metal film types. Among the major advantages of the oxide films are the higher ohms per square, the control afforded over the resistance by chemical constitution, low temperature coefficients, thermal stability and intrinsic toughness of the films. In addition, the method of preparation was rather more suited to quantity production than that of the metal film. One of the present difficulties was the making of satisfactory electrical end connections. The films consist normally of tin oxide in combination with one or more oxides—for example, antimony, indium, bismuth, cadmium. Films are normally deposited by spraying the hot substrates in a solution of the mixed chlorides. First stage development of the oxide film potentiometer consisted in determining the relation between composition resistivity and temperature coefficient and film thickness. By requisite control, temperature coefficients can be held to less than $\pm 0.01\%$ per °C over a wide temperature range. Two types of potentiometer track have been developed, the infinite resolution type (consisting of a narrow continuous track), and the meandering type(for very high values). In the first type the number of ohms per square is normally about 200, while for the meandered type values up to 5 megohms can be obtained on the track of 2 in. diameter. The relatively simple photographic method has been developed for producing the meandered tracks. A reinforcing wiper track is again laid down to improve wear resistance. Rotational noise values of the order of 22 millivolts per volt are obtained. Development, particularly of the meandered type of oxide potentiometer, is continuing but a fair amount of work remains on production methods and performance.

177

Recent High-K Capacitor Developments in France

J. Peyssou*

Developments of high K dielectrics had been based, as elsewhere, on the titanates with stannate zirconate additions. These give very high dielectric constants but suffer very large temperature coefficients and unreliability at high temperature. These have, to a large extent, been overcome by the French work and a number of uses become possible.

To reduce temperature dependence of capacitance, two methods have been tried. First the standard one of mixing barium and strontium titanates to give a split maximum: the firing conditions for this are critical. Secondly, addition of bismuth gives a much flatter curve with or without a pronounced peak at high temperatures. Finally, the addition of pentavalent oxides lowers the power factor at high frequencies.

To obtain high temperature dielectrics lead barium titanates are used. The basic lead barium titanates are fired with trivalent and pentavalent oxide additions and the conditions of firing need careful control. As a result a material in which the dielectric constant does not change by more than $\pm 20\%$ in the range $-60°$ to $200°C$ has been aimed at.

Miniaturization has called for the development of particularly thin sheets, and a thickness of $0\cdot15$ mm is considered the safe limit at present. In this way flat capacitors having a value of 50,000 pF per square or wound types giving $0\cdot5$ μF for 2 cm² had been obtained. Stack types giving values ranging from $0\cdot5$ to $5\mu F$ and test voltages of 1000V, rated 200, have also been constructed.

Reliability is largely determined by the leakage current in inferior dielectrics. The insulation resistance increases with time for good dielectrics. The chief cause is believed to be ionic current and it is thought that in inferior dielectrics the movement of the ions produces a space charge effect.

Generally speaking, the behaviour of dielectrics shows noticeable improvement if the following points are observed: —

Alkaline-free metallic oxides.

Small additions of ZrO_2 in place of TiO_2.

Original fineness of the particle size of the powders and extended bulk milling in alkaline-free mills.

Special purity with a view to avoiding the introduction of iron oxide from the shaping machinery.

Mixing with the organic binders as homogeneously as possible.

Adjustment of the firing programme in order to check the growth of the grains.

And, of course, great care in metallizing, soldering and fitting operations.

In the course of experiments it has been found possible to extend the use of high K dielectrics to very low frequencies of the order of 50 c/s. Briefly, it may be said that the higher the d.c. resistance the more suitable is the material for these applications, and the materials are finding use both for interference suppression units and for high voltage capacitor use in power distribution.

The accompanying table shows the nature of the improvements and some new uses for these materials.

Nature of Improvements	New Use
Stabilization of the curve $(\varepsilon/\theta)/°C$	Coupling capacitors, padding, more even by-passing, low frequency
Higher rated temperature increased from $90°C$ to $200°C$	Airborne equipments for use on supersonic aircraft, guided missiles, nuclear reactors control, geophysics
Miniaturized capacitors for low voltages	Transistorization
Better reliability at $90°C$ and higher	Security of utilization: equipments of service-free use
Lower power factor at V.L.F.	Uses at 50 c/s interference suppressors, high frequency measuring instruments under very high tension

* Compagnie Generale de Telegraphie sans Fil, France.

THE EXPERIMENTAL DETERMINATION
OF SYSTEM TRANSFER FUNCTIONS FROM
NORMAL OPERATING DATA*

by

J. G. Henderson, B.Sc.† and C. J. Pengilley, B.E.,Ph.D.‡

SUMMARY

It is often not possible to remove a plant or system from service in order to measure its transfer function by the usual process of applying sinusoidal or impulse test signals. Use can, however, be made of statistical data of input and output when the system is operating in normal service, since in a linear system, undisturbed by noise, the cross-correlogram between the input and output signals is given by the convolution of the system weighting function and the auto-correlogram of the input. The experimental determination of the system transfer function or weighting function involves finding the function which, when convoluted with the auto-correlogram of input, will most closely fit the cross-correlogram between the input and output signals. The paper discusses various methods of doing this, with particular emphasis on analogue methods.

1. Introduction

This paper attempts to show that it is advantageous to use correlation analysis of normal operating data as a means for determining experimentally the transfer function of a system, especially when it is disturbed by noise. The method has especial merit in those applications where only a limited amount of time is available for actual experimental testing, as is often the case in the flight testing of aircraft controls, etc., or wherever it is necessary to determine the transfer function of a plant, such as a manufacturing process plant, that must remain in normal operation.

This method of analysis requires the calculation of the auto-correlation function of the input signal and the cross-correlation function between the input and the output signals. In the case of linear systems the cross-correlation process eliminates the effect

of noise and the system weighting function is that function which when convoluted with the auto-correlation function gives the cross-correlation function. The paper shows how system transfer functions, or their corresponding weighting (or impulse-response) functions, can be derived (*a*) by numerical methods which are appropriate for solution by a digital computer and (*b*) by analogue methods. The latter are essentially processes of curve fitting, in which the auto-correlation function is reproduced as a voltage waveform which is applied to an analogue with adjustable parameters, which simulates either the process of weighting or the functional dependence of the system under examination. The parameters of the analogue are then adjusted until the output-voltage waveform most closely fits a voltage replica of the cross-correlation function. The impulse response of the analogue is then closely approximate to that of the system to which the correlograms relate. In addition, the system frequency-response, which is usually the data that is required for the further application of the results of this analysis in control system design, can be obtained by direct frequency-response measurements on the analogue.

2. Relationship between Auto and Cross-correlation Functions

Consider a linear system with a weighting function, i.e. a response to unit impulse, defined by $w(x)$. The Laplace Transform of $w(x)$, given by

$$W(p) = \int_0^\infty w(x)\,e^{-px}\,dx$$

may be defined as the transfer function of the system, and when $j\omega$ is substituted for p in $W(p)$, the operator $W(j\omega)$ defines the relationship between the output and the input of the system when subjected to a sinusoidal input.

In response to an arbitrary input $f_i(t)$ the output of the system $f_o(t)$ is given by the convolution integral

$$f_o(t) = \int_0^\infty w(x)\,.\,f_i(t-x)\,dx \quad \ldots\ldots\ldots(1)$$
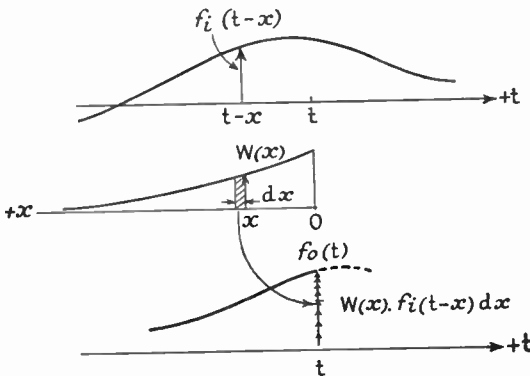
Fig. 1. The process of convolution

$$f_o(t) = \int_0^\infty w(x)\,.\,f_i(t-x)\,dx$$

The corresponding physical process is shown in Fig. 1, where the output $f_o(t)$ is composed of weighted sums of preceding values of $f_i(t)$. In time series notation, which will be adopted at a later stage, the process can be described by summation

$$f_o(m) = \sum_{n=0}^{n=\infty} w(n)\,.\,f_i(m-n)$$

where $m = t/\Delta$ and Δ is the time interval between ordinates of the time series representing the functions $f_i(t)$ and $f_o(t)$.

It follows from this process of weighting that there must be correlation between the output $f_o(t)$ and preceding values of the input $f_i(t)$. If we define a "cross-correlation" function $C(\tau)$

$$= \lim_{T\to\infty} \frac{1}{2T} \int_{-T}^{+T} f_i(t-\tau)\,.\,f_o(t)\,.\,dt$$

and then substitute for $f_o(t)$ we obtain

$$C(\tau) = \lim_{T\to\infty} \frac{1}{2T} \int_{-T}^{+T} f_i(t-\tau) \int_{x=0}^{x=\infty} w(x)\,.\,f_i(t-x)\,.\,dx\,.\,dt$$

Interchanging the order of integration gives

$$C(\tau) =$$
$$\int_{x=0}^{x=\infty} w(x)\,.\,\left[\lim_{T\to\infty} \frac{1}{2T} \int_{-T}^{+T} f_i(t-\tau)\,.\,f_i(t-x)\,dt\right]dx$$
$$\ldots\ldots\ldots(2)$$

If we now define the square bracketed term as the auto-correlation function of the input signal, $A(\tau-x)$, equation (2) can be written as

$$C(\tau) = \int_0^\infty w(x)\,.\,A(\tau-x)\,.\,dx \quad \ldots\ldots\ldots(3)$$

That is the cross-correlation function is given by the convolution of the system weighting function and the auto-correlation function of the input signal.

$A(\tau)$ and $C(\tau)$ may be regarded respectively as a statistically representative stimulus and response, and the aim of this paper is to exploit the relationship between $C(\tau)$ and $A(\tau)$ as a method for deriving system weighting functions $w(x)$ from correlograms computed from normal operating data.

The auto-correlation function is a symmetrical function of τ, whilst in general the cross-correlation function is asymetrical.

In the limit, if $A(\tau)$ were to degenerate to a unit impulse at the origin, which corresponds to the auto-correlation function of a random signal of infinite bandwidth, the cross-correlation function $C(\tau)$ would become identical to the weighting function $w(x)$.

2.1. Discrimination Against Noise

The power of correlation analysis is primarily its capacity to discriminate against random noise. If it were not for this, the rest of this

paper might just as well be in terms of the *actual* input and output signals instead of their correlograms.

If in the system shown in Fig. 2 a random disturbance $N(t)$ is directly additive to the output, $f_{oi}(t)$, of a linear system, then the net output $f_o(t) = f_{oi}(t) + N(t)$. If $f_i(t)$ were a sinusoidal signal such as is used in frequency response testing and $N(t)$ had substantial components of the same frequency it would prove difficult to perform conventional amplitude and phase measurements, and the problem would be more difficult still if the frequencies concerned were very low, as in process control plant.
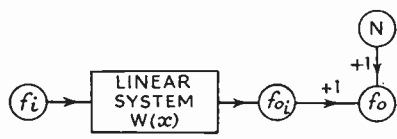
Fig. 2. Linear system with noise added directly to the output.

If, however, the input and output were recorded and then correlated we would have the cross-correlation between input and output

$$C(\tau) = \lim_{T \to \infty} \frac{1}{2T} \int_{-T}^{+T} f_i(t - \tau) \cdot (f_{oi}(t) + N(t)) \, dt$$

and if $N(t)$ and $f_i(t)$ were uncorrelated, we would be left with

$$C(\tau) = \lim_{T \to \infty} \frac{1}{2T} \int_{-T}^{+T} f_i(t - \tau) \cdot f_{oi}(t) \, dt$$

and once again

$$C(\tau) = \int_{0}^{\infty} w(x) \cdot A(\tau - x) \, dx$$

That is, provided the system is linear, $w(x)$ may still be derived from the relationship between the auto-correlation of the input and its cross-correlation with the output even though random noise is present in the output.

3. The Derivation of Transfer Functions from Correlograms

In the practical application of equation (3) as a method of determining system transfer functions it is first necessary to compute the correlograms, $C(\tau)$ and $A(\tau)$ from records of $f_i(t)$ and $f_o(t)$. The merit of this technique is that these records may be associated with the normal operation of the system whose transfer function is desired.

If $f_i(t)$ and $f_o(t)$ are records on paper it may be most expedient to read off equally spaced ordinates and compute the correlograms by digital computer using the time series equations

$$A(m) = \frac{1}{N} \sum_{n=0}^{n=N-1} f_i(n) \cdot f_i(n+m)$$

$$\ldots\ldots\ldots(4)$$

$$C(m) = \frac{1}{N} \sum_{n=0}^{n=N-1} f_i(n) \cdot f_o(n+m)$$

It is, of course, essential to compute these correlograms for a range of $\tau = m\Delta$ that is sufficiently large for the weighting function to have converged to a negligibly small value within this time. On the other hand this whole process of data recording and processing is one well suited to analogue computation and in many cases it would be feasible to record $f_i(t)$ and $f_o(t)$ on magnetic tape and determine correlograms by the operations of delaying one signal by physically displacing one play-back head with respect to the other, multiplying the two signals $f_i(t)$ and $f_o(t+\tau)$ and integrating the product.

There are two important restrictions on the recorded data:

(a) the bandwidth of the frequency spectrum of the input signal should ideally be wider than the bandwidth of the system under examination, otherwise there is insufficient high frequency data present in the output records from which to determine the system response at high frequencies with any exactitude.

and

(b) the records should be long enough to constitute a stationary time series. A rough guide is that the record should be about ten times as long as the lowest periodicity evident in the input signal.

Having determined the correlation functions $A(\tau)$ and $C(\tau)$ it is then necessary to determine the weighting function $w(x)$ which when

convoluted with $A(\tau)$ will give a cross-correlogram which is identical with $C(\tau)$. This operation can be performed by either numerical methods or by analogue methods. In practice, the process of curve fitting is restricted to the positive region of $C(\tau)$ in order to avoid spurious contributions from the discontinuous start of $A(\tau)$ which is defined only for a finite range of τ.

3.1. Numerical Method of Deriving $w(x)$

The equation (3) can be defined in time series notation as

$$C(m) = \sum_{j=0}^{j=\infty} w(j) \cdot A(m-j)$$

where $W(j)$ is a time series representation of $w(x)$. Now if $w(x)$ is substantially convergent to zero in a time $k\Delta$, the range of the summation can be limited to k terms and $w(j)$ can be derived from the following matrix, in which ordinates of the auto-correlogram are represented by the series $A_{-k}...A_o...A_k$ and those of the cross-correlogram by the series $C_o...C_k$. We have

$$
\begin{bmatrix} C_0 \\ \cdot \\ \cdot \\ \cdot \\ \cdot \\ \cdot \\ \cdot \\ \cdot \\ C_k \end{bmatrix}
=
\begin{bmatrix}
A_0 & A_1 & \cdot & \cdot & \cdot & \cdot & \cdot & A_k \\
A_1 & A_0 & \cdot & \cdot & \cdot & \cdot & \cdot & \cdot \\
\cdot & \cdot & \cdot & & & & & \cdot \\
\cdot & \cdot & & \cdot & & & & \cdot \\
\cdot & \cdot & & & \cdot & & & \cdot \\
\cdot & \cdot & & & & \cdot & & \cdot \\
\cdot & \cdot & & & & & \cdot & \cdot \\
\cdot & \cdot & & & & & & \cdot \\
A_k & \cdot & \cdot & \cdot & \cdot & \cdot & \cdot & A_c
\end{bmatrix}
\cdot
\begin{bmatrix} W_0 \\ \cdot \\ \cdot \\ \cdot \\ \cdot \\ \cdot \\ \cdot \\ \cdot \\ W_j \end{bmatrix}
$$

By inverting the matrix, a process most suited to a digital computer, the time series $w(j)$ may be derived.

Although this method seems attractive because both correlograms and weighting functions can be determined by digital computer, it must be stressed that in a general case the range of time $k\Delta$ for $w(x)$ to become convergent will not be known and it may be necessary to repeat the process for a range of values of k before a consistent result is found. For example, too small a range of $k\Delta$ will give a truncated type of weighting function that will satisfy the equations at k values of $C(\tau)$, but the series $w(j)$ need bear no resemblance to the actual weighting function. At the other extreme too large a range of $k\Delta$ will result in a weighting function in which only the first few ordinates are important, but through which it would be difficult to draw a smooth function. Obviously without some prior knowledge of the system it may be necessary to repeat the solution of the matrix for different values of ordinate spacing Δ.

Since most control system design is done by way of frequency response analysis it would often be necessary to deduce the system frequency response from the time series $w(j)$. Computing programmes exist which enable this to be done on a digital computer, and thus it is feasible to determine system transfer functions from normal operating data entirely by operations on a digital computer. On the other hand, suitable analogue devices have been described[1,2] which perform the conversion from time-function to frequency-function, and these may often prove cheaper and more convenient.

3.2. Determination of System Transfer Functions by Analogue Methods

Analogue methods of computation require that correlograms $A(\tau)$ and $C(\tau)$ should be reproduced as voltage waveforms $V_A(\tau)$ and $V_C(\tau)$ respectively. This can be done by making opaque masks of the functions, $A(\tau)$ and $C(\tau)$ and rotating them in front of cathode-ray tube curve followers in which the beams are constrained to follow the edges of the masks.

The process of determining $w(x)$ is simply that of applying the voltage $V_A(\tau)$ to some form of analogue capable of simulating the dynamics of the system under examination and then varying the parameters of the analogue until its output voltage most closely matches the positive region of the cross-correlogram represented by $V_C(\tau)$. The impulse response of the analogue, so adjusted, will approximate that of the system under examination and by direct frequency response measurements between the input and output of the analogue its frequency-response $W(j\omega)$ may be obtained.

The quality of the fit that has been obtained can be determined by measuring the mean-square value of the difference in voltage, e, between the cross-correlogram $V_C(\tau)$ and the

output voltage of the analogue $V_a(\tau)$ and comparing it with the mean-square value of the positive region of $V_c(\tau)$, that is the quality

of fit is proportional to $\dfrac{e^2}{V_c{}^2(\tau)}$: an operation

that can be easily performed by an electronic multiplier combined with a moving-coil meter, or by a thermal milliammeter, if the signals are repetitive. This general scheme is shown in Fig. 3.
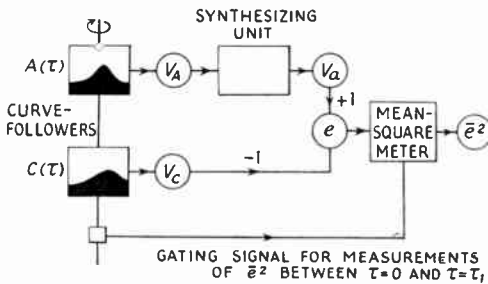

Fig. 3. Scheme for the experimental determination of system transfer function.

Any of the following devices may be used to simulate weighting functions.

3.2.1. Delay-line synthesizers

In these the process of convolution is simulated by a tapped delay-line from which is available a series of delayed replicas (ideally, they should be undistorted replicas) of the input signal. By passing each of these signals through an adjustable attenuator and summing them, positively or negatively as required, the operation of weighting is simulated. A number of delay lines[3,4] used for this purpose have been described and when they have been required to produce section delays of the order of 1–10 millisec they have usually consisted of a number of R-C stages with intermediate buffer amplifiers. Tolerably good approximations to pure delay are produced if the signal frequencies only occupy about 1/10th of the pass-band of the delay line. However, it is apparent that with such delay lines a unit impulse applied to the input is dispersed as it passes along the delay line and consequently the outputs from the tap points do not form an orthogonal set of functions, and therefore the settings of the attenuators do not

correspond directly to the ordinates of the system weighting functions.

L-C delay lines are a little better in this respect and they have been used in process analogues[4] and in high speed correlators[5] involving total delays of 2 millisec but they become impractical when total delays approaching 0·2 sec are required. However, a recent development by Girling and Good[6] who have made an electronic analogue of one cell of an L-C ladder makes it possible to simulate L-C ladder networks with a very low cut-off frequency, and this may prove to be an attractive alternative to buffered R-C ladders.

The problem of producing long delays can be solved by changing from a continuous to a discontinuous "delay-line" synthesizer[7,8]. This synthesizer involves sampling the input signal, and storing this value for a time interval Δ. At the commencement of the next time interval the first signal is passed to a second storage stage, whilst the first samples the input signal again. By having some 20 stages in cascade, 20 delayed replicas of the sampled input signal are made available, and by suitably attenuating them and adding them the discontinuous delay line may be used to synthesize system weighting functions.

3.3.2. Function simulators

In contrast to the delay-line synthesizers, which give a time series approximation to the weighting function, electronic simulators can be constructed which reproduce, section by section, the same scheme of dependence as is envisaged in the system under examination and again by adjustment of the parameters the system that will best fit the given auto- and cross-correlograms may be obtained. This technique is worth while if the principal operations in the system under examination are well defined.

If it is desired to find the parameters of a prescribed, and usually simple, law of form $W(p)$, that will best fit correlation data, it is convenient to simulate, by means of d.c. amplifiers and feedback circuits[9] a series of

simple factors such as p, $\dfrac{1}{p}$, $p+a$, $\dfrac{1}{p+b}$, and

$\dfrac{\omega_0{}^2}{p^2+2\alpha p+\omega_0{}^2}$ from which all stable, linear

transfer-functions must be composed. The system transfer-function is then obtained by connecting such elements in series or in parallel and summing their outputs with appropriate amplitudes until the output voltage of the analogue approximates that corresponding to the cross-correlogram.

4. Experimental Work

In order to examine the utility of this method of analysis experiments have been performed on two systems—first, on a theoretical system, and secondly, on a small servo-system which was subjected to a quasi-random input signal.

In each case the appropriate correlograms were produced by cathode-ray-tube curve-followers at a repetition rate of three times per second. The signal corresponding to the auto-correlogram was fed into a function simulator which could reproduce transfer functions of the form

$$W(p) = K \cdot \frac{p+a}{p+b} \cdot \frac{\omega_0^2}{p^2 + 2\alpha p + \omega_0^2}$$

The output of the simulator was compared with the cross-correlogram $V_c(\tau)$, either directly on an oscilloscope or by displaying the mean square error on a meter. The general scheme was the same as that shown in Fig. 3. The gating signal for the error measurement was obtained from a mono-stable multivibrator triggered by a contact on the shaft of the curve-followers, and this signal was used to open and close a high-speed relay in the input circuit of the mean-square-error meter.

4.1. Experiments based on a Theoretical Example

To obtain data, from a theoretical system, which can be used to test the process described above, a cross-correlogram was calculated for a theoretical system with the transfer function

$$W(p) = \frac{100(p+5)}{p^2 + 12p + 100}$$

which was presumed to be subjected to an input signal with an auto-correlation function of the form $A(\tau) = e^{-5}$, shown in Fig. 4. The calculation proceeded thus: using the two-sided Laplace transform in order to deal with time functions in negative τ, the transform of $A(\tau)$ becomes
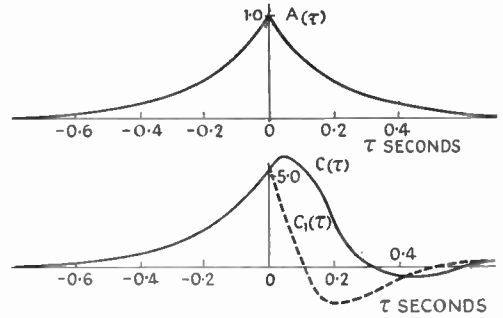
$$A(p) = \frac{1}{(5+p)} + \frac{1}{(5-p)}$$

Fig. 4. Correlograms for the theoretical example.

where the inverse transform of $1/(5+p)$ exists only for $\tau > 0$ and the inverse transform of $1/(5-p)$ exists for $\tau < 0$.

The transform of the cross-correlogram is given by the product $W(p) \cdot A(p)$ and in order to simplify the analysis, one of the factors of $W(p)$ was chosen to correspond with one in $A(p)$, thus

$$C(p) = \frac{100(p+5)}{p^2 + 12p + 100} \left(\frac{1}{5+p} + \frac{1}{5-p} \right)$$

Expanding this in two parts corresponding to the two parts of $A(\tau)$, the negative side of $A(\tau)$ yields

$$C(\tau) = 5 \cdot 41 \, e^{5\tau} \text{ for } \tau < 0$$

and

$$C_1(\tau) = 5 \cdot 41 \, e^{-5\tau} \left(\cos 8\tau - \frac{15}{16} \sin 8\tau \right) \text{ for } \tau > 0$$

which is shown dotted in Fig. 4.

The positive side of $A(\tau)$ yields

$$C_2(\tau) = \frac{100}{8} \, e^{-5\tau} \sin 8\tau \text{ for } \tau > 0,$$

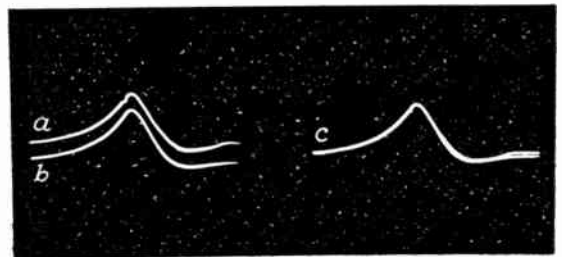and on combining them we obtain the cross-correlogram $C(\tau)$ shown in full in Fig. 4.

Fig. 5. Oscillograms of actual and synthesized cross-correlograms.
(a) Cross-correlogram $C(\tau)$
(b) Synthesized cross-correlogram $V_c(\tau)$
(c) Superposition of (a) and (b)

In applying the method of analysis described in Section 3.3.2 to these data, the correlograms were reproduced by the curve-followers, and the analogue was adjusted to give minimum mean-square error. The oscillograms shown in Fig. 5 show the quality of fit between the synthesized and the actual cross-correlograms. The corresponding frequency-response vector loci are compared with the theoretical locus $W(j\omega)$ in Fig. 6, where it will be seen that the agreement is good. The functional form of $W(p)$ and $W(j\omega)$ can be found, if desired, from the settings of the controls of the various units of the analogue circuit.

Fig. 6. Comparison of theoretical and experimental frequency-response loci.

4.2. *Tests on a Servo-System*

In this case a small servo-system was subjected to a fluctuating input signal produced by manual movements of a potentiometer. The aim was to simulate a random signal with a bandwidth as wide as that of the servo-system. In the event it proved that the bandwidth of the perturbations fell short of this requirement.

The correlograms of the input and output data were computed by equations such as equation (4), and once again the transfer function was synthesized by the function simulator. The experimental correlograms are shown in Fig. 7, and in Fig. 8 two synthesized frequency-response vector-loci are compared with the measured response of the actual servo-system, where it will be seen that there is good agreement up to 1·4 c/s. In fitting this correlogram in the time domain the relative mean-square-error $\dfrac{e^2}{V_{c^2}(\tau)}$ was of the order of 1·0 per cent. and equally good qualities of fit were obtained for each of the two transfer functions, although they differed by a factor $1/(p+b)$. The reason for this is that the
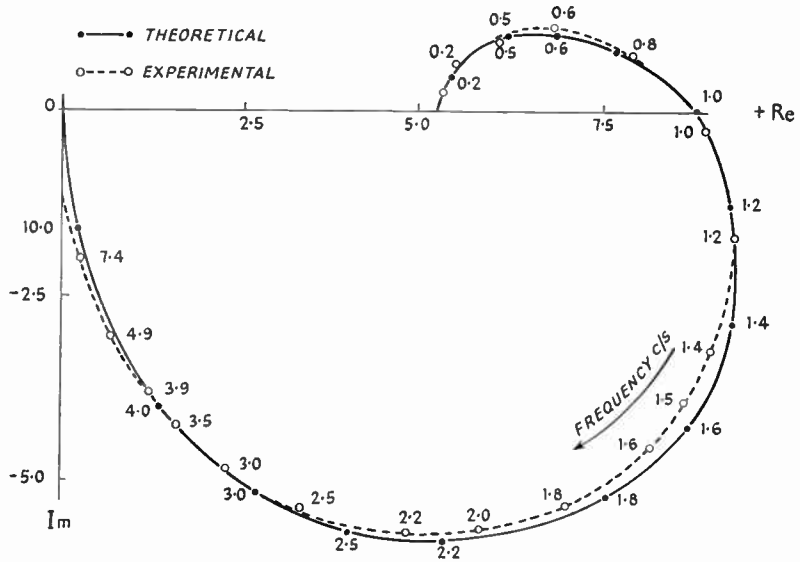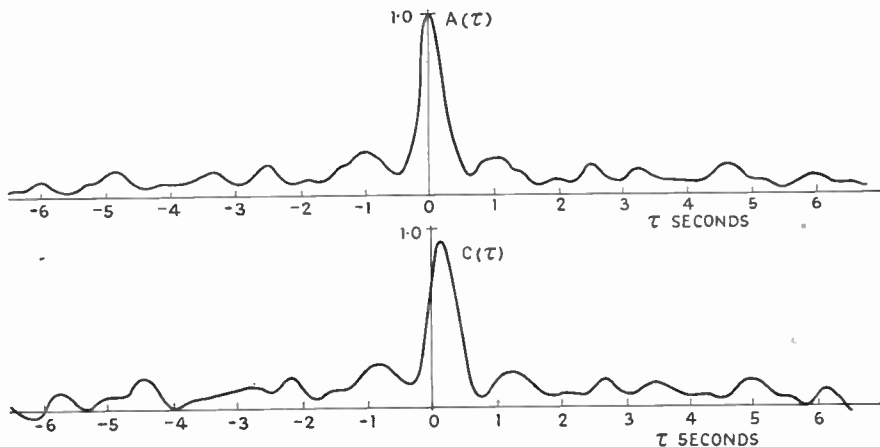

Fig. 7. Normalized correlograms for the servo-system.

frequency spectrum of the input signal is deficient in high frequency components and there is therefore an inadequate stimulus to reveal, with certainty, the existence of the $1/(p+b)$ term, which is apparent in the measured frequency response.

In this case the frequency spectrum of the input signal extended from $0-1$ c/s, whilst the cut-off frequency of the servo was about 1.5 c/s. These results serve to remind one that the bandwidth of the stimulus should be wider than that of the system under examination. A further point that should be noted is that calculating correlograms from time series, with an ordinate spacing of $\triangle$, eliminates all frequencies greater than $f_c = 1/2\triangle$; in our case $f_c = 3$ c/s, so frequency-response data for higher frequencies is of no value.

————————measured response of servo

$$\frac{104}{p^2 + 10 \cdot 2p + 103}$$

o ——— o) synthesized
• ——— •) responses

$$\frac{152}{(p^2 + 10 \cdot 9p + 146)(1 + 0 \cdot 052p)}$$

Fig. 8. Comparison of frequency-response loci for the servo-system.

5. Conclusions

The experimental results show that provided certain conditions are satisfied by the input signal, namely

(a) that its bandwidth is wider than the bandwidth of the system under examination;

(b) that the records are long enough to approximate to a stationary time series;

(c) that the sampling interval used in the numerical calculation of correlograms is short enough;

then it is practicable to derive system transfer functions from normal operating data. If the normal operating data is deficient in respect of (a) there is no objection to deliberately superimposing additional perturbations on the input signal.

In general, one should be cautious in attempting to identify terms in the transfer functions, so derived, with operations in the actual system unless some further information is available, for the transfer function is merely a best approximation using a limited number of terms. However, this is a temptation that few will resist.
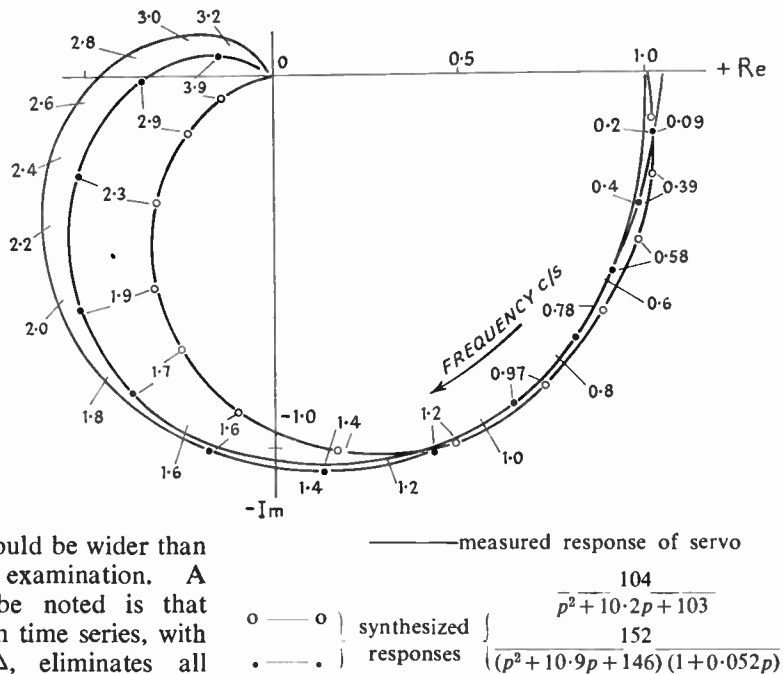
6. References

1. J. G. Henderson, "A mechanical harmonic analyser and some applications to servo systems," *Engineering,* **173**, p. 52 and p. 68, 1952.

2. D. G. Tucker, "An analogue computer for Fourier transforms," 1957 Convention paper. *J.Brit.I.R.E.,* **18**, April 1958 (To be published).

3. T. P. Goodman and J. B. Reswick, "The determination of system characteristics from normal operating data," *Trans. Amer. Soc. Mech. Engrs,* **79**, p. 259, 1956.

4. J. M. L. Janssen and L. Ensing, "The electroanalogue, an apparatus for studying regulating systems," *Philips Tech. Rev.,* **12**, p. 257 and p. 319, 1950-51.

5. H. Bell and V. C. Rideout, "A high-speed correlator," *Trans. Inst. Radio Engrs,* **EC-3**, No. 2, p. 30, June 1954.

6. F. E. J. Girling and E. F. Good, "The Leapfrog Feedback Filter," R.R.E. Memo. No. 1176.

7. J. M. L. Janssen, "Dis-continuous low-frequency variable delay-line with continuously variable delay," *Nature,* **169**, p. 148, 26th January 1952.

8. R. M. F. Houtappel, "Properties of a feed-back system analogue based on a dis-continuous delay-line synthesizer," *Proc. Instn Elect. Engrs,* **103**, Part C, p. 367, 1956.

9. G. A. Korn and T. M. Korn, "Electrical Analogue Computers." (McGraw Hill, New York, 1952.)

621.317.351.029.6 : 621.3.018.7

Wave-form observation of electron current using travelling-wave cathode-ray tubes. H. MAIDA. *J. Inst. Elect. Commun. Engrs., Japan* **11**, pp. 1171-1177, November 1957.

The anode currents in a v.h.f. beam tetrode operating at 100 Mc/s are observed on an experimental cathode-ray-tube. The effects on the oscillogram of termination of the deflecting line are shown. Some typical bunched electron currents in a velocity modulated beam, which have been only estimated by the electron ballistic theory, are experimentally observed for the first time by oscillograms. It is considered that high-frequency oscillography of the electron currents shows the possibility of profitable use of the travelling-wave c.r.t. for experimental study of microwave tube operation.

621.317.799 : 621.385.3 / 5.012

A measuring device for transmitting tube characteristics. J. W. A. VAN DER SCHEER. *Het PTT-Bedrijf*, **8**, pp. 95-100, January 1958.

A measuring device for transmitting tube characteristics is described, which for any anode dissipation enables all voltages and currents to be read simultaneously on meters. The measurements can also be made in case of positive grid voltages, without the admissible dissipation being exceeded. The measuring device is suitable for transmitting tubes of a power of not more than about 50 kW, and it can be operated by semi-skilled personnel.

621.372.56

The frequency response of cut-off attenuators with coaxial launching and pick-up probes. A. SANDER. *Nachrichtentechnische Zeitschrift*, **11**, pp. 1-5, January 1958.

The frequency response of two types of capacitively-coupled cut-off attenuators is calculated. The attenuation ratio is independent of wavelength in the first case and proportional to wavelength in the second case. Equivalent circuits are given.

621.372.62

On the synthesis of three-terminal networks composed of two kinds of elements. K. M. ADAMS. Doctorate Thesis, Technological University of Delft, 66 pp. October 1957.

The synthesis of series-parallel LC three-terminal networks is investigated. A set of necessary and sufficient conditions and a method of realization of all sets of series-parallel LC three-terminal-network functions from the zeroth to the sixth degree are given. Some of these conditions are essentially new, i.e., independent of any previously derived conditions. They are necessary for the synthesis of series-parallel LC three-terminal networks, but it is not known whether they are also necessary for the synthesis of three-terminal networks of arbitrary structure. In principle, it is possible to apply the method to functions of higher degree than the sixth, but the amount of computation required increases in general very rapidly with the degree.

A selection of abstracts from European and Commonwealth journals received in the Library of the Institution. Members may borrow these journals under the usual conditions. All papers are in the language of the country of origin of the journal unless otherwise stated. The Institution regrets that translations cannot be supplied.

621.372.823.2 : 621.372.814

Mode conversion losses in transmission of $TE_{01}{}^0$ modes through conically tapered waveguides. S. KUMAGAI, N. KUMAGAI and H. OHBA. *J. Inst. Elec. Commun. Engrs., Japan*, **11**, pp. 1203-1209, November 1957.

Some general expressions are derived for the coupling coefficients between the circular electric normal modes in the cylindrical and conical waveguides. The mode conversion losses of the incidental $TE_{01}{}^0$ mode propagation through a conically tapered guide which connects two cylindrical guides of different sizes are reated mathematically and estimated numerically. The normal modes of transmission through conical waveguide are also discussed. The "equivalent cut-off wavelength" and the "equivalent attenuation constant" of the transverse circular electric normal modes of conical guide, $TE_{0p}{}^v$, are obtained by using the first order perturbation. ($TE_{01}{}^0$ refers to a TE_{01} mode in a cylindrical guide whereas $TE_{0n}{}^v$ refers to a TE_{0n} mode in a conical guide). Some numerical examples of the equivalent attenuation constants of $TE_{01}{}^v$ mode are illustrated for various parameters.

621.374.3 : 621.314.7

Non-saturating junction transistor flip-flop circuits. K. AOYAGI, K. MIYAWAKI and J. SASAKI. *J. Inst. Elec. Commun. Engrs., Japan*, **11**, pp. 1196-1202, November 1957.

Describes the principle of bistability and the steady state non-saturation from the results of analysing and synthesizing the junction transistor multivibrator circuit.

621.374.4.029.6 : 621.314.63

The efficiency of microwave frequency multiplier using a crystal diode. S. OKAMURA and T. OHKOSHI. *J. Inst. Elect. Commun. Engrs., Japan*, **11**, pp, 1190-1196, November 1957.

The optimum matching and bias-voltage conditions are investigated and the maximum efficiencies are calculated. The matching and the bias-voltage correlate with each other, and both depend on the characteristic of the crystal diode and the order of the harmonic desired.

621.374 / 5.02965

The generation and amplification of millimetric waves. W. KLEEN and K. POSCHL. *Nachrichtentechnische Zeitschrift*, **11**, pp. 8-19, January 1958.

The various methods for generating and amplifying millimetric waves are summarized. A wavelength of

187

approximately 0·6 mm. has been obtained from frequency multiplication by means of crystal diodes. Retarding field valves, reflex klystrons, double slot oscillators, backward-wave oscillators and multi-slot magnetrons are also suitable. Amplification at these frequencies has been achieved so far only with travelling-wave tubes. The highest frequencies produced with electronic valves have a wavelength of approx. 1·5 mm. Methods for radiation excitation of electrons are described also. The utilization of quantum effects in molecules appears to have particular possibilities as oscillators as well as amplifiers. Amplifiers operating on this principle are of a particular interest since noise figures can be expected which are one or several orders of magnitude smaller than those obtainable at present by means of other methods.

621.385.832

Automatic tracing of electron trajectories. O. CAHEN. *L'Onde Electrique, 37,* pp. 1098-1103, December 1957.

The data furnished by a rheostatic tank traces the trajectories of electrons in a space where the electric and magnetic fields possess a symmetry of revolution. A model, exactly reproducing the system under study, is immersed in the tank without taking account of the space charge. The model is therefore very easy to make. Corrections for space charge and for the magnetic field which can be calculated once and for all, are introduced with great precision by preset functional potentiometers, and are valid for all gun models. The first trace recorded gives directly the trajectory sought. This method avoids long calculations by successive approximations. It is the fastest known precision method.

621.395.623.43

Condenser (earphone) receiver. T. HAYASAKA and M. SUZUKI. *J. Inst. Elect. Commun. Engrs., Japan,* **11,** pp. 1151-1157, November 1957.

A condenser type earphone receiver using a titanium diaphragm of 0·0007 cm. thick is described. It is able to produce a sound pressure of about 15 dyne/cm^2 in a 6 cm^3 coupler (3% distortion), and is practical for use as a receiver in a master reference system for telephone transmission.

621.396.11

Interaction between radiated and surface waves and its application to long distance propagation. J. ROBIEUX. *L'Onde Electrique, 37,* pp. 1089-1097, December 1957.

Consideration is given to the propagation of guided waves along layers with dielectric constant greater than that of the surrounding substance. These waves radiate a part of their energy when they encounter an irregularity in the structure of the guide. The properties of this radiation are considered. They are applied to the description of a mechanism which explains the nature of tropospheric propagation for metre waves. The energy radiated can be captured by the horizontal layers which stratify the troposphere, and this energy can then be radiated towards the receiver which may be below the horizon from the transmitter.

621.396.677

A new way to the solution of the problem of wideband aerials. H. MEINKE. *Nachrichtentechnische Zeitschrift,* **10,** pp. 594-609, December 1957.

A novel explanation for the process of wave formation at a radiator is used for showing why the input

impedance and the radiation pattern of most aerials are a function of frequency. This also points a way for precautions which will lead to the design of aerials with very little frequency sensitivity. By means of a non-linear coordinate system the field equations are represented in a form, which will result in a suitable approximate solution for wide-band aerials of comparatively simple shapes.

621.396.75(93)

A new receiver for the Australian DME beacon. B. R. JOHNSON. *Proceeding of the Institution of Radio Engineers Australia,* **18,** pp. 423-430, November 1957.

A new beacon receiver which was designed to overcome problems of coverage and echo interference in the Australian DME system is described. The arrangement of the r.f. stages which provide a beacon triggering sensitivity of 3 V is briefly described and and operation and design criteria for the instantaneous automatic gain control used for echo suppression are discussed. The introduction of instantaneous automatic gain control imposes requirements on the video circuits of the receiver which are analysed. Result of field trials of a prototype equipment are given.

621.397.74

Transmission of video signals over local telephone lines. J. APPELDOORN and C. BAKKER. *Het PTT-Bedriff,* **8,** pp. 87-94, January 1958.

It appears possible to use local telephone lines for transmitting video signals for the 625-line television system. After a brief survey of the requirements and possibilities, amplifiers developed for this purpose are described. Some results of an experimental link are given.

681.142

A.D.A.—a transistor decimal digital differential analyser. M. W. ALLEN. *Journal of the Institution of Radio Engineers, Australia,* **29,** pp. 255-262, October-November, 1957.

The basic computing process of the digital differential analyser is described and alternative forms of machine organization are indicated. This is followed by illustrative examples of special functions and by a description of the logical organization of A.D.A. Circuit techniques and assembly and construction methods are discussed. To conclude, the specification of the machine is summarized and several problem diagrams are considered.

681.142 : 621.039

Analogue representation of heat exchange circuits. Application to exchangers in nuclear power stations. J. CARTERON. *L'Onde Electrique, 37,* pp. 1075-1082, December 1957.

The study on an analogue machine of the transient behaviour of a nuclear power station, leads to the solution of a number of problems which confront engineers engaged in projects of this type, but the amount of apparatus required for the analogue becomes greater as the accuracy of simulation is increased. Heat exchangers are particularly difficult to represent, and the paper suggests a practical method of simulation requiring only a small amount of apparatus but which gives a representation of real phenomena with good accuracy.

188

FREQUENCY MODULATION BY INDUCTANCE VARIATION:

A MAGNETICALLY-STABLE FERRITE MODULATOR*

by

F. Slater (Associate Member) †

SUMMARY

The factors affecting the production of frequency modulation are considered when the modulator is either a reactance valve or a variable inductance employing magnetic variation of the core permeability. It is shown that whilst the effectiveness of the reactance valve is reduced at high oscillator frequencies or with large fractional frequency deviations, the inductance modulator is not affected to the same extent. The losses inherent in the magnetic core of the inductance modulator are considerably reduced by using magnetic ferrites; such a ferrite modulator is described. The effects of magnetic hysteresis, in producing oscillator frequency instability, are minimized by applying a specific level of polarization from a permanent magnet. A figure of merit is developed by which the frequency instability can be calculated from a knowledge of the prevailing magnetic conditions. The ferrite frequency modulator is particularly suitable for use with variable frequency oscillators where the equipment is to be portable and free from spurious sub-harmonic outputs. Results are given which serve to indicate the performance of this modulator.

1. Introduction

The principle of the variable-inductance frequency modulator—that of changing the frequency of a *L-C* oscillator by magnetic alteration of the oscillator inductance—is not new, and there are many early examples of its use as a remote tuning device.[1] The main disadvantages, which prevented its ready acceptance, were those of low current sensitivity, high radio-frequency loss, and hysteresis.

In 1951, H. Boucke published in Germany[2] the description of a successful variable-inductance frequency modulator using a laminated nickel-iron core in preference to one of metallic dust. The magnetizing current requirements, however, were very large—being of the order of 100 mA for steady magnetization and 50 mA for modulating current, for a frequency deviation of 1 Mc/s at a carrier frequency of 80 Mc/s.

A satisfactory solution to the problem of current sensitivity did not occur until the mixed

magnetic ferrite had been commercially developed. This homogeneous material with a high initial permeability was readily responsive to variations in the modulating current and furthermore its radio-frequency loss properties were excellent.

In the ferrite modulator—later to be described—the effect of magnetic hysteresis was reduced to a minimum by a choice of the level of polarizing field, and the modulator is now used in several commercially available signal generators. It has the advantage that by its use the range over which a variable-frequency oscillator can be tuned and also frequency modulated is considerably extended without the use of multipliers.

2. The Reactance Valve Modulator

The reactance valve is the most commonly used frequency modulator either singly or in push-pull forms. Its limitations spring, in the main, from the need to maintain, at the oscillator frequency a 90-deg. phase shift between anode and grid of the reactance valve, and from the need for a linear change of slope with grid voltage.

As a result of these limitations a reduction in efficiency occurs at the ultra-high frequencies and at the low frequencies—where high

fractional frequency deviations are more likely to be encountered.

It is desirable with the frequency-modulated tuned oscillator that the frequency deviation be independent of the oscillator frequency. Yet in fact the sensitivity of the modulator changes when the tuning element is changed, the law depending upon whether the modulator is inductive or capacitive and upon which element of the L-C circuit is changed. To compensate for this variation in modulator sensitivity the modulating input is usually varied with the tuning element. However, at the higher oscillator frequencies the reactive polarity of the modulator may be determined by the valve and associated components—such as the stray capacitances—giving an intractable law to the modulator sensitivity. Furthermore, the reactive polarity may change in an arbitrary manner as the oscillator is tuned, making it impossible to track the audio input to the modulator sensitivity.
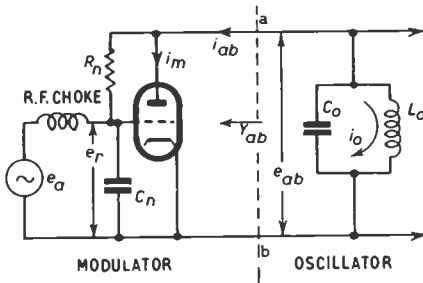
Fig. 1. Circuit of the reactance valve modulator.

The grid base of the modulator valve is occupied by a selected fraction of the oscillator radio-frequency voltage and also by the audio-frequency voltage. When both oscillator and audio-frequency voltages are high the limits of the linear mutual conductance grid base are exceeded and distortion of the modulation results. These factors are considered in more detail in the next few sections.

2.1. *The Reactance Valve Modulator—Ultra High Frequency Operation*
The importance of maintaining the desired 90 deg. phase relationship between anode and grid of the reactance valve has already been mentioned; the polarity and magnitude of the simulated reactance being dependent upon this relationship. The circuit of the modulator is shown in Fig. 1. In this circuit the phase-shifting network $R_n C_n$ is connected so as to retard the phase of the radio-frequency voltage applied to the grid; hence the valve will normally simulate an inductance connected across points a and b.

When the oscillator is tuned over a wide range of frequencies, the electron transit time changes with frequency, and this can modify the reactive polarity.

An approximate relationship between g_m and the transit angle θ of the modulator valve is given by

$$\theta = \frac{4\pi . f_c . C_{gc}}{g_m} \qquad \ldots\ldots\ldots(1)$$

The transit angle is equal to ωt radians where t is the electron transit time in seconds.

Equation (1) shows that the transit angle is affected by the mutual conductance of the valve and by the oscillator frequency f_c. When the transit angle has a value between zero and π the input admittance (Y_{ab}) of the reactance valve is approximately represented by a shunt conductance and a shunt inductive susceptance, as for the low-frequency case.[3] The low-frequency case does not hold at u.h.f. If θ is equal to 2π the susceptance becomes capacitive with the same $R_n C_n$ configuration. Using lumped circuits at u.h.f., changes in mutual conductance and in oscillator frequency are able to alter the transit angle sufficiently to cause the modulator to simulate a capacitance. The modulator sensitivity and its law with respect to the tuning element (Sect. 2.2) are changed by this.

The phase-shifting network at lower frequencies is unaffected by stray capacitances of the valve and circuit, but becomes increasingly sensitive to these as the frequency is raised. This is an additional factor in the reduction of efficiency of the modulator at u.h.f.

2.2. *Change in Sensitivity with Oscillator Frequency*
In a tuned oscillator which is frequency modulated, the frequency deviation is usually required to be independent of the tuning over

190

a band of frequencies. The nearest approach to this which is obtainable with the standard reactance valve circuit is when the deviation is either directly or inversely proportional to the oscillator frequency over the band. This occurs when the reactances of the tunable element and the modulator are of different polarity, i.e. one capacitive and one inductive or vice versa. The four conditions for an L-C circuit are as follows:

(a) Inductive modulator, capacitor tuned: The frequency deviation is directly propor-·tional to the oscillator frequency over the range of the tuning element.

(b) Capacitive modulator, inductor tuned: as for (a).

(c) Inductive modulator, inductor tuned: frequency deviation is inversely proportional to the oscillator frequency over the range of the tuning element.

(d) Capacitive modulator, capacitor tuned: The frequency deviation is directly proportional to the third power of the frequency over the range of the tuning element.

In the majority of cases arrangement (a) is used, and a variable resistance is ganged to the tuning capacitor linearly reducing the audio input to the modulator as the oscillator frequency is increased. At oscillator frequencies of about 100 Mc/s the capacitive type is frequently used, the anode–grid capacitance providing, together with a low value resistor from grid to earth, the phase-shifting network. A circuit using this type of modulator, if free from the effects of transit angle changes, will have a modulator sensitivity proportional to the third power of the oscillator frequency.

The wide-range modulated oscillator giving continuous cover from, say, 10 to 500 Mc/s obviously presents difficulties both in obtaining the modulation and in making it independent of the tuning. The modulator could not be allowed to change its polarity over this frequency range.

In practice such wide-range modulated oscillators have, in the past, employed frequency multipliers, tuned and ganged, to cover this tuning range.

2.3. Fractional Frequency Deviation

Limits are imposed upon the fractional

frequency deviation by the available linear mutual conductance base, and by the peak value of the oscillator tuned circuit voltage.

The maximum deviational sensitivity of an ideal reactance valve modulator operating in Class A conditions is obtained when $e_r = e_a = \frac{1}{2}E_g$. Then the maximum fractional frequency deviation is given by Winlund[4] as

$$\frac{\delta f_c}{f_c} = \frac{g_m \cdot e_r}{8\pi \cdot f_c \cdot e_{ab} \cdot C_0} \qquad \ldots\ldots\ldots(2)$$

When e_{ab} is large compared with e_r (large angle of lag of e_r) then

$$\frac{e_r}{e_{ab}} = \frac{1}{\omega \cdot C_n \cdot R_n} = \frac{1}{\tan\theta_n} \qquad \ldots\ldots\ldots(3)$$

where θ_n is the angle of phase shift provided by the network $C_n R_n$. And if $\theta_n = 84°\ 18'$ $e_r/e_{ab} \cong 0.1$, then eqn. (2) becomes

$$\frac{\delta f_c}{f_c} = \frac{0.1\ g_m}{8\pi \cdot f_c \cdot C_0} \qquad \ldots\ldots\ldots(4)$$

At high frequencies the stray capacitances across R_n and C_n affect the values and properties of the phase-shifting network; whereas at low frequencies, say 1 Mc/s, the available fractional deviation for minimal distortion is usually inadequate. The closer θ_n is taken to 90 deg. the smaller the fractional deviation, however, the spurious amplitude modulation is also reduced.

2.4. General Comments

The two main factors affecting the operation· of the reactance valve modulator are thus the need for a grid base in which the mutual conductance is linear with applied voltage, and the need for a phase-shifting network.

The sum of the peak r.f. and a.f. voltages applied to the grid has to be accommodated in the linear mutual conductance range and the sensitivity of the modulator is affected by the relative proportions of these voltages.

The phase-shifting network is affected at high frequencies, by stray capacitances and there are electron transit time effects within the valve.

At low frequencies a compromise may have to be reached between the attenuation of the phase-shifting network, so as to reduce e_r when

e_{ab} becomes high, and the attainment of an adequate fractional frequency deviation.

3. Inductance Variation

An alternative method of obtaining frequency modulation is to vary the core permeability of an inductance in sympathy with the modulating
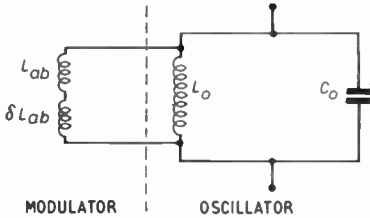
Fig. 2. Showing the modulator inductance connected across the oscillator tank circuit.

signal and to connect the inductance across the resonant circuit of an oscillator (Fig. 2). It is a method attractive in its fundamental simplicity.

The frequency of the oscillator will be determined, at any instant of the modulating cycle, by the permeability of the core at that instant.

3.1. Fractional Frequency Deviation

The fractional frequency deviation, using the circuit of Fig. 2, is given by

$$\frac{\delta f_c}{f_c} = - \frac{\delta L_{ab} \cdot L_t}{2 \cdot L_{ab}^2} \qquad \text{........(5)}$$

for which proof is given in the Appendix.

For a toroidal coil former, δL_{ab} is given by

$$\delta L_{ab} = \delta \mu_s \left(\frac{2 \cdot N_2^2 \cdot A_2}{r_2} \times 10^{-9} \right) \text{........(6)}$$

The fractional frequency deviation of eqn. (5) is thus directly proportional to a small change in the permeability of the radio-frequency core of the modulator.

3.2. Radio-frequency Core Loss

An important factor in the operation of this type of modulator is the radio-frequency core loss since this will be reflected across the tank circuit of the oscillator. The loss is apparent as an increase in the series resistance of the inductance upon the core and is caused by the power dissipation in the core. The characteristics of the core material are important in

determining the extent of this loss.

At low flux densities the losses of the core material can be expressed in terms of the total equivalent loss resistance (R_{tot}) as follows[5,6]:

$$\frac{R_{tot}}{\mu_a \cdot f \cdot L} = C_e \cdot f + C_h \cdot B_{max} + C_r \text{........(7)}$$

where the individual losses are represented by their loss coefficients which are dimensionless. These are as follows:

C_e is the eddy current loss coefficient. It is inversely proportional to the resistivity of the material and proportional to the diameter of the metal particles in the case of dust cores, or to the form and dimensions of the core in the case of ferrites.

C_h is the hysteresis loss coefficient. Hysteresis loss is proportional to the cube of the flux density for small flux densities, whilst C_h is proportional to B_{max}. In the case of ferrites this coefficient is affected by frequency, its value increasing with an increase in frequency.

C_r is the residual loss coefficient[7]; it does not contribute to harmonic distortion.[8] The residual loss coefficient, in the case of ferrites, is dependent to some extent upon frequency; for this reason eqn. (7) is rewritten for ferrites as

$$\frac{R_{tot}}{\mu_a \cdot f \cdot L} = C_e \cdot f + C_h \cdot B_{max} + C_r \cdot (f) \text{........(8)}$$

Equations (7) and (8) are based upon the Rayleigh hysteresis loop equations and are completely true only for materials obeying that relationship and for low flux densities where the measured permeability is not more than 10–20 per cent. greater than the initial permeability.

In ferrites, particularly of the nickel-zinc variety, the eddy-current losses are very small and residual loss usually accounts for the greatest part of the total loss. Although the losses of the core material increase with frequency the effect of such an increase can, to a great extent, be offset by the way in which the modulator is connected to the oscillator; this will be dealt with more fully later.

3.3. Harmonic Distortion

One effect of introducing magnetic materials into the modulating process is to increase the

harmonic distortion since the relationship between B and H is non-linear. However this can be minimized by applying a knowledge of the factors involved.

The distortion is a function of the core material and the conditions under which it is operated, [9, 10, 11]. The inverse ratio of the amplitude (V_1) of the modulating frequency to that (V_3) of its third harmonic is given by

$$\frac{V_3}{V_1} = \frac{0 \cdot 6}{2\pi} \cdot \mu \cdot C_h \cdot B_{max} \qquad \ldots\ldots\ldots(9)$$

The relationship is correct only for small values of a.c. magnetizing force.

3.4. R.F. Inductance and Self Capacitance

The self-capacitance of the radio-frequency winding is not a limiting factor in the performance of the modulator, since it is thrown across the oscillator circuit in the same way as the inductance of the modulator. The whole circuit is tuned to resonance and consequently a change in the modulator inductance produces an inductive change in the oscillator frequency. Tests on signal generators using the ferrite modulator have shown that the law of deviation sensitivity plotted against oscillator frequency consistently follows that to be expected from an inductive modulator.

3.5. Sensitivity and R.F. Loss

It is easily possible with this type of modulator to proportion the sensitivity and the radio-frequency loss. This is done by con-
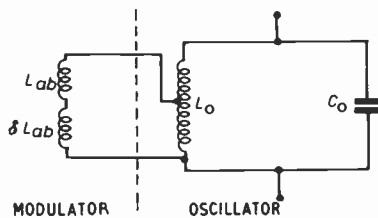

Fig. 3. To exchange sensitivity for a reduction in r.f. core loss the modulator coil, L_{ab}, can be tapped down the oscillator tuning inductance, L_0, as shown.

necting the modulator inductance (L_{ab}) across a smaller portion of the oscillator coil, as shown in Fig. 3. The overall sensitivity will be reduced but so will the circuit loss due to the presence of the modulator.

In this way, for a given deviation, the effect of the increase in modulator core loss, with increasing frequency, can be made quite small. This proportioning is particularly advantageous at the highest frequencies where the required fractional deviation, and consequently the modulator sensitivity, is small but where the inherent r.f. core loss is increasing. A reduction in spurious frequency modulation, which is not in the oscillator, can be accomplished in a similar way.

4. Core Materials

4.1. Dust Cores

The need to reduce eddy-current loss at high frequencies resulted in the development of metal dust cores where the metallic particles used had a high intrinsic magnetic permeability, but were diluted by an insulating binder. The effective permeability of such cores is much less than that of the metallic particles of which they are composed. The many gaps between the magnetic particles has the effect of making the effective permeability independent of the intrinsic permeability of the particles. This will be seen in the following equation for the effective permeability (μ_{eff}) of a gapped core. Thus

$$\frac{1}{\mu_{eff}} = \frac{(1 - a_a)}{\mu_c} + a_a \qquad \ldots\ldots\ldots(10)$$

where the intrinsic permeability is μ_c and a_a is the relative air-gap length. This equation shows that when the intrinsic permeability is large, the effective permeability will be independent of it and dependent only upon the relative air-gap length. In a dust core with many air-gaps the effective permeability is almost completely independent of μ_c and, consequently, of the magnetizing force H.

A modulator using a radio-frequency core of this material would be certain to possess a low sensitivity, since the greatest sensitivity is achieved by using a material in which the permeability changes readily with a change of magnetizing force. This is confirmed by the results obtained by Boucke[2] who in 1951 compared two modulators having radio-frequency cores of metallic dust and of laminated nickel-iron. On the basis of current sensitivity the laminated core was preferred

even at the operating frequency of 80 Mc/s. The current requirements of the modulator were very large, being of the order of 100 mA for steady magnetization and 50 mA for modulating current. The maximum deviation was 1 Mc/s and this limit was imposed by the restriction on the operating temperature of the modulator to 50°C.

4.2. *Mixed Magnetic Ferrites*

The magnetic ferrite as commercially developed is a homogeneous material of high electrical resistivity and high magnetic permeability. The permeability of the material is readily changed by a magnetizing force and the eddy-current loss is negligible. The greatest component of the loss is the residual loss. Magnetic ferrites are normally available in mixtures of manganese-zinc and nickel-zinc ferrites, the former having the higher permeability whilst the latter has the lower losses.

4.3. *Comparison between Dust Core and Ferrite*

To enable a comparison to be made between the dust core and the ferrite, the loss coefficients and the permeability for materials designed for approximately similar frequency ranges are shown in Table 1. The materials are a molybdenum-Permalloy dust core and a manganese-zinc ferrite—Ferroxcube A1. Some higher grade radio-frequency dust cores use carbonyl iron which ensures metal particles of spherical shape. The losses for these cores can vary widely, but average figures are given in the Table together with figures for a nickel-zinc ferrite—Ferroxcube B2.

Comparing the values given in these tables for dust cores and for ferrites, the most striking feature is the much greater permeability and lower eddy-current loss of the ferrites. In the B grades the eddy-current loss is sufficiently small for it to be neglected. Moreover, despite the fact that the initial permeability of ferrite is many times greater than that of the dust core, the loss coefficients are smaller.

However, these factors alone are not in themselves sufficient to account for the complete success of the material when used in a frequency modulator; it is the homogeneity of the material which is of paramount importance; it is this which makes it possible to change the permeability quite readily by a change in the magnetizing force.

5. The Ferrite Modulator
5.1. *General Form*

The commercial availability of the mixed magnetic ferrite has made possible the design of this compact frequency modulator with a high current sensitivity and low radio-frequency loss.

Some work has been done upon the design of magnetic circuits for use as magnetic tuning devices prior to 1938 in Germany and also in this country[1] and in the ferrite modulator the general form was followed. That is to say, a primary low-frequency winding of many turns was built up on a U-shaped core of thin Ni-Fe laminations (Fig. 4). This primary magnetic circuit served to provide the polarizing and modulating flux for the secondary magnetic circuit. The secondary magnetic circuit consisted of a small square sided "toroid" of nickel-zinc ferrite (Ferroxcube B3), supported in a mating fit between the open ends of the primary circuit U-laminations, and carrying the radio-frequency winding of the modulator. Sinusoidal flux variations in the primary

Table 1

Loss co-efficients of dust and ferrite core materials

	Mo —Permalloy	Ferroxcube A1	Carbonyl Iron	Ferroxcube B2
$C_e \times 10^9$	14	0·5	2·5	$4·5 \times 10^{-5}$
$C_h \times 10^6$	14·3	4·6	50	
$C_r \times 10^6$	143	40	250	80
Average μ_a	—	1200	—	200
μ_{eff}	14	—	20	—

magnetic circuit flowing through the ferrite core of the secondary circuit could evoke a sympathetic variation in permeability and, consequently, in the inductance of the radio-
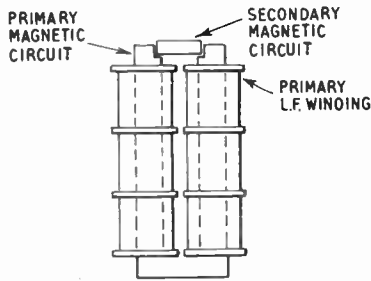

Fig. 4. The primary and secondary magnetic circuits of the ferrite modulator. The primary low frequency winding is also shown.

frequency coil. The radio-frequency coil connected across the oscillator inductance changed the oscillator frequency in sympathy with the original flux variation.

A steady polarizing flux is necessary to avoid magnetic frequency doubling when the sinusoidal flux is applied and the presence of this gives rise to a small amount of second harmonic distortion which is present in addition to the third harmonic "iron" distortion occurring through the non-linear relationship between B and H.

5.2. *Hysteresis Instability.*

The non-linear relationship between B and H also causes a form of frequency instability which is too great to be acceptable in most frequency modulator applications. This can be overcome by using a large polarizing flux.[12]

Let a section of a ferrite hysteresis loop be considered, as in Fig. 5. Here a ring of Ferroxcube B4 material has been placed in a steady magnetic field of 3 oersteds and the resulting flux density is 250 gauss. The permeability, B/H, at the working point is indicated by point 1.

Now let it be assumed that the ring of ferrite has a few turns of wire around it and that this inductance is connected across the tank circuit of the oscillator, having a frequency, f_1. The radio-frequency field across the ferrite is small.

If now a low-frequency field is applied to the ferrite, changing the magnetization by $+$ or -1 oersted, the permeability will vary from that at point 2 to that at point 4, with a mean
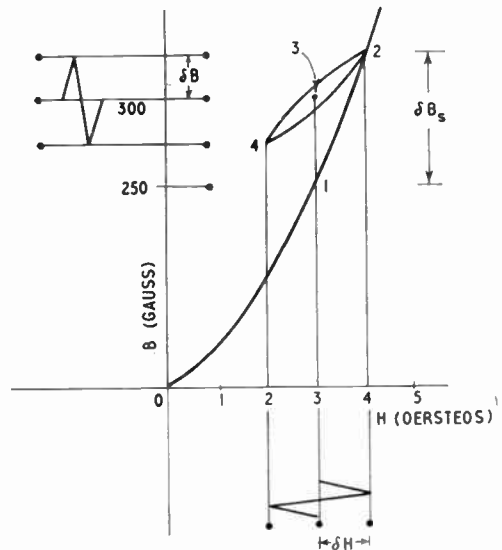

Fig. 5. A section of the ferrite hysteresis loop for Mullard Ferroxcube grade B4.

flux density of 300 gauss at point 3. The corresponding oscillator frequency variations, due to this change in permeability, will be from f_2 to f_4 with a mean at f_3.

If the alternating field is now reduced to zero, but the steady field left as before, the permeability will be that of point 3; this is the same as the mean permeability when the sinusoidal field was applied. Thus the application of a sinusoidal magnetizing force superimposed on a steady magnetizing force has resulted in a change of mean oscillator frequency from f_1 to f_3 and upon subsequent removal of the sinusoidal force the oscillator frequency remains at f_3.

To put it another way, the oscillator frequency before application of the modulation was f_1, but during and after modulation was f_3. The greater the amplitude of the sinusoidal magnetizing force, the greater will be the difference between f_1 and f_3.

Should the steady field now be reduced to

195

zero and then reapplied by increasing it to 3 oersteds, the permeability of the material will be that at point 1 and the oscillator frequency will have returned to f_1. A further application of the same sinusoidal force would again cause the mean oscillator frequency to be transferred to f_3.

5.3. Analysis of Hysteresis Instability

It is assumed that the radio-frequency magnetic field set up in the ferrite is very small compared with the modulating field. The frequency of the oscillator is determined at any instant of the modulating cycle by the radio-frequency permeability of the ferrite at that instant. The radio-frequency permeability is decided by two things: the inherent characteristics of the ferrite at the radio frequency concerned and the magnetic state of the ferrite at that time. The locus of the ferrite permeability as it changes over the modulating cycle is the minor hysteresis loop. It follows that the frequency deviation of the oscillator is caused by the variation of the radio-frequency permeability in its progress round the minor hysteresis loop.

The magnitude of the hysteresis instability is determined by the difference between the slopes of the major and the minor hysteresis loops at the operating point. The slope of the major loop at that point is the differential permeability, μ_d; this is shown in Fig. 6(a), the incremental permeability being shown in Fig. 6(b).

From Fig. 6(a) the differential permeability, μ_d, is given by

$$\mu_d = \frac{\delta B_s}{\delta H_s} \qquad \ldots\ldots\ldots(11)$$

The incremental permeability, μ_{inc} (Fig. 6(b)) is given by

$$\mu_{inc} = \frac{\delta B}{\delta H} \qquad \ldots\ldots\ldots(12)$$

The application of a steady magnetizing force to the ferrite, followed by the superimposition of a sinusoidal force, of amplitude δH (Fig. 6), changes the mean operating flux by $\delta B_s - \delta B$.

It is apparent from Fig. 6(b) that if the incremental and differential permeabilities were made equal the change $\delta B_s - \delta B$ would be zero and there would be no frequency instability

from this cause. By selecting a value of the steady magnetic field, H, this condition can be closely approached. An increase in H beyond the steep centre region of the major curve will reduce both the differential and the incremental permeabilities simultaneously. The sensitivity of the modulator—which is proportional to μ_{inc}—is reduced by this procedure but in a smaller proportion than the hysteresis instability since the later is affected by the reduction in both μ_d and μ_{inc}.

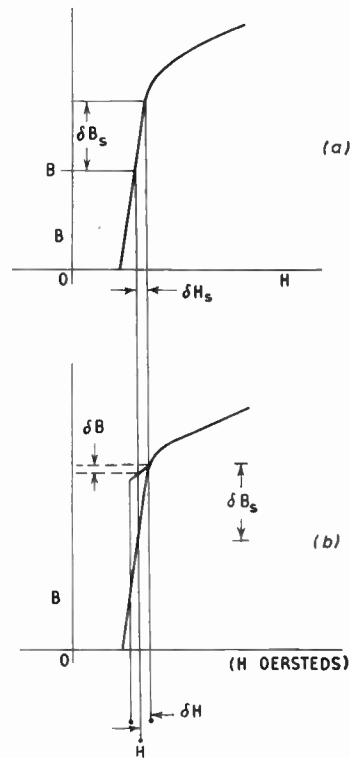In Fig. 6 the changes δB_s and δB are shown as caused by the same peak value of sinusoidal

Fig. 6. The differential permeability, μ_d, is shown in (a) whilst the incremental permeability, μ_{inc}, is shown in (b).

field, δH. Since this is a valid assumption an expression can be arrived at for the ratio of the oscillator frequency instability to the frequency deviation prevailing. Thus

$$\frac{\text{oscillator frequency instability}}{\text{frequency deviation}} = \frac{\delta f_{c1}}{\delta f_c} \ldots\ldots\ldots(13)$$

196

When δH is small compared with H_{dc},

$$\frac{\delta f_{c1}}{\delta f_c} = \frac{\delta B_s - \delta B}{\delta B} \qquad \ldots\ldots(14)$$

$$= \frac{\delta B_s}{\delta B} - 1 \qquad \ldots\ldots(15)$$

Then since

$$\frac{\delta H_s}{\delta B_s} = \frac{1}{\mu_d}$$

and $\quad \delta H_s = \delta H$

and $\quad \delta H = \dfrac{\delta B}{\mu_{inc}}$

$$\frac{\delta B}{\delta B_s} = \frac{\mu_{inc}}{\mu_d} \qquad \ldots\ldots(16)$$

Substituting eqn. (16) into eqn. (15) provides

$$\frac{\delta f_{c1}}{\delta f_c} = \frac{\mu_d}{\mu_{inc}} - 1 \qquad \ldots\ldots(17)$$

and $\quad \dfrac{\delta f_{c1}}{\delta f_c} \parallel \sigma - 1 \qquad \ldots\ldots(18)$

where $\sigma \ (= \mu_d/\mu_{inc})$ is to be known as the figure of merit for oscillator instability.

Equation (17) expresses the fractional frequency instability in terms of kc/s oscillator shift per kc/s frequency deviation. It thus takes into consideration both the stability and the modulator sensitivity.

When the figure of merit (σ) is equal to unity the slopes of the major loop and the minor incremental loop will be the same, and the frequency shift due to hysteresis instability will be zero. Using the curves of Figs. 7 and 8,
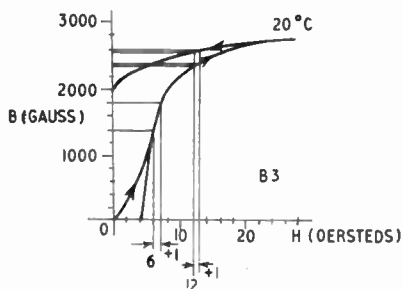

Fig. 7. B-H loop of Mullard Ferroxcube B3 with fields superimposed.

taken from a manufacturers' catalogue, the differential permeability, μ_d, and the incremental permeability, μ_{inc}, can be found for a given value of steady magnetizing field H. By this means, using eqn. (17), different projected

modulator designs can be compared for frequency stability.

Thus from Fig. 7, for a value of $H = 6$ oersteds and a variation of 1 oersted, the differential permeability, μ_d, will be 400. And the incremental permeability, μ_{inc}, will be 40—assuming that μ_{inc} is substantially independent of B_{max} at these values, the curve of Fig. 8 being taken for $B_{max} = 10$ gauss.
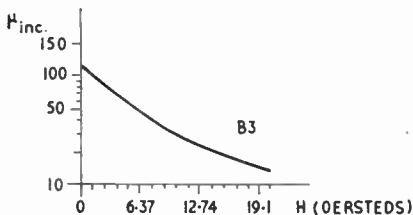

Fig. 8. Incremental permeability of Mullard Ferroxcube B3.

For these values the figure of merit will be given by:

$$\sigma = \frac{\mu_d}{\mu_{inc}} = \frac{400}{40} = 10$$

In the case of a steady magnetizing field of 12 oersteds and a variation of $+1$ oersted on the ascending curve of the B/H loop—

$\mu_d = 40; \quad \mu_{inc} = 35; \quad \sigma = 1 \cdot 6.$

With the same magnetizing field of 12 oersteds $+1$ oersted variation but occupying a position on the descending curve of the B/H loop—

$\mu_d = 20; \quad \mu_{inc} = 25; \quad \sigma = 0 \cdot 8.$

Substituting in eqn. (17) these values for σ gives—

(a) Steady field 6 oersteds—$\delta f_{c1}/\delta f_c = 9$.

(b) Steady field 12 oersteds—ascending curve:
  $\delta f_{c1}/\delta f_c = 0 \cdot 6$.

(c) Steady field 12 oersteds—descending curve:
  $\delta f_{c1}/\delta f_c = -0 \cdot 2$.

The improvement between (a) and (b) is 15 times, whilst that between (a) and (c) is 45 times. The negative field of (c) indicates that with the values of steady and alternating magnetic fields used the fractional frequency instability has been slightly over-corrected.

In illustrating the effect upon the fractional frequency instability of changes in the value of the steady magnetizing field a sinusoidal field of $+$ or $-$ 1 oersted was used, this was chosen

mainly for ease of illustration when using the reproduced curves. In practice, however, the amplitude of the normal sinusoidal variation would be much smaller than this.
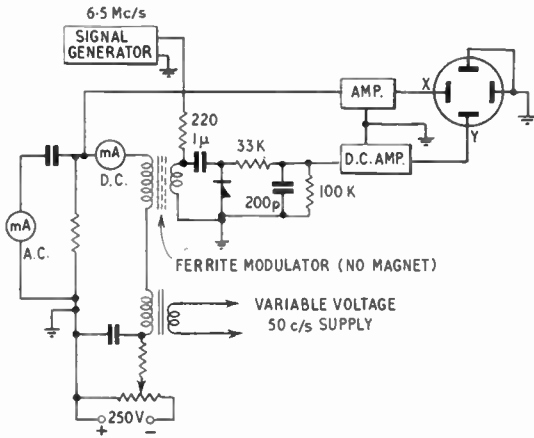

Fig. 9. A circuit for the display of r.f. inductance v. magnetizing current of the ferrite modulator.

5.4. Experimental Confirmation.

Experiments were carried out to check the assumptions made in sections 5.3 and 5.4. A ferrite modulator with variable d.c. magnetizing field was connected in the circuit shown in Fig. 9. A sinusoidal modulating field was applied and the frequency deviation checked for various values of d.c. field. The ferrite was demagnetized before each experiment. One trace obtained showing the position and angle of the incremental permeability loops is shown in Fig. 10. The graph shown in Fig. 11 has been prepared from the actual oscillograph traces and, therefore, shows the characteristics of the particular sample of ferrite under test. The modulator was later connected across an oscillator circuit at a fixed carrier frequency and the frequency deviation noted when a sinusoidal voltage, of the same amplitude as in the previous experiment, was applied.

5.4.1. Frequency deviation

It is assumed that the frequency deviation is caused by the variation of the radio frequency permeability of the ferrite core around a minor hysteresis loop. This is borne out by Fig. 11

which shows the change of the radio-frequency inductance produced by a sinusoidal field superimposed upon different values of d.c. magnetizing fields. These can be correlated against the frequency deviation produced.

Referring to the descending section of the curve shown in Fig. 11: at 6 or 12 mA d.c. the change of inductance expressed as trace length in millimetres for the respective minor loops is as follows:—

6 mA; 2·5 mm |
12 mA; 2 mm | An increase at 6 mA of 25%.

The comparative frequency deviations obtained with the same d.c. input were:

6 mA; 65 kc/s |
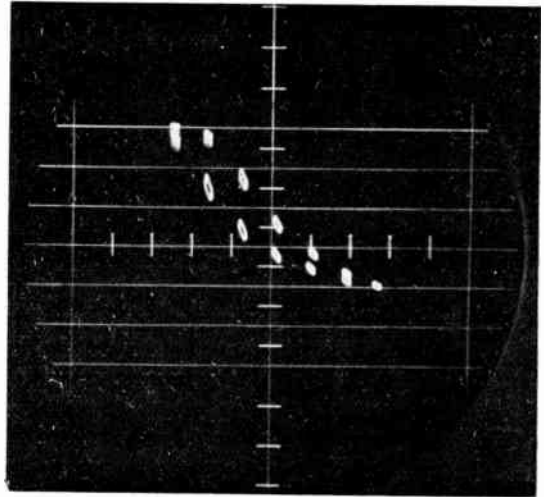12 mA; 48 kc/s | An increase at 6 mA of 35%.

Fig. 10. An oscillogram of some minor hysteresis loops obtained with the ferrite modulator using Ferroxcube B3.

Results which can be considered to coincide when allowance is made for the errors of measurement. If however the slopes of the two minor loops are compared then:

$$6 \text{ mA}; \tan 80° = 5·67$$
$$12 \text{ mA}; \tan 60° = 1·73$$

The change in inductance evoked by the minor loops is clearly correlated with the frequency deviation, whereas the change in slope of the minor loop is not.

198

5.4.2. Oscillator frequency instability (δf_{c1})

This is caused by a change in the radio-frequency permeability of the ferrite when the minor loop is first formed. On the rising curve (I increasing) the change of permeability is

Fig. 11. A graph prepared from the oscillogram showing the major and minor hysteresis loops Ferroxcube B3.

negative. on the falling curve (I decreasing) it is positive. The phenomenon can be seen in action on an oscillograph screen using the circuit of Fig. 9. The change observed in terms of trace length is shown in Fig. 11 from the point marked with a cross to the point marked with a circle.

5.4.3. Relation between carrier frequency instability (δf_{c1}) and frequency deviation (δf_c)

If the inductance change causing the change of carrier frequency is given as L_x and that causing the frequency deviation L_y then

$$\frac{L_x}{L_y} = \frac{\delta f_{c1}}{\delta f_c}$$

and eqn. (14) provides

$$\frac{\delta f_{c1}}{\delta f_c} = \frac{\delta B_s - \delta B}{\delta B} \qquad \dots\dots\dots(14)$$

Now $\qquad \dfrac{L_x}{L_y} = \dfrac{K_x \cdot \mu_x}{K_y \cdot \mu_y}$

and if $K_x = K_y$ and $H_x = H_y = H_{dc}$ also that δH is small compared with H_{dc}.

Then—

$$\frac{L_x}{L_y} = \frac{B_x}{B_y}$$

Referring to Figs. 6(a) and (b) it is apparent that

$$B_x = \delta B_s - \delta B$$

also $\quad B_y = \delta B$

Therefore,

$$\frac{L_x}{L_y} = \frac{\delta B_s - \delta B}{\delta B} = \frac{\delta f_{c1}}{\delta f_c}$$

Since both δf_{c1} and δf_c can be represented in terms of inductance change (or oscillograph trace length) derived from Fig. 11 and since values have also been obtained in terms of frequency for δf_{c1} and δf_c, it should be possible to correlate the ratios of these results and so to justify the theory upon which eqn. (14) is based:—
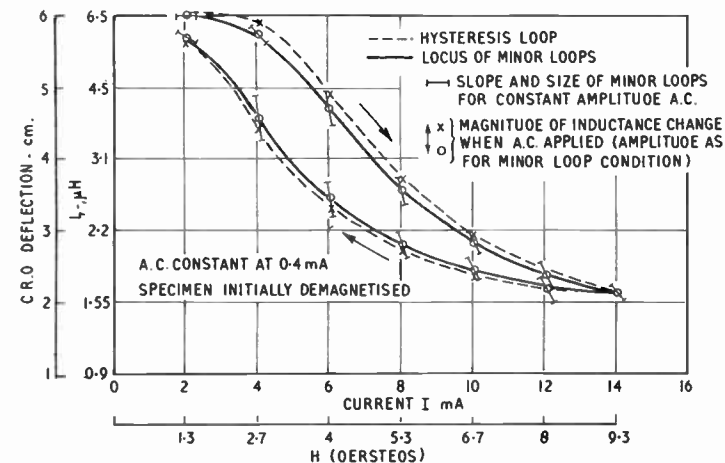
I_{dc}	Using Fig. 11 $\dfrac{\delta f_{c1}}{\delta f_c}$	Using modulated oscillator $\dfrac{\delta f_{c1}}{\delta f_c}$
4 mA ($>$)	$\dfrac{1 \cdot 5}{1 \cdot 25} = 1 \cdot 2$	$\dfrac{50}{40} = 1 \cdot 25$
6 mA ($>$)	$\dfrac{2}{3} = 0 \cdot 67$	$\dfrac{50}{65} = 0 \cdot 77$
19 mA ($>$)	$\dfrac{1}{2} = 0 \cdot 5$	$\dfrac{30}{64 \cdot 5} = 0 \cdot 465$
4 mA ($<$)	$\dfrac{1 \cdot 5}{3 \cdot 25} = 0 \cdot 46$	$\dfrac{40}{80} = 0 \cdot 5$

5.4.4. Validity of eqn. (17)

Equation (17) is given as

$$\frac{\delta f_{c1}}{\delta f_c} = \frac{\mu_d}{\mu_{inc}} - 1$$

According to results of the previous paragraph which were obtained experimentally, it is possible to check eqn. (17) against values from the standard curves for B3 Ferroxcube. However an exact correlation cannot be expected since the tolerance allowed on the

199

initial permeability of B3 is 100% (i.e. from 100–200). (See Fig. 12.)

$$4 \text{ mA} (>) \qquad \mu_d = \frac{40}{0.27} = 148$$

$$\mu_{inc} \text{ (from Fig. 8)} = 75.$$

Therefore $\quad \dfrac{\mu_d}{\mu_{inc}} = \dfrac{148}{75} = 1.92$

and $\quad \dfrac{\delta f_{c1}}{\delta f_c} = 1.92 - 1$

$$= 0.92.$$

as against 1·25 found experimentally.

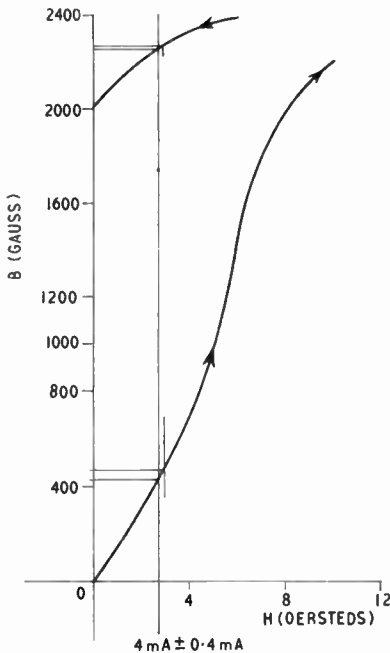$$4 \text{ mA} (<) \qquad \mu_d = \frac{12}{0.27} = 44.5$$

$$\mu_{inc} = 75$$

Fig. 12. B3 Ferroxcube. Enlarged typical *B-H* loop section. (From manufacturer's catalogue.)

Therefore $\quad \dfrac{\mu_d}{\mu_{inc}} = \dfrac{44.5}{75} = 0.59$

and $\quad \dfrac{\delta f_{c1}}{\delta f_c} = 0.59 - 1$

$$= -0.4$$

compared with 0·5 for the experimental result.

The improvement obtained is 2·5 times in the case of the experimental results whereas using the catalogue results it is 2·3 times.

It is apparent from this comparison that the ratio $\delta f_{c1}/\delta f_c$ can be calculated with greater precision when based upon the values obtained with a given sample of material. However, the general importance of the method is not affected since by using catalogue information the trend of any change in the steady magnetizing force is readily seen, and the ratio of improvement reliably indicated.

5.5. *Working Point Ambiguity*

During the theoretical comparison between modulators having steady fields of 6 and 12 oersteds, it was shown that the fractional carrier frequency instability could have two values for a given steady field, this was so since the operating point could be placed either on the ascending or on the descending curve of the *B/H* loop. The transference of the working point from the ascending to the descending curve can be caused by an excessively large sinusoidal field. If the working point is located on the descending curve this effect will be avoided. This is done by applying a large sinusoidal "conditioning" field. The "conditioning" field can be applied immediately after the application of the steady field; moreover, if the steady field is obtained from a permanent magnet the field need only be applied once, that is, immediately after assembly and magnetization.

5.6. *Permanent Magnet Polarization*

The use of a strong permanent magnet built into the modulator as part of the primary magnetic circuit has several other advantages besides the minimization of hysteresis instability; thus the modulator requires no external supplies other than the audio-frequency modulation current—a factor of importance in reducing the complexity. The stability of the polarizing field is determined almost solely by the magnetic stability of the permanent magnet and therefore voltage pulses on the direct current supply line, caused by switching surges, etc., have no effect upon such a modulator.

5.7. *Temperature Effects*

The effect of an increase of temperature upon the mixed magnetic ferrite is to change

the shape of its hysteresis loop by a reduction in saturation flux density. The magnitude of the effect is less for materials with a high Curie point. However, high Curie point materials have relatively low initial permeabilities at ambient temperatures of 25°C. The initial permeability can be increased by reducing the Curie point of the material and in mixed ferrites this is usually done by admixing the non-magnetic zinc ferrite to another ferrite. Such ferrites then have permeabilities in the region of 1,500, but are sensitive to temperature variations in respect of their permeability and saturation flux density. Examples of this type of mixed ferrite are the Mullard Ferroxcube A grades which are manganese-zinc ferrites.

The Mullard B grades of Ferroxcube are nickel zinc ferrites with a higher Curie point than the A grades and, consequently, exhibit less temperature sensitivity and also a smaller initial permeability. The electrical resistivity of this material is greater than for the A grades and the radio frequency losses are also smaller.

The temperature coefficient of the initial permeability of mixed ferrites is positive; however, with a steady magnetizing field applied the temperature coefficient of the incremental permeability can be either positive or negative, the polarity being dependent upon the change of slope of the hysteresis loop with temperature at the working point.

The ferrite modulator uses a B3 grade of Ferroxcube with a magnetic polarizing field of about 10 oersteds. The temperature coefficient of the radio-frequency inductance is -0.005% per °C over the temperature range 20°C to 50°C, whilst the temperature coefficient of the modulator sensitivity is plus 0.05% per degree centigrade for the same temperature change. The effect of a change in temperature is, therefore, about ten times as great in the case of the modulator sensitivity as in that of the radio-frequency inductance.

5.8. Construction of the Ferrite Modulator

The construction of the modulator is shown in Fig. 13. The audio frequency coils are wound upon two limbs of the specially shaped Radiometal laminations. The coils are connected in series and are sectionalized to improve the response at higher audio frequencies. A
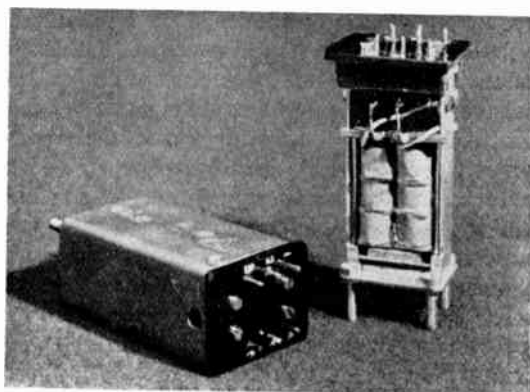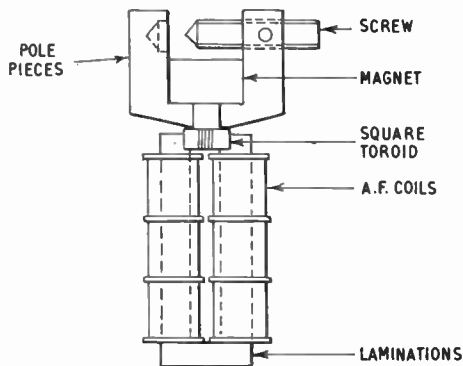

Fig. 13. The construction of the ferrite modulator is shown in the diagram above and also below in the photograph of the prototype unit.

square sided "toroid" Mullard Ferroxcube FX.1606 grade B3, is fixed in the open end of the U-shaped laminations with a mating fit made between the laminations and the ground faces of the "toroid". Performance artefacts arising from magnetostriction of the ferrite have not been observed. The polarizing field for the ferrite is provided by a small sintered magnet of Alcomax III alloy. It is supported between the pole pieces as the cross-arm, in an H arrangement, the ferrite being across the open end of this shape whilst a soft-iron screw is provided to shunt the other end. This screw provides a small adjustment of the field through the ferrite.

There are two main paths for the flux from the permanent magnet, these are through the ferrite and through the Radiometal laminations. The paths are in parallel and the one through

the Radiometal laminations is essentially a leakage path. The relative reluctances are approximately in the ratio of 2:1 for Radiometal as against ferrite paths.

The leakage flux through the laminations can be reduced by passing a direct current through the low-frequency windings in a direction to cause an opposing flux; however, this flux will add to the permanent magnet flux already present in the ferrite. Any audio-frequency harmonic distortion caused by the presence of the leakage field in the Radiometal laminations can be reduced in this way.

The "toroidal" core carrying the radio-frequency winding provides a low reluctance path to the radio-frequency flux—which is usually very small—and thereby minimizes the leakage into the low-frequency circuit. With a balanced winding upon this toroid the audio-frequency controlling flux will develop audio-frequency potentials in opposition across each half of the r.f. winding and hence the total audio-frequency e.m.f. across the winding will be zero. This form of construction is particularly valuable for a modulator operating at a low carrier frequency with a r.f. coil of many turns where the induced audio-frequency e.m.f. would otherwise cause spurious modulation of the oscillator. Where the balanced r.f. winding is not practicable the effect of the induced audio-frequency e.m.f. can be made small by connecting a capacitor between the modulator r.f. winding and the oscillator tank circuit connection. The value of the capacitance is chosen to provide a high impedance to audio frequencies and a low impedance to radio frequencies.

The sizes of the various component parts of the modulator are determined for a particular application by the type of ferrite, the operating frequency and r.f. losses, the sensitivity, and the audio-frequency response.

5.9. Electrical Circuit

The greatest stability of operation for the ferrite modulator is realized when it is used in the circuit of Fig. 14. The modulator is parallel fed with audio-frequency current from the anode of the modulation valve. The voltage across the anode choke rises with frequency by 6 db per octave, whilst the reactance of the

modulator winding increases at the same rate. Over the frequency range that this applies the current through the modulator primary circuit coil will be independent of audio frequency and, hence, the frequency modulated signal will be the same.
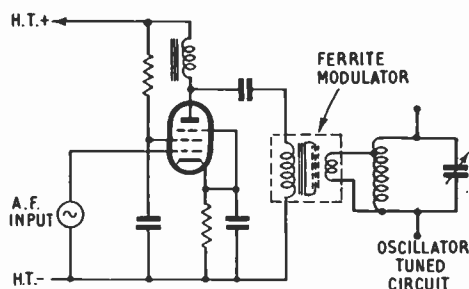

Fig. 14. The parallel-feed connection for the ferrite modulator.

5.10. Production Techniques

Because of the wide variations in the magnetic properties of the materials used in the modulator—as an example the initial permeability of the B3 Ferroxcube can vary between 100 and 200—particular attention was paid to production techniques and these became an integral part of the design. It was expected that unsuspected variations would give rise to difficulties but in the event the number of rejects was small and continues to be so. The main reason for this is seen in the compensating influence of the permanent magnet which tends to correct for variations in the permeability of the ferrite by a compensating flux variation. Thus it was possible to wind a fixed number of turns on the ferrite core and, despite the wide tolerances of initial permeability, to expect the inductance to be reasonably consistent when assembled in the modulator.

So far, in the applications to which this modulator has been put, it has not been necessary to control the loss factor (tan δ/μ) of the material. Moreover, no difficulties have been caused by spurious resonances even over the wide frequency range in which this modulator is used.

It was mentioned earlier when considering working point ambiguity that an increase in stability under varying conditions of audio input could be realised if the completed

modulator were saturated by a large sinusoidal field. This procedure is carried out on each modulator.

5.11. *Performance Details*

A summary of figures obtained on the performance of the ferrite modulator is given below: —

5.11.1. Operational frequency range

Generally 400 kc/s to 500 Mc/s if slight changes are made to the winding on the ferrite core. It would appear that these figures do not express extreme limits of operation.

5.11.2. Inductance of r.f. coil

When mounted in the modulator and polarized with the permanent magnet the inductance is 3·6 μH.

5.11.3. Temperature coefficient of r.f. inductance

The change of inductance with temperature for the fully assembled modulator is approximately − 0·01 % / °C.

5.11.4. Current sensitivity

The current sensitivity of the modulator, for small variations in the inductance of the r.f. coil is approximately 0·1 μH change per mA of current in the low frequency coil.

5.11.5. Temperature coefficient of sensitivity

The change in current sensitivity with temperature is approximately +0·1% / °C.

5.11.6. Q of the r.f. coil

The Q of the r.f. coil is in the region of 25 at 4 Mc/s.

5.11.7. A.f. characteristic

In the circuit shown in Fig. 14 the a.f. response characteristic will be within ±0·5 db between 50 c/s and 15 kc/s—with the proviso that the other components used exert no limiting influence.

5.11.8. Demodulated audio frequency distortion

The following figures show the harmonic distortion to be expected at various oscillator frequencies with this modulator, after the frequency-modulated wave has been demodulated.

Oscillator frequency	Frequency deviation	Total distortion
400 kc/s	15 kc/s	5%
30 Mc/s	90 kc/s	5%
170 Mc/s	100 kc/s	2%

A sinusoidal audio-frequency current of 1 kc/s was applied to the modulator. The harmonic distortion in the auxiliary circuits to the parallel-fed ferrite modulator was less than 1%.

The figures for an oscillator frequency of 400 kc/s were taken with a larger r.f. coil on the ferrite core, the inductance of this being 22 μH.

5.11.9. Hysteresis frequency stability

The magnitude of the shift in oscillator frequency caused by an excessively large audio-frequency voltage initially applied to the modulator will be less than 50 c/s per kc/s deviation.

5.11.10. Spurious frequency modulation

Adequate magnetic screening and a rigid mechanical construction served to reduce the spurious frequency modulation to a small level. Further by proportioning audio frequency sensitivity as mentioned earlier in section 3.5 levels of spurious frequency modulation can be reached which are small compared with other types of frequency modulators. Thus, in a typical circuit, the level of spurious frequency modulation was less than 30 c/s when the circuit was adjusted for a normal frequency deviation of 100 kc/s at 100 Mc/s.

6. Conclusion

The limitations of the reactance valve modulator have been examined and an attempt has been made to place the ferrite modulator in perspective against them. The limitations are shown to be of particular importance in equipment where a tuned oscillator is frequency modulated. At low oscillator frequencies the fractional frequency deviation obtainable is often inadequate whilst at the ultra high frequencies the effects of electron transit time, lead inductance and valve capacitance dominate the performance. Modulation distortion, deviation v. oscillator frequency tracking, microphony, reproducibility with valve replacements are problems which are eased by the use of the ferrite modulator at these high frequencies.

The large radio-frequency losses usually associated with magnetic materials can be made small in nickel-zinc ferrites. The effects arising from magnetic hysteresis are shown to be unimportant if suitable magnetic polarization is employed.

In contrast to the reactance valve modulator the ferrite modulator can be operated in simple variable frequency oscillator circuits up to 500 Mc/s. Likewise at frequencies of 1 Mc/s and below, large fractional deviations of 5 per cent. and more can be obtained without additional circuit complexity.

The ferrite modulator was designed for factory production and has proved to be both reliable and reproducible.

7. References and Bibliography

1. L. de Kramolin, "Magnetic tuning devices," *Wireless World*, **42**, p. 160, and p. 186, 1938; *ibid.*, **43**, p. 5, 1938.

2. H. Boucke, "Uber eine Einrichtung zur Frequenz Modulation von Sendern mit hilfe Vormagetisierter Hf-Eisenkernspulen," *Fernmeldtechnische Zeitschrift*, **4**, p. 201, 1951.

3. C. L. Cuccia, "Certain aspects of triode reactance-tube performance for frequency modulation at ultra-high frequencies," *R.C.A. Review*, **10**, p. 74, 1949.

4. E. S. Winlund, "Drift analysis of the Crosby frequency-modulated transmitter circuit," *Proc. Inst. Radio Engrs*, **29**, p. 390, 1941.

5. V. E. Legg, "Magnetic measurements at low flux densities," *Bell System Technical Journal*, **15**, p. 39, 1936.

6. J. L. Salpeter, "Developments in sintered magnetic materials," *J.Brit.I.R.E.*, **13**, p. 499, 1953.

7. J. L. Snoek, "New Developments in Ferro-magnetic Materials" (Elsevier Publishing Co. Ltd., Amsterdam, 1947).

8. V. E. Legg, *Loc. cit.*, p. 49.

9. E. Peterson, "Harmonic production in ferromagnetic materials at low frequencies and low flux densities," *Bell System Technical Journal*, **7**, p. 762, 1928.

10. H. P. J. and J. J. Went, "The magnetization process in ferrites," *Physica, s'Gravenhage*, **17**, p. 976, 1951.

11. H. P. J. Wijn, "Frequency dependence of Magnetization processes in ferrites and its relation to the distortion caused by ferrite cores," "Soft Magnetic Materials for Telecommunications," p. 51, Ed. C. E. Richards and A. C. Lynch (Pergamon Press, London, 1953).

12. F. Slater, "A ferrite frequency modulator," *Marconi Instrumentation*, **4**, p. 186, 1954.

8. Appendix: Freqnency Modnlation by Indnctance Variation

Referring to Fig. 2 in the paper, the total inductance, L_t, without modulation, is given by

$$L_t = \frac{L_0.L_{ab}}{L_0+L_{ab}} = L_0\left(1+\frac{L_0}{L_{ab}}\right)^{-1} \quad\ldots\ldots(19)$$

Now, f_o, the tuned anode circuit resonant frequency, is given by:—

$$f_o = \frac{1}{2\pi\sqrt{(L_0.C_0)}} \qquad \ldots\ldots\ldots(20)$$

and the resonant frequency when the modulator inductance, L_{ab} is connected without modulation being applied is

$$f_c = \frac{1}{2\pi\sqrt{(L_t.C_0)}} \qquad \ldots\ldots\ldots(21)$$

Therefore

$$f_c = f_o\left(1+\frac{L_0}{L_{ab}}\right)^{\frac{1}{2}} \qquad \ldots\ldots\ldots(22)$$

and

$$\frac{\delta f_c}{\delta L_{ab}} = -\frac{f_o.L_0}{2\,L_{ab}^2(1+L_0/L_{ab})^{\frac{1}{2}}}$$

By substituting f_c in terms of f_o from eqn. (22)

$$\frac{\delta f_c}{\delta L_{ab}} = -\frac{f_o.L_0}{2\,L_{ab}^2(1+L_0/L_{ab})} \ldots\ldots(23)$$

and from eqn. (19)

$$\frac{\delta f_c}{\delta L_{ab}} = -\frac{f_o.L_t}{2\,L_{ab}^2}$$

or

$$\frac{\delta f_c}{f_c} = -\frac{\delta L_{ab}.L_t}{2\,L_{ab}^2} \qquad \ldots\ldots\ldots(24)$$

In eqn. (24), δf_c represents the frequency deviation of the resonant frequency, f_c, when the modulator is connected and a modulating signal is applied. The change of the modulator inductance, L_{ab} producing this frequency deviation is represented by δL_{ab}.